#10 50

(1)

NATL AERONAUTICS AND SPACE ADM; NASA-CR-144835
COST ITEM $10.50

DO NOT DESTROY
RETURN TO LIBRARY

# DEVELOPMENT OF ELECTROLUMINESCENT DIODE-PUMPED Nd: YAG LASERS SUITABLE FOR SPACE USE

GaAlAs Diode Development

G. I. Farmer, J. M. Woodall, R. J. Lynch
IBM Corporation
18100 Frederick Pike
Gaithersburg, Maryland 20760

June 1972
Final Report for Period June 1971 — January 1972

23 MAR 1982
MCDONNELL DOUGLAS
RESEARCH & ENGINEERING LIBRARY
ST. LOUIS

Prepared for

GODDARD SPACE FLIGHT CENTER
Greenbelt, Maryland 20771

N77-72747

(NASA-CR-144835) DEVELOPMENT OF ELECTROLUMINESCENT DIODE Nd: YAG LASERS SUITABLE FOR SPACE USE. GaAlAs DIODE DEVELOPMENT Final Report, Jun. 1971 - Jan. 1972 (International Business Machines Corp.) 70/90 Unclas 55028

REPRODUCED BY
NATIONAL TECHNICAL
INFORMATION SERVICE
U.S. DEPARTMENT OF COMMERCE
SPRINGFIELD, VA. 22161

M82-12131

NOTICE

THIS DOCUMENT HAS BEEN REPRODUCED FROM THE BEST COPY FURNISHED US BY THE SPONSORING AGENCY. ALTHOUGH IT IS RECOGNIZED THAT CERTAIN PORTIONS ARE ILLEGIBLE, IT IS BEING RELEASED IN THE INTEREST OF MAKING AVAILABLE AS MUCH INFORMATION AS POSSIBLE.

TECHNICAL REPORT STANDARD TITLE PAGE

| 1. Report No. | 2. Government Accession No. | 3. Recipient's Catalog No. |
|---|---|---|
| | | |

**4. Title and Subtitle**
DEVELOPMENT OF ELECTROLUMINESCENT DIODE-PUMPED Nd:YAG LASERS SUITABLE FOR SPACE USE
GaAlAs Diode Development

**5. Report Date**
June 1972

**6. Performing Organization Code**

**7. Author(s)**
G. I. Farmer, J.M. Woodall, J. R. Lynch

**8. Performing Organization Report No.**
72-L25-002

**9. Performing Organization Name and Address**
IBM Corporation
18100 Frederick Pike
Gaithersburg, Maryland 20760

**10. Work Unit No.**

**11. Contract or Grant No.**
NAS 8-11447

**12. Sponsoring Agency Name and Address**
Mona Tyze
Goddard Space Flight Center
Greenbelt, Maryland 20771

**13. Type of Report and Period Covered**
Final Report

**14. Sponsoring Agency Code**

**15. Supplementary Notes**

**16. Abstract**

Electroluminescent diodes for Nd:YAG laser pumping have been fabricated which show several advantages over previous technology. The semiconductor material used was GaAlAs grown by liquid phase epitaxy on GaP substrates. The GaP gives the necessary physical strength and is a good window for the 8000 Å to 8100 Å pump radiation. The diodes have both electrical contacts on the same face while light is emitted from the opposite face. This eliminates mechanical interference from contact wiring and shadowing of the junction by the top contact. Because the epitaxial growth can be very thin (20 μm) growth times are short and heat conduction from the p-n junction is improved.

Contact metallurgy was optimized empirically for both n- and p-type GaAlAs using Au-Ge-Ni and Au-Zn mixtures respectively.

| 17. Key Words (Selected by Author(s)) | 18. Distribution Statement |
|---|---|
| Light Emitting Diodes<br>GaAlAs<br>GaP<br>Nd: YAG Lasers | |

| 19. Security Classif. (of this report) | 20. Security Classif. (of this page) | 21. No. of Pages | 22. Price* |
|---|---|---|---|
| UNCLASSIFIED | UNCLASSIFIED | | |

*For sale by the Clearinghouse for Federal Scientific and Technical Information, Springfield, Virginia 22151.

Reproduced from best available copy.

## PREFACE

The work performed under this contract represents the first phase in development of a diode-pumped Nd:YAG laser. A space-qualified version of this device is a candidate for use as a transmitter in space communications. The objective addressed in this task was the specialization and improvement of GaAlAs diodes for Nd:YAG pumping. Improvements were sought in the form of increased external quantum efficiency and better thermal design. The diode design was made so that the device packing density could be maximized, and so that there would be no masking of emitted light or mechanical interference by electrical contacts.

Beginning with epitaxial growth of diode material, this program extended through fabrication of diode devices and their evaluation. Also included was the investigation of some low melting point glass material to be used as an adhesive in anticipated laser designs. The main feature of this program was the growth of GaAlAs by liquid phase epitaxy on GaP wafers. Since GaP is transparent to the 8100Å emission from the diodes, it can serve well as a supporting substrate on which very thin layers of GaAlAs of a minimum band-gap emission structure can be grown.

Efficient GaAlAs diodes were grown on GaP and, for the small sample produced, showed as much as 2 to 3 times the efficiency expected for previously produced homojunction diodes. Techniques for contacting and bonding the diodes were developed. Diodes of the desired form were produced and shown to exhibit the predicted characteristics. Problems which appear to be related to the crystal growth direction were found in mesa etching. Additional problems have been found in layer cracking and surface roughness of wafer.

Further development of these diodes is recommended. As the next step toward utilization in a laser device, a relatively large number of these diodes should be produced to establish production procedures and give a statistical base for further evaluation. There remain some problems discovered, during the course of this work, which appear tractable and merit further attention. The causes and elimination of layer cracking should be studied more extensively, and the appropriate conditions for growth on (100) crystal planes should be established.

Reproduced from best available copy.

## TABLE OF CONTENTS


| Section | | | Page |
|---|---|---|---|
| 1 | INTRODUCTION AND STATEMENT OF THE PROBLEM | | 1-1 |
| 2 | PROGRAM GOAL AND PROPOSED APPROACH | | 2-1 |
| | 2.1 | INNOVATION REQUIRED BY THIS TECHNICAL APPROACH | 3-5 |
| 3 | EXPERIMENTAL PROCEDURE AND RESULTS | | 3-1 |
| | 3.1 | SEMICONDUCTOR GROWTH | 3-1 |
| | | 3.1.1 Experimental Procedure | 3-1 |
| | | 3.1.2 Target LED Structure | 3-4 |
| | | 3.1.3 Results - MBG Structure on GaAs | 3-6 |
| | | 3.1.4 Results - MBG Structures on GaP | 3-8 |
| | | 3.1.5 Surface Morphology and Imperfection | 3-18 |
| | | 3.1.6 Back-Contact LED Fabrication | 3-22 |
| | | 3.1.7 Summary | 3-22 |
| | | 3.1.8 Future Studies | 3-22 |
| | 3.2 | METAL-GaAlAs CONTACTS AND CONTACT RESISTANCE | 3-24 |
| | | 3.2.1 Introduction | 3-24 |
| | | 3.2.2 Application of Metallurgy | 3-24 |
| | | 3.2.3 Experimental | 3-25 |
| | | 3.2.4 Discussion | 3-25 |
| | | 3.2.5 Conclusions | 3-27 |
| | 3.3 | REFLECTIVE COATINGS | 3-31 |
| | 3.4 | LOW MELTING POINT GLASS ADHESIVE | 3-34 |
| | 3.5 | LED CONSTRUCTION AND EVALUATION | 3-40 |
| | | 3.5.1 Device Description | 3-40 |
| | 3.6 | PROJECTED LIFE TESTING | 3-54 |

Table of Contents (cont)


| Section | | Page |
|---|---|---|
| 4 | RECAPITULATION AND DISCUSSION OF PROGRAM RESULTS | 4-1 |
| 5 | NEW TECHNOLOGY | 5-1 |
| | 5.1 EPITAXIAL GROWTH OF GaAlAs on GaP | 5-1 |
| | 5.2 MINIMUM BANDGAP LED STRUCTURE | 5-1 |
| | 5.3 TECHNIQUES FOR FABRICATION OF DOMED LEDs | 5-1 |
| | 5.4 LED PUMP ARRAY DESIGN AND ASSEMBLY | 5-1 |
| 6 | CONCLUSIONS | 6-1 |
| 7 | RECOMMENDATIONS FOR FURTHER ACTIVITY | 7-1 |
| Appendix | | |
| A | GaP DOMED DIODE PREPARATION | A-1 |
| B | PROCEDURE FOR DEVICE FABRICATION | B-1 |
| C | APPLIED PHYSICS LETTERS | C-1 |
| REFERENCES | | R-1 |

## LIST OF ILLUSTRATIONS


| Figure | | Page |
|---|---|---|
| 1-1 | Homojunction Diode | 1-2 |
| 1-2 | Detailed Absorption Spectrum of Nd:YAG in the Transitions from $^4I_{9/2}$ to $^4F_{5/2}$ & $^2H_{9/2}$ States at Room Temperature | 1-2 |
| 2-1 | Back Contact Diode | 2-1 |
| 2-2 | Bandgap Energy vs Aluminum Content | 2-3 |
| 2-3 | Idealized MBG Diode Structure | 2-4 |
| 2-4 | Suggested Semielliptical Pumping Cavities | 2-4 |
| 2-5 | Typical Homojunction Diode Array Performance | 2-6 |
| 3-1 | Apparatus for LPE Growth | 3-2 |
| 3-2 | Composition Profile of P 160, an Optimal MBG Structure Grown on GaAs | 3-8 |
| 3-3 | Electron Beam Profile of Al and P for P 171 | 3-11 |
| 3-4 | Electron Beam Profile of Al and P for P 174 | 3-12 |
| 3-5 | Light Output and Forward Current vs Voltage for P 176B | 3-14 |
| 3-6 | Light Output and Forward Current vs Voltage for P 176B | 3-15 |
| 3-7 | Electron Beam Profile of Al and P for P 179 | 3-16 |
| 3-8 | Photomicrographs of a Typical MGB Structure on GaP | 3-17 |
| 3-9 | Surface of Growth on (100) GaP Surface | 3-18 |
| 3-10 | Electron Beam Profile of P 180 | 3-20 |
| 3-11 | Surface of P 180 after HCl Removal of Surface Layer | 3-21 |
| 3-12 | Cracked Layer of P 196 | 3-21 |
| 3-13 | Photomicrograph of a Back Contacted Graded $Ga_{1-x}Al_xAs$ Layer Grown on GaP - Run P 203 | 3-23 |
| 3-14 | Specific Contact Resistance of AuGeNi on N type $Ga_{1-x}Al_xAs$ As a Function of Carrier Concentration | 3-26 |
| 3-15 | Specific Contact Resistance of AuZn on P-type $Ga_{1-x}Al_xAs$ As a Function of Carrier Concentration | 3-26 |
| 3-16 | Specific Contact Resistance of AuGeNi on N-type $Ga_{1-x}Al_xAs$ As a Function of Percent Aluminum | 3-28 |
| 3-17 | Specific Contact Resistance of AuZn on P-type $Ga_{1-x}Al_xAs$ As a Function of Percent Aluminum | 3-29 |
| 3-18 | Specific Contact Resistance of AuGeNi on N-type $Ga_{1-x}Al_xAs$ As a Function of Resistivity | 3-30 |
| 3-19 | Reflectively Coated GaAs Chip | 3-33 |
| 3-20 | Refraction in Multilayered Medium | 3-30 |

## List of Illustrations (cont)


| Figure | | Page |
|---|---|---|
| 3-21 | Transmission of Pump Radiation vs Interface Incidence Angle | 3-37 |
| 3-22 | Diode Output (Relative) vs Drive Current | 3-39 |
| 3-23 | Glass Vapor Pressure vs Temperature | 3-41 |
| 3-24 | LED Structure | 3-42 |
| 3-25 | Cross Section of Solution Grown Wafer Before Processing | 3-42 |
| 3-26 | Series Embodiment for a LED Pumping Array | 3-43 |
| 3-27 | Assembled Device for Evaluation | 3-43 |
| 3-28 | Emission Spectrum from Flip Chip Device | 3-45 |
| 3-29 | DC Current-Voltage Characteristic, GaAlAs LED with GaP Window, Diode Area: 10 mil by 100 mil, Diode DI | 3-46 |
| 3-30 | DC Current-Voltage Characteristic, GaAlAs LED with GaP Window, Diode Area: 10 mil by 100 mil, Diode DII | 3-47 |
| 3-31 | DC Current-Voltage Characteristic, GaAlAs LED with GaP Window, Diode Area: 10 mil by 100 mil, Diode DIII | 3-48 |
| 3-32 | Voltage Dependence of Diode Current | 3-49 |
| 3-33 | Voltage Dependence of Diode Current | 3-50 |
| 3-34 | AC Measurement Circuit for Device Evaluation | 3-51 |
| 3-35 | AC Current-Voltage Characteristic, Pulse Width: 500 $\mu$s, PRF: 20 Hz, Diode Area: 10 mil × 100 mil, Diode DII | 3-52 |
| 3-36 | AC Current-Voltage Characteristic, Pulse Width 500 $\mu$s, PRF: 20 Hz, Diode Area: 10 mil × 100 mil, Diode DIII | 3-53 |


## LIST OF TABLES


| Table | | Page |
|---|---|---|
| 2-1 | Substrate Material Characteristics | 2-2 |
| 3-1 | Minimum Band Gap Active Region LED Structure on GaAs | 3-7 |
| 3-2 | Growth Specifications for Optimal LED Structure on GaAs | 3-9 |
| 3-3 | Minimum Band Gap Active Region LED Structures on GaP | 3-10 |
| 3-4 | $Ga_{1-x}Al_xAs$ Layers with Graded Composition on GaP | 3-19 |
| 3-5 | Device Characteristics Summary | 3-44 |


Reproduced from best available copy.

## LIST OF ABBREVIATIONS AND SYMBOLS

| | |
|---|---|
| Å | Angstrom |
| AuGeNi | Gold Germanium Nickel |
| AuZn | Gold Zinc |
| GaAlAs | Gallium Aluminum Arsenide |
| GaAs | Gallium Arsenide |
| GaP | Gallium Phosphide |
| ISM | Isothermal Solution Mixing |
| LED | Light Emitting Diode |
| LPE | Liquid Phase Epitaxy |
| MBG | Minimum Band Gap |
| Nd:YAG | (Neodymium doped) Yttrium Aluminum Garnet |
| p-n | Semiconductor doping types |
| SiO | Silicon Oxide |
| m | Micrometer |
| ≃ | Approximately |

## Section 1

# INTRODUCTION AND STATEMENT OF THE PROBLEM

This report describes the work performed in electroluminescent diode development during the period beginning in June, 1971 and ending in January, 1972. Stimulated by the eventual need for optical communications systems for space application, much attention has been directed toward several laser transmitters. Of these potential candidates, the Nd:YAG laser is presently preeminent. This laser derives, from a crystalline active medium, an emission at 1.06 $\mu$m, a near infrared wavelength for which reasonably good detectors exist. Since the Nd:YAG laser can be mode-locked to produce subnanosecond pulses, communications systems utilizing it can meet and exceed gigahertz information bandwidths.

The choice of Nd:YAG for further development presents an additional design selection. Three promising excitation sources exist for this laser: arc lamps, solar energy, and electroluminescent diodes. Before the ultimate selection of one, or a combination, of these sources as most advantageous for space application, each is being developed experimentally.

Since the experimental feasibility of planar GaAlAs diodes as pump sources was shown earlier; this program was initiated to develop diodes specifically designed for Nd:YAG pumping. Several diode improvements were conceived. These improvements can be understood by studying the homojunction GaAlAs diode. Figure 1-1 shows a transverse section of a homojunction diode. Light is created, by carrier recombination at the p-n junction, when a forward bias voltage is applied to the diode. The wavelength of the light created in this process depends on the fractional content of aluminum in the GaAlAs crystal. To be used as an excitation source for Nd:YAG, the most desirable emission wavelength is about 8070Å. This emission wavelength is produced when the GaAlAs crystal contains about 11 mole percent aluminum. The efficiency of the radiative recombination process, in material of that composition, is very high — approaching 100%. The bandwidth of the light emitted is dependent, in part, upon the gradient of the aluminum in the junction region. The bandwidth varies from 250Å to 400Å in average homojunction diodes, and is generally a little greater than 300Å. A reduction in the bandwidth of the diode emission would increase the Nd:YAG pumping efficiency through a better match to the neodymium absorption spectrum. This can be seen from the Nd:YAG absorption spectrum, shown in Figure 1-2, which was measured using a 1.5 mm thickness of lutetium compensated Nd:YAG. The neodymium doping level is approximately 1% which is the same as that used in present laser rods.

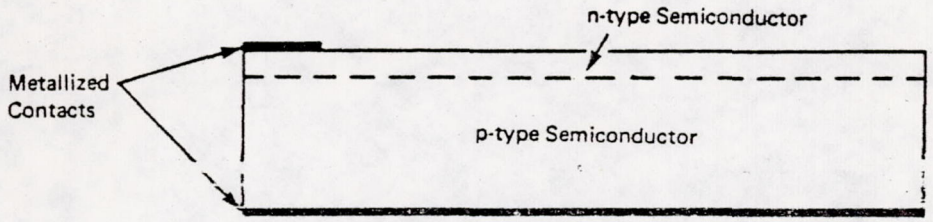


Figure 1-1. Homojunction Diode

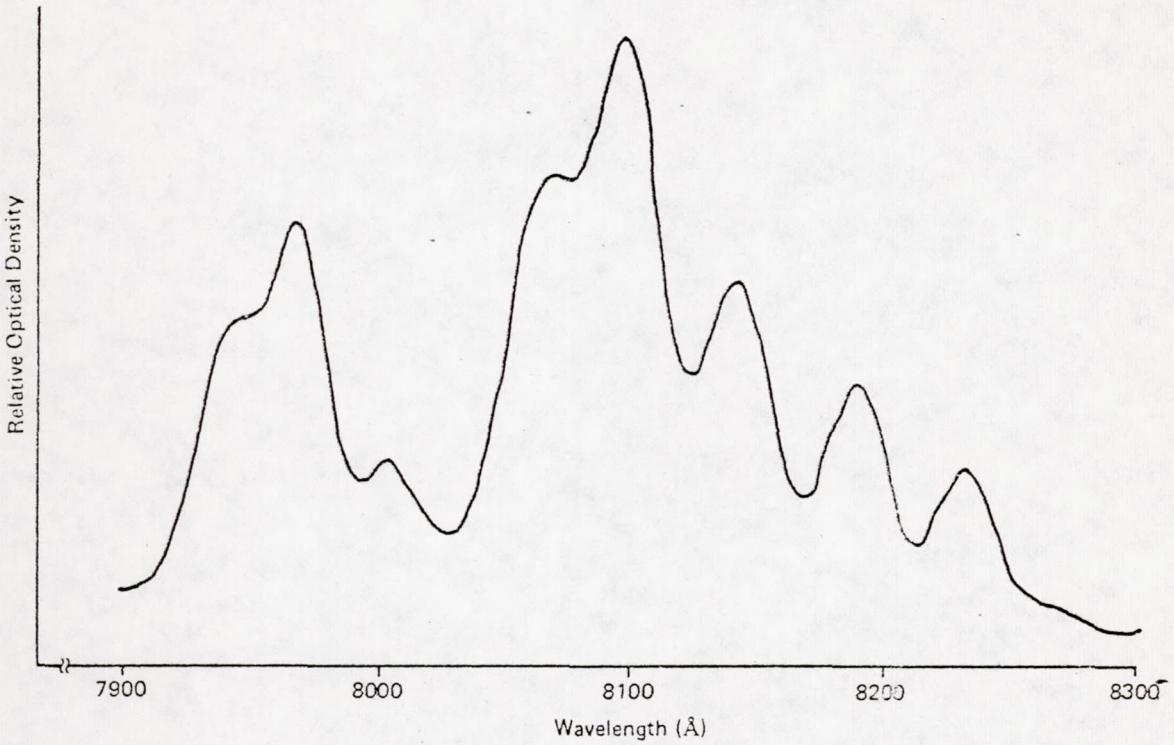


Figure 1-2. Detailed Absorption Spectrum of Nd:YAG in the Transitions from $^4I_{9/2}$ to $^4F_{5/2}$ & $^2H_{9/2}$ States at Room Temperature

Although light is efficiently generated at the p-n junction of this device, the external efficiency is much lower (≈1% into air). The degradation in efficiency results from the high refractive index of the semiconductor material, which makes the critical angle for total internal reflection at interfaces very small (≈15° at GaAlAs-air interfaces). (See Equation 3.4-2.) Light reflected at these boundaries is eventually absorbed within the material. The absorption in the n-type region of the material is not very high ($\alpha \approx 10\ cm^{-1}$), but virtually all light passing into the p-region is lost. This absorption results from free carriers and from the reduced bandgap in the p-region. To understand the situation fully, a brief summary of the diode growth and fabrication technique is helpful.

Customarily, liquid phase epitaxial growth begins with the introduction of an n-type GaAs seed wafer into an n-doped GaAlAs melt containing a higher concentration of aluminum than that producing the desired emission wavelength. Growth is initiated by varying the melt temperature. As the growth proceeds, variation in temperature and melt aluminum concentration determine the stoichiometry of the growth. As the temperature is decreased and growth proceeds, the aluminum concentration in the crystal decreases. After about 25 $\mu$m of growth, the aluminum concentration has reached that characteristic of the desired emission wavelength, and a p-type counter doping is added to form the p-n junction. Growth is then continued to add about 100 $\mu$m of p-type material necessary for physical strength of the diode devices. During this final growth, the aluminum concentration continually decreases so that the bandgap energy of all this material is lower than that at the p-n junction. This condition produces the strong absorption previously mentioned. To complete the processing, the seed crystal of GaAs is completely lapped off, leaving only the epitaxial growth layers. Application of the electrical contacts, dicing, and bonding operations complete the diode device fabrication. (See Figure 1-1.)

Another source of loss is the presence of the n-type electrical contact above a portion of the p-n junction. This contact consists of AuGeNi metallurgy and is opaque to the emitted radiation. This contact degrades the output efficiency by the ratio of the total junction width to the contact width since light is emitted from all the junction width but the portion under the contact is blocked. Therefore, a minimum contact width of about 90 $\mu$m on a total device width of 340 $\mu$m reduces the efficiency by 26.5%. This loss of efficiency exacerbates an already troublesome thermal problem which is also incumbent on this diode structure.

There are two mechanisms of heating in electroluminescent diodes. One is the direct conversion through ohmic heating due to bulk resistivity and contact resistance. The other is the reabsorption of light. In the use of the homojunction diode, it is reasonable to assume that almost all of this heat is deposited in the p-region between the p-type contact and the junction. This heat must be conducted through the 100 $\mu$m layer of GaAlAs to the heat sink. This heating can result in a significant (30° C or more) temperature rise between the diode base and junction. Because the external quantum efficiency is also dependent on the temperature, decreasing as the temperature increases, such temperature increases are undesirable.

The temperature dependence of the quantum efficiency, $\eta$, can be empirically characterized by the relationship

$$\eta_{int}(T) \propto \exp(E_a/kT)$$

The apparent activation energy, $E_a$, has observed values in the range 0.02 to 0.09 eV for several GaAlAs LEDs measured.

## Section 2

## PROGRAM GOAL AND PROPOSED APPROACH

The goal of this program was to develop an improved electroluminescent diode for Nd:YAG laser excitation. Potential improvements in several diode characteristics were desirable and feasible, e.g., internal and external quantum efficiency, thermal characteristics and form factors. Specific improvement of internal quantum efficiency was sought through optimization of band gap structure and doping density. External quantum efficiency could be improved by reducing internal absorption and eliminating contact masking of the junction region. A new diode shape would improve heat conduction and optical coupling efficiency. To achieve this goal a diode structure was proposed which is shown schematically in Figure 2-1.

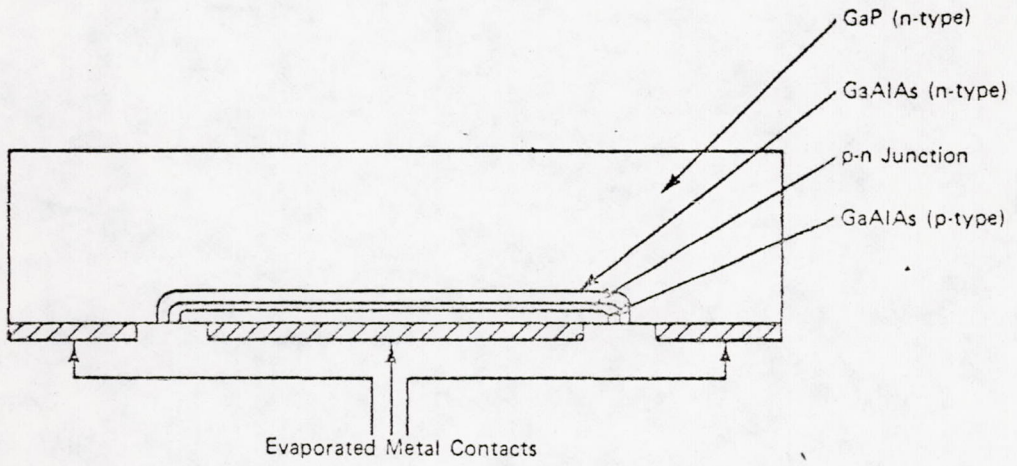


Figure 2-1. Back Contact Diode

The proposed diode consists of epitaxial layers of GaAlAs grown on GaP. The ideal starting material for epitaxial growth is a crystal lattice seed wafer of dimensions perfectly matched to the dimensions of the overgrowth layers, having good thermal conductivity and being transparent to radiation at the desired emission wavelength.

Table 2-1 lists possible substrate materials which are transparent to 8100Å light. However, all materials except for GaP were rejected as substrates for one of the following reasons: (1) not available in suitable sizes, (2) noncompatible lattice constant, (3) no growth of $Ga_{1-x}Al_xAs$ by the liquid phase epitaxial method. Although there exists a small lattice mismatch with the GaAlAs lattice, single crystal GaP satisfies most of the requirements for the seed wafer. GaP is available in wafer sizes which are useful for epitaxy and therefore was chosen as the supporting substrate for the diode design.

Reproduced from best available copy.

**Table 2-1**

SUBSTRATE MATERIAL CHARACTERISTICS

| Material | Band Gap[1] (eV) | Lattice Constant[2] (Å) | Average Substrate Area ($cm^2$) |
|---|---|---|---|
| SiC | 2.2-3 | 4.36 | 0.1 |
| AlAs | 2.16 | 5.66 | none |
| GaP | 2.25 | 5.45 | 1-2 |
| AlSb | 1.6 | 6.09 | 1-2 |
| ZnSe | 2.80 | 5.66 | 0.1-0.2 |
| ZnTe | 2.26 | 6.1 | 1-2 |
| $Al_2O_3$ | >3.0 | 4.75[3] | 1-6 |
| MgO | >3.0 | 4.2 | 1-6 |

Notes:
1. 8100 Å = 1.53 eV
2. GaAs = 5.65 Å
3. Hexagonal-Rhombic Structure

In addition to the use of a transparent substrate, it is also desirable to be able to form the EL diode structure in such a manner that the material adjacent to (on both sides of) the active recombination region is also a window. At the same time it should not introduce competitive nonradiative centers which reduce efficiencies in the active region. Such a condition is ideally met with the $Ga_{1-x}Al_xAs$ system. As seen in Figure 2-2, the band gap energy increases with Al concentration. Furthermore, changes in composition can occur without significant changes in lattice constant. This situation can be contrasted with the $GaAs_{1-x}P_x$ system where compositional changes are accompanied by detrimental lattice constant changes. It is the lack of lattice constant mismatch which is responsible for the success of the $Ga_{1-x}Al_xAs$ heterojunction laser devices.

Thus, it is possible to grow a structure in which all the material outside the active region where radiative recombination occurs has a larger band gap than the active region. Such a structure is shown schematically in Figure 2-3. The optical consequences of this structure will be discussed in more detail in Subsection 3.1.2.

This structure can be shown in the following manner. On the prepared surface of the GaP seed wafer, a high bandgap n-type GaAlAs layer is grown to a thickness of 10 to 15 $\mu$m. This layer is followed by two p-type layers of GaAlAs, the first of the desired emission bandgap, and the next of a higher bandgap. These layers have a total thickness of 15 to 20 $\mu$m. The diode fabrication is completed by mesa etching, application of contact stripes, dicing, and bonding in suitable arrays.

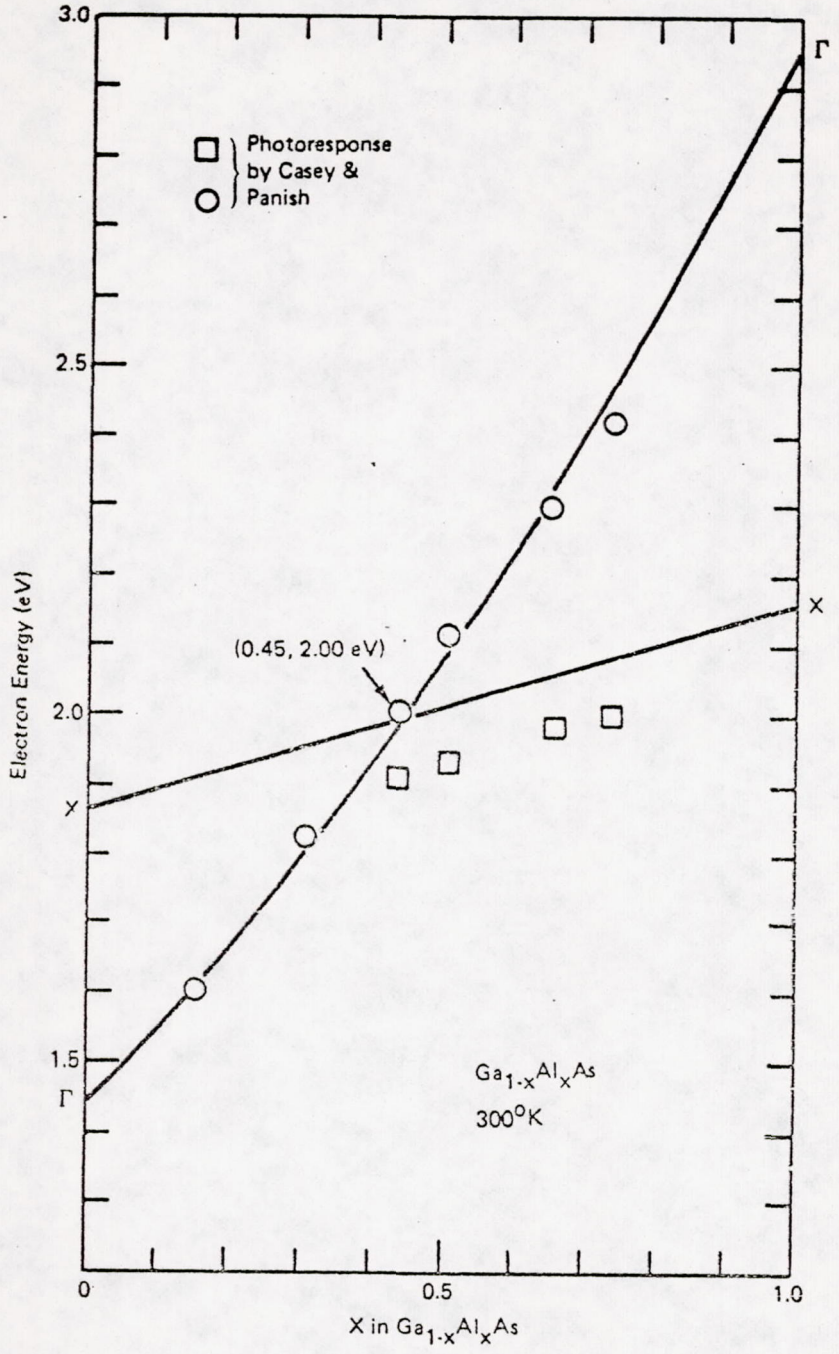


Figure 2-2. Bandgap Energy vs Aluminum Content

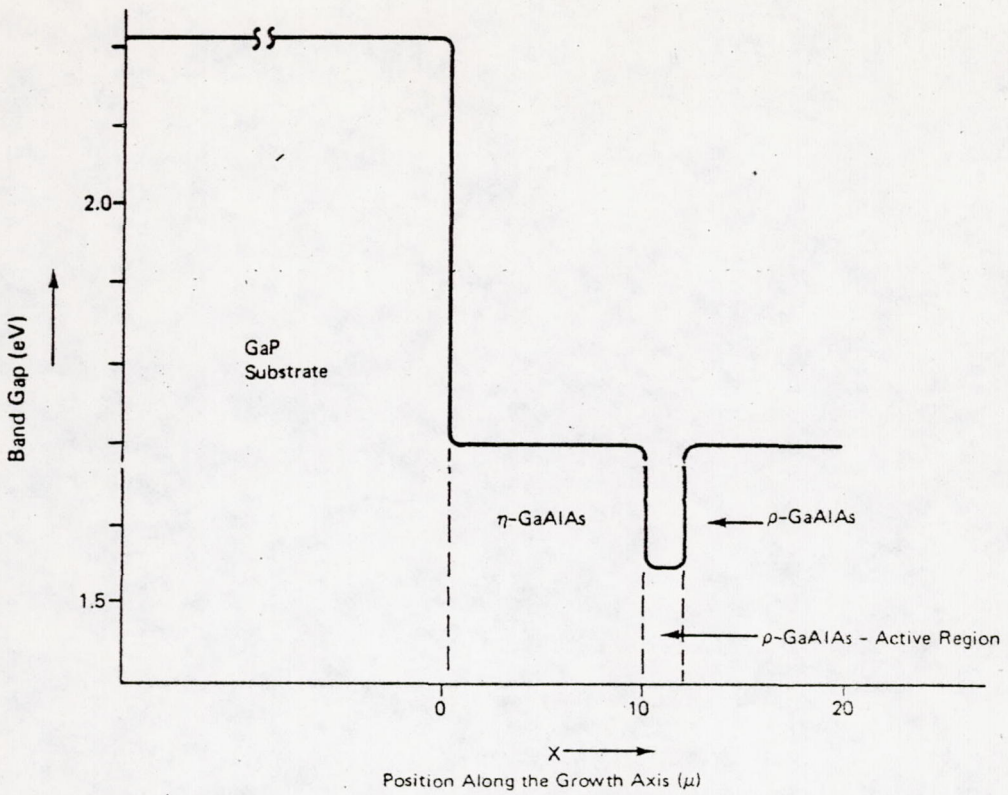


Figure 2-3. Idealized MBG Diode Structure

In this diode structure, light again originates at the p-n junction and is emitted through the n-layer and the GaP substrate. Efficiency of this diode can be increased, because the absorption of the layers is reduced by bandgap tailoring and the absorbing layer thickness is substantially reduced from the case where the seed wafer must be lapped away from the epitaxy. The position of the electrical contacts on this design satisfies the requirement for avoiding masking of the junction and also allows the diode to be used in a design suggested schematically in Figure 2-4.

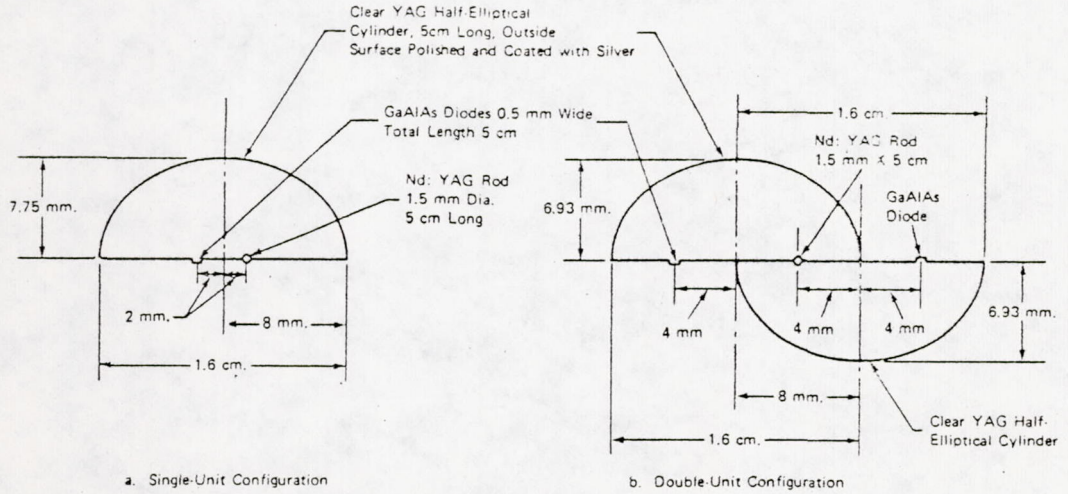


Note: These configurations are central sections through the pump cavity perpendicular to the rod axis.

Figure 2-4. Suggested Semielliptical Pumping Cavities

In this design, the diode array is bonded directly to a solid cylinder of yttrium aluminum garnet (YAG) crystal. The GaP interfaces directly with this material of refractive index n = 1.82, and the critical angle for total internal reflection is then increased from 15° to about 32°, thus increasing the diode emission by a factor of 4.

The "back-contact" diode design achieves the other important goal sought by reducing the thermal problem. By locating the junction only 10 $\mu$m from the heat sink, approximately ten times the heat load can be applied to the new diodes for an identical temperature rise, $\Delta T$. This estimate is based on the expression derived for one dimensional heat flow.

$$\Delta T = \frac{l}{KA} Q$$

In this equation l represents the distance from the junction to the heat sink; K, the thermal conductivity; A, the junction area; and Q, the total heat to be conducted. This advantage is particularly important since thermal effects on previously constructed diodes have been manifested by a nonlinear relation between drive current and light output. When operated in a pulsed mode ($\approx$500 $\mu$s pulses) the light output increases linearly with the current, up to current densities of 400A/cm$^2$ or higher. However, when DC excitation is applied, the diode output reaches a maximum typically at 125 to 150 A/cm$^2$ and further increases in current actually reduce the light output. This is shown for a typical homojunction diode in Figure 2-5.

## 2.1 INNOVATION REQUIRED BY THIS TECHNICAL APPROACH

Most significant of the technological steps required by this program was the growth of the efficient GaAlAs semiconductor material on single crystal GaP. No similar system has ever been reported and many details of growth such as direction, thermal profile, phosphorous contamination of the junction, and growth rates had to be ascertained.

Another significant innovation was the fabrication of the new devices. Photolithography and chemical etching techniques had to be developed to produce mesa diodes of the proper size and shape. Flip-chip solder connections for use on evaporatively coated berylium oxide circuit boards had to be devised.

Metallurgical contacting techniques were carefully explored to find the lowest contact resistance for both n- and p-type material, requiring the study of the particular alloys and the method of application to the material.

The necessity for bonding the diode array directly on the solid reflector without air interface, as depicted in Figure 2-4, suggests the use of high refractive index adhesive between the diodes and the reflector. Otherwise, the total internal reflection advantage would be reduced. One candidate for this adhesive is a low melting point glass made from arsenic, sulfur, selenium, bromine, or iodine. Some investigation of this material was made under this program to show the feasibility of its use.

Application of a reflective coating to the sides of the diode offers a further increase in the useful light output. The reflectivity of electrical contacts were measured and techniques for application of reflective coatings to other surfaces required further innovation.

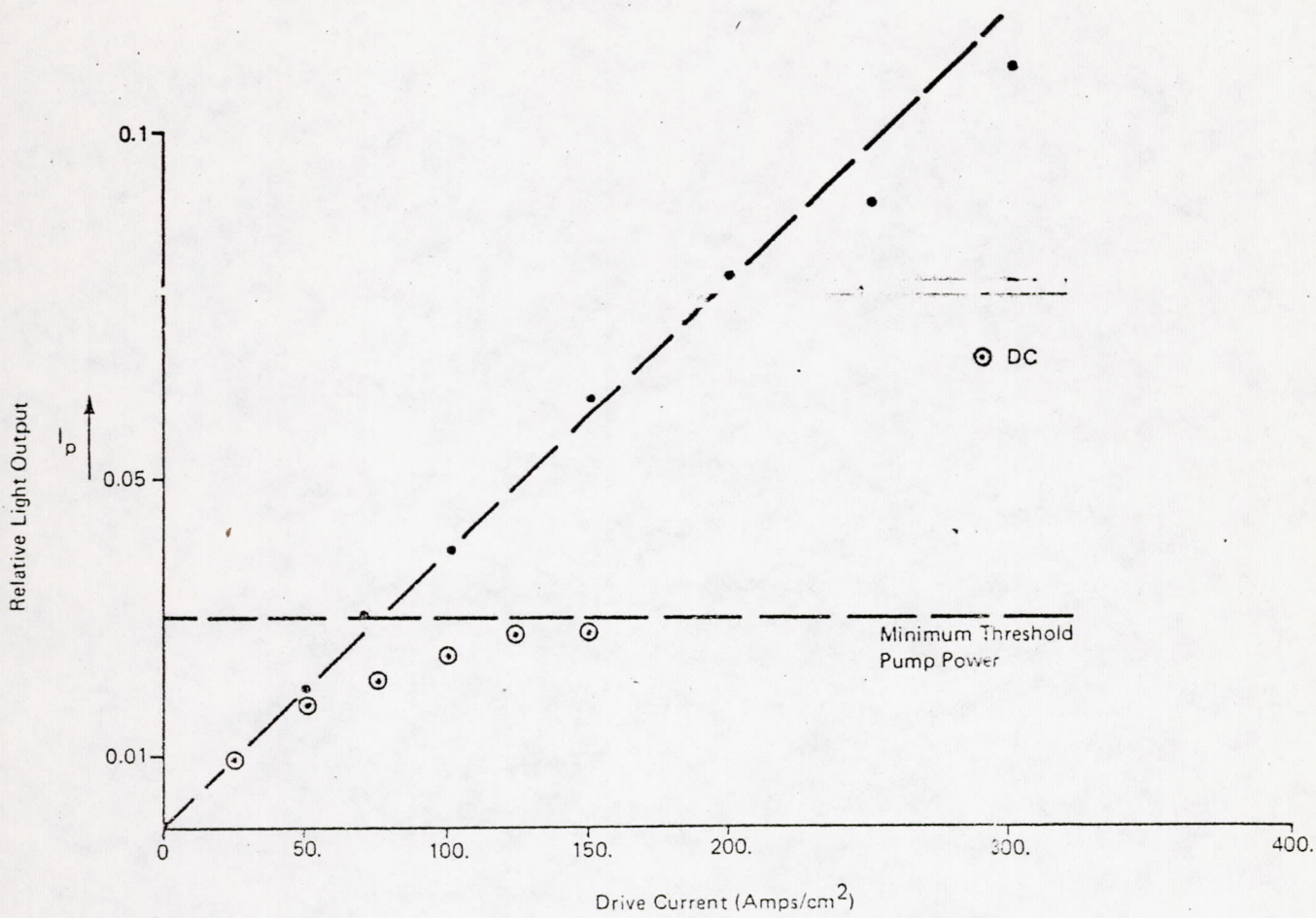


Figure 2-5. Typical Homojunction Diode Array Performance

## Section 3

# EXPERIMENTAL PROCEDURE AND RESULTS

## 3.1 SEMICONDUCTOR GROWTH

The purpose of the semiconductor growth experiments was to explore the growth of new light emitting diode structures on a nonabsorbing semiconductor substrate. The material used for the light emitting diode (LED) structures was $Ga_{1-x}Al_xAs$, and the nonabsorbing substrate was GaP. $Ga_{1-x}Al_xAs$ has been previously used for both efficient electroluminescent sources[1] and much improved room temperature laser devices.[2,3,4,5] For these previous devices, $Ga_{1-x}Al_xAs$ layers have been grown on GaAs substrates by the liquid phase epitaxial (LPE) method.[6,7] It was felt that the only impediment to further enhancement of electroluminescent efficiencies in $Ga_{1-x}Al_xAs$ LED structures was the use of GaAs substrates, which absorb radiation emitted by $Ga_{1-x}Al_xAs$. In order to remove the GaAs substrate, it is necessary to grow thick layers of $Ga_{1-x}Al_xAs$. This requires a complicated and time consuming brute force crystal growth technology. However, it has been shown recently that thick layers of $Ga_{1-x}Al_xAs$ grown on GaAs can lead to devices with improved quantum efficiencies.[8] For this program, it was assumed that, if $Ga_{1-x}Al_xAs$ would epitaxially deposit on GaP substrates by LPE, further improvements in external quantum efficiencies could be expected, provided the $Ga_{1-x}Al_xAs$ layers grown on GaP had the same optical and electronic properties as those grown on GaAs. Therefore, the following experimental design plan was adopted:

1) Develop growth procedures for an optimal $Ga_{1-x}Al_xAs$ LED structure on GaAs which produces the expected efficiencies.

2) Substitute GaP substrates for GaAs.

3) Adjust growth procedure to accommodate the GaP, if necessary.

4) Conduct auxiliary experiments to study unexpected results, if any.

### 3.1.1 EXPERIMENTAL PROCEDURE

The LPE methods used in these experiments have been described previously.[9,10,11] However, to orient the reader, a schematic diagram of the apparatus is shown in Figure 3-1. The apparatus has four main parts which are made of high purity, high density graphite. Part a is an outer crucible, which contains parts b, c, and d when assembled. Part a also prevents rotation of the four melt chambers, within part d, with respect to the substrate holder, part b, and the carbon spacer for melt transfer, part c.

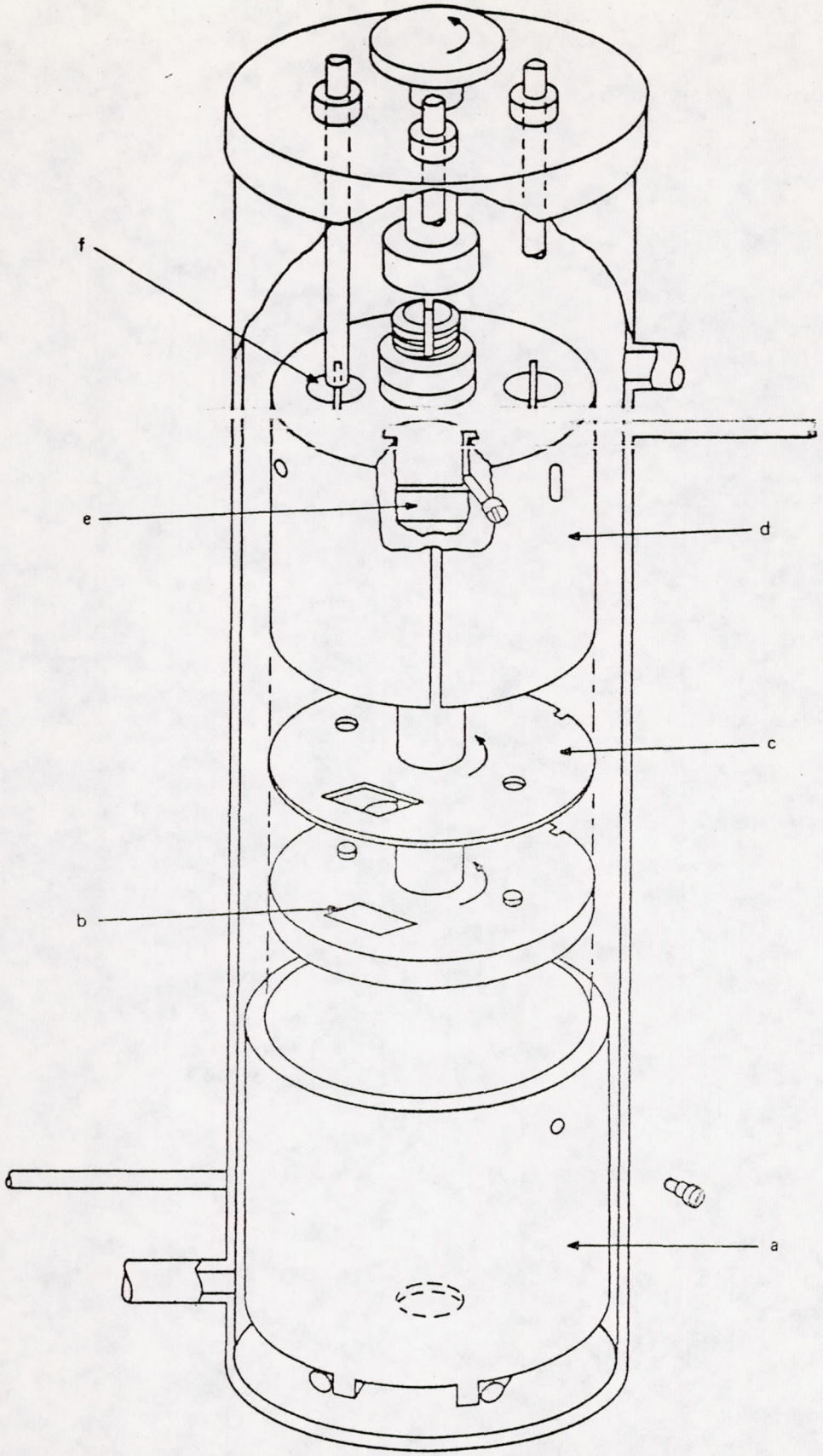


Figure 3-1. Apparatus for LPE Growth

The additional features which can be seen are: (1) a cutaway view of a melt chamber with a GaAs source bar, e; (2) a melt chamber, f, with a quartz tube, leading to the exterior, used to insert a dopant into the melt during growth; and (3) the manner in which the carbon spacer, c, is fixed to the substrate holder, b. In operation, the substrate holder and the spacer for melt transfer are rotated from one melt chamber to another via a quartz rod connected from part b to a handle outside of the quartz containing vessel. The vessel containing the quartz is constructed to facilitate vacuum baking, hydrogen back filling, and continuous flushing.

To prepare a growth, a GaAs (100) substrate is lapped to the proper thickness; etched in 1:3:4, $HF:HNO_3:H_2O$ for 30 s; and rinsed in deionized water. The etched wafer is placed into a recess in part b, then part c is placed on part b, thus holding the GaAs wafer in place. Part d is then placed on the b and c assembly so that the wafer is located under the venting hole between two of the melt chambers. Next, the melt chambers are charged with an etched polycrystalline slab of undoped GaAs. Then, the proper amount of Ga, Al and dopant are loaded into the chambers. Assembled parts b, c and d are loaded into part a, and the entire assembly is placed into the quartz containing vessel. The apparatus is generally vacuum baked at 300°C for about 30 minutes to remove any absorbed water from the carbon parts. After back filling with palladium diffused hydrogen and continuous flushing, the apparatus is brought to the crystal growth temperature using a resistance furnace having a uniform temperature profile and controlled to ±0.1°C. The temperature is held constant for about 1 hour to allow each melt to achieve solid-liquid equilibrium. Then, the GaAs wafer is rotated into a position under one of the melt chambers, thus bringing the wafer into contact with one of the melts. At this point, crystal growth can be initiated by one of several procedures. In one method, the temperature can be lowered at a programmed rate, producing growth by the normal liquid phase epitaxy mode of growth. A procedure modification is to rotate the substrate to a position between the melt chambers. This procedure transfers and confines a small volume of melt from the chamber under which the wafer had been positioned. Next, the normal liquid phase epitaxy procedure is used. However, by using small melt volumes, the growth thickness and uniformity can be controlled better than the growth thickness uniformity obtained using larger melt volumes for the same cooling rates and total temperature span.

Alternatively, growth can be initiated by maintaining the temperature constant and rotating the substrate back and forth between two melts of different Al concentrations. Growth by the latter method (ISM) occurs when a small volume of a Ga-rich solution of GaAlAs, at solid-liquid equilibrium, is isothermally mixed with a GaAlAs melt at solid-liquid equilibrium and having a different composition than the first solution. The mixing of the two solutions results in a new supersaturated solution. If a GaAs or $Ga_{1-x}Al_xAs$ single crystal solid-liquid interface is located near the solution mixing interface, $Ga_{1-x}Al_xAs$ epitaxial layers will deposit. The degree of supersaturation and, hence, the amount of growth, increases with the volume of transferred melt. In the previous apparatus, this volume was 0.2 $cm^3$ and it could not be changed easily. However, the transfer volume of the present apparatus is proportional to the thickness of carbon spacer that is used. Furthermore, the spacer design permits smaller transfer

volumes than before. For example, a spacer as thin as 0.025 cm, or 0.037 $cm^3$ in volume, can be used without the loss of the solid-liquid interface during transfer. Thus, layers grown with this spacer are about 0.2 times as thick as the layers grown in the previous apparatus, with the other growth conditions constant.

The apparatus can be operated in yet another mode which can be important for some applications. By leaving out part c, the carbon spacer, and adjusting the position of substrate surface to be 0.001-0.002 cm below the surface of part b, the melt can be wiped away from the substrate during transfer between melt chambers.

### 3.1.2 TARGET LED STRUCTURE

The target $Ga_{1-x}Al_xAs$ LED structure for this program was described in Section 2 and shown in Figure 2-3. This structure is called the minimum band gap (MBG) structure, because all of the $Ga_{1-x}Al_xAs$ outside the planar region were radiative recombination occurs has an energy band gap larger than that of the action region. The consequence of this is that the peak energy of the light emitted in the active layer is less than the absorption edge of the material outside the active layer; hence, light produced in the active layer will not be strongly absorbed outside the active layer. Thus, if all the surfaces of a not quite parallelepiped structure, except one with an area equal to the surface area of the active layer, are coated with a good reflective coating, $T_1 = .01$, then an expression can be derived which will approximately relate external efficiencies to internal efficiencies. (Reference 16)

The light power absorbed in the active region of the device is:

$$\rho \, v_g \, V \, \alpha$$

where

$\rho$ = energy density (joules/$cm^3$)

$v_g$ = group velocity of light (cm/s)

$V$ = volume of active layer ($cm^3$)

$\alpha$ = absorption constant in active layer; $\approx 100\ cm^{-1}$

flux out of surface is:

$$1/4 \, \rho \, v_g \, T_2$$

where $T_2$ = transmissivity of window area flux lost to reflective coated surfaces = $0.1\ cm^{-1}$

$$1/4 \, \rho \, v_g \, T_1$$

where $T_1$ = transmissivity of coated area $\approx 0.01\ cm^{-1}$

$$\frac{\text{power out surface}}{\text{total light power}} = \frac{1/4\ \rho\ v_g\ T_2\ A_1}{1/4\ \rho\ v_g\ T_2\ A_1 + \rho\ v_g\ V\ \alpha + 1/4\ \rho\ v_g\ T_1\ A_2}$$

where

$A_1$ = area of surface = area of active region

$A_2$ = area of coated surface

then

$$V = L \times A_1$$

where

L = thickness of active region $\approx 1\mu$

The final result is:

$$\eta_{ext} \cong \eta_{int} \left( \frac{T_2}{T_2 + XT_1 + 4\,\alpha\,L} \right)$$

where

$$\eta_{int} = \frac{\text{photons/s}}{\text{electron/s}}$$

X = area of reflective coating ÷ area window $\approx 2$

thus

$$\eta_{est} \approx 0.6\ \eta_{int}$$

For a diode emitting into air without the benefit of reflecting surfaces the external efficiency is not high. An estimate of that efficiency can be derived for purposes of growth evaluation. Consider an element of junction area, dA, which radiates isotropically such that the flux which passes through the cone between the angles $\theta$ and $\theta + \Delta\theta$ is

$$\frac{I_o}{2\pi} \cos\theta\, d\theta$$

where $I_o$ is the total radiant flux emitted by dA. The total flux emitted by dA toward the window is

$$\int_{\phi=o}^{\phi=2\pi} \int_{\theta=o}^{\theta=\frac{\pi}{2}} \frac{I_o}{2\pi} \cos\theta \sin\theta\, d\phi\, d\theta = \frac{I_o}{2}$$

The total flux falling within the core of the critical angle for total internal reflection is

$$\int_{\phi=0}^{\phi=2\pi}\int_{\theta=0}^{\theta_c} \frac{I_o}{2\pi} \cos\theta \sin\theta \, d\theta \, d\phi = I_o \frac{\sin^2\theta_c}{2}$$

Therefore, the fraction of the total radiation that could be emitted is

$$\frac{\sin^2\theta_c}{2}$$

or in the best case

$$\eta_{ext} \simeq \frac{\sin^2\theta_c}{2} \eta_{int}$$

If this structure were grown on an absorbing GaAs, and assuming all the light that is refracted at the window at an angle greater than critical angle is absorbed, then,

$$\eta_{ext} \approx (0.035) \eta_{int}$$

for diodes in which the area of the surface is much larger than the sum of the area of the side faces. When the Fresnel reflection coefficients are used in the analysis (Subsection 3.4) the external quantum efficiency is given by

$$\eta_{ext} \approx (0.025) \eta_{int}.$$

Thus, we have performance criteria for evaluating MBG structures grown on GaAs substrates.

Using this criteria of efficiency, the growth procedures were adjusted for the MBG structure on GaAs until $\eta_{ext} > 0.01$ was achieved.

### 3.1.3 RESULTS - MBG STRUCTURE ON GaAs

Table 3-1 shows a summary of the growth conditions and results of 10 MBG growths on GaAs substrates. The fourth column indicates the weight of Al added to a 5 g Ga melt. The letter p or n, above each number, indicates the conductivity type of each melt. These melts were doped with 1.5, 1.5, 3.5, and 200 mg of Zn, Zn, Te, and Sn respectively. It can be seen that efficiencies of >1% were achieved three times and that for most of those cases for which either the efficiencies were lower or the run failed, some parameter had been changed. It appears from Table 3-1 that changes in Al concentration, cooling rate, and growth temperature greatly affect quantum efficiencies. However, the manner in which changes in these parameters affect the electrical and optical properties is not yet understood and many more experiments must be performed in order to verify these effects. The composition profiles of an optimal MBG structure, P 160, is shown in Figure 3-2. The growth conditions of an optimal structure are listed in Table 3-2.

Table 3-1

MINIMUM BAND GAP ACTIVE REGION LED STRUCTURE ON GaAs

| Run No. | Orient. | Type | Al Weight per Melt (mg) | | | | Cooling Span per Melt (°C) | | | | Start Temp. | Upheat | Cool Rate (°C/min) | $\eta_{ext}$ |
|---|---|---|---|---|---|---|---|---|---|---|---|---|---|---|
| | | | 1 | 2 | 3 | 4 | 1 | 2 | 3 | 4 | | | | |
| | | | p | p | n | n | | | | | | | | |
| P 160 | 100 | p | 3.1 | 1.7 | 3.5 | 200 | 5 | 2[a] | 7 | - | 840 | -- | 0.1 | $1.4 \times 10^{-2}$ |
| | | | p | p | n | n | | | | | | | | |
| P 162 | 100 | p | 3.1 | 1.8 | 3.0 | 200 | 6 | 2[a] | 2 | - | 835 | -- | 0.1 | -- |
| | | | p | p | n | n | | | | | | | | |
| P 170 | 100 | p | 3.0 | 1.7 | 3.0 | 200 | 10 | 2 | 4 | - | 840 | -- | 0.1 | -- |
| | | | p | p | n | n | | | | | | | | |
| P 175 | 100 | p | 3.0 | 1.7 | 3.2 | 200 | 25 | 2 | 11 | - | 890 | 5°C melt | 0.17 | $0.4 \times 10^{-2}$ |
| | | | p | p | p | n | | | | | | | | |
| P 176B | 100 | p | 3.0 | 3.4 | 1.6 | 3.0 | 12 | 18 | 2 | 10 | 890 | 5°C melt | 0.17 | $1\text{-}2 \times 10^{-3}$ |
| | | | p | p | n | n | | | | | | | | |
| P 184 | 100 | p | 4.3 | 1.5 | 6.2 | 200 | 7 | 2[a] | 8 | - | 840 | -- | 0.17 | $1\text{-}2 \times 10^{-3}$ |
| | | | p | p | n | n | | | | | | | | |
| P 186 | 100 | p | 2.9 | 1.5 | 2.9 | 200 | 5 | 2[a] | 5 | - | 840 | -- | 0.1 | $1\text{-}2 \times 10^{-2}$ |
| | | | p | p | n | n | | | | | | | | |
| P 188[b] | 100 | p | 3.3 | 1.7 | 3.4 | 200 | 10 | 2 | 10 | - | 840 | -- | 0.17 | NA |
| | | | p | p | n | n | | | | | | | | |
| P 189[b] | 100 | p | 3.0 | 1.6 | 3.0 | 200 | 10 | 2 | 10 | - | 840 | | 0.17 | NA |
| | | | p | p | n | n | | | | | | | | |
| P 190[b] | 100 | p | 3.1 | 1.5 | 3.2 | 200 | 5 | 1 | 5 | - | 840 | | 0.1 | $1\text{-}2 \times 10^{-2}$ |

Notes:

a) Cooling done between melts with 0.020 inch span.
b) Melt wipe.

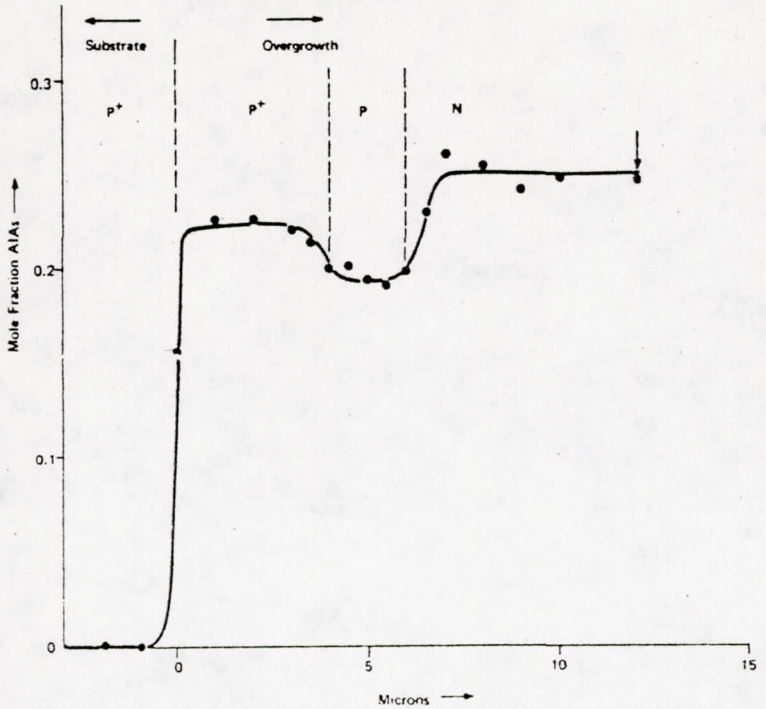


Note:
Composition profile of three layer electroluminescent diode structure. The arrow refers to the surface composition associated with melt quenching.

Figure 3-2. Composition Profile of P 160, an Optimal MBG Structure Grown on GaAs

Having established the growth conditions and composition profile which produce optimal LED structures on GaAs, the next step was to replace the GaAs substrate with GaP.

### 3.1.4 RESULTS - MBG STRUCTURES ON GaP

The first attempts to use the same growth conditions on GaP resulted in either no growth or, at best, poor growth. Table 3-3 lists the sequence of the experimental condition tried for the MGB on GaP. Runs 163 and 164 were attempts at achieving good growth at higher growth temperatures than those normally used. The growth characteristics were much improved. Finally a 5°C upheat, in the presence of the entire melt at a growth start temperature of 890°C, and etching the substrate with 1:1, $HCl:H_2O_2$ resulted in acceptable growth. However, the LED structure emitted light either weakly or not at all. An electron beam probe study of phosphorous contamination is shown in Figures 3-3 and 3-4 for two of these structures. It can be seen that the phosphorus contamination level is about 0.05 weight fraction near the GaP-$Ga_{1-x}Al_xAs$ interface, and that it is about one order of magnitude less in the active

Table 3-2

GROWTH SPECIFICATIONS FOR OPTIMAL LED STRUCTURE ON GaAs

| P 160 | |
|---|---|
| Substrate | (100) GaAs p-type p = $2X10^{19}$ |
| Layer 1 | $Ga_{0.78}Al_{0.22}As$<br>melt - 5g Ga; 0.0031g Al; 0.0015g Zn; excess GaAs<br>cooling span 5°C<br>cool rate 0.1°C/min |
| Layer 2 | $Ga_{0.81}Al_{0.19}As$<br>melt - 5g Ga; 0.0017 Al; 0.0015g Zn; excess GaAs<br>cooling span - 2°C between melts with 0.020 inch spacer<br>cool rate 0.1°C/min |
| Layer 3 | $Ga_{0.75}Al_{0.25}As$<br>melt - 5g G; 0.0035g Al; 0.0035 Te; excess GaAs<br>cooling span - 7°C<br>cool rate 0.1°C/min |
| Layer 4 | Growth termination melt.<br>5g Ga; - 0.200g Al |

## Table 3-3

## MINIMUM BAND GAP ACTIVE REGION LED STRUCTURES ON GaP

| Run No. | Orient. | Type | Al Weight per Melt (mg) | Cooling Span per Melt (°C) | Start Temp. | Upheat | Cool Rate (°C/min) | $\eta_{ext}$ |
|---|---|---|---|---|---|---|---|---|
| | | | 1 2 3 4 | 1 2 3 4 | | | | |
| | | | p p n n | | | | | |
| P 163 | 111B | p | 3.0 1.4 3.2 200 | 8 3 2 – [a] | 890 | — | 0.1 | -- |
| | | | p p n n | | | | | |
| P 164 | 111B | p | 3.0 1.7 3.3 200 | 9 2 3 – | 890 | — | 0.1 | -- |
| | | | p p n n | | | | | |
| P 166 | 111B | n | 3.3 1.7 3.5 200 | 10 3 4 – | 890 | 5°C melt | 0.1 | -- |
| | | | p p n n | | | | | |
| P 168 | 111B | p | 3.2 1.6 3.5 200 | 11 3 5 – | 890 | 5°C melt | 0.1 | -- |
| | | | p p n n | | | | | |
| P 171* | 111B | p | 3.4 1.5 3.5 200 | 15 3 6 – | 890 | 5°C melt | 0.1 | -- |
| | | | p p n n | | | | | |
| P 172 | 111A | p | 3.5 1.6 3.3 200 | 13 2 7 – | 890 | 5°C melt | 0.1 | -- |
| | | | p p n n | | | | | |
| P 174* | 111B | p | 3.4 1.6 3.0 200 | 30 2 10 – | 890 | 5°C melt | 0.17 | -- |
| | | | p p p n | | | | | |
| P 176A | 111B | p | 3.0 3.4 1.6 3.0 | 12 18 2 10 | 890 | 5°C melt | 0.17 | $0.6 - 1.5 \times 10^{-3}$ |
| | | | p p p n | | | | | |
| P 179* | 111B | p | 3.1 3.2 1.5 10.0 | 10 10 1 5 | 890 | 5°C spacer[b] | 0.17 | $0.4 - 0.7 \times 10^{-3}$ |
| | | | p p p n | | | | | |
| P 182 | 111B | p | 3.5 3.1 1.6 10.0 | 10 9 1 5 | 840 | 5°C spacer[b] | 0.17 | $0.3 - 0.7 \times 10^{-4}$ |
| | | | n p p p | | | | | |
| P 187 | 100 | n | 12 - 16 - | 6 1 2 – | 840 | -- | 0.1 | N.G. |
| | | | n n p p p | | | | | |
| P 192[c] | 100 | n | 10 10 - 10 - | 3 5 1 2 $\frac{3}{2}$ | 840 | -- | 0.1 | N.G. |
| | | | p p p n | | | | | |
| P 194 | 031 | p | 3.2 3.2 1.6 3.6 | 6 4 1[a] 1 | 900 | 5°C spacer[b] | 0.1[d] | N.G. |
| | | | p p p n | | | | | |
| P 196 | 111 | p | 3.0 3.1 1.5 3.0 | 5 4 1[a] 4 | 855 | 5°C spacer[b] | 0.1[d] | N.G. |
| | | | n n p p p | | | | | |
| P 197 | 111 | p | 10 10 - 10 - | 4 4 2 2 $\frac{3}{2}$ | 845 | 2°C melt | 0.1 | N.G. |
| | | | p p p n | | | | | |
| P 198*[c] | 111 | p | 3.4 3.4 1.6 3.3 | 5 4 1 5 | 840 | 5°C melt | 0.1 | $4 - 6 \times 10^{-4}$ |
| | | | n p p p | | | | | |
| P 202 | 111 | n | 12.2 - 16.1 - | 10 1 2 1 | 855 | 5°C melt | 0.1 | N.G. |
| | | | n n p p | | | | | |
| P 210 | 100 | n | 6.2 6.2 - 6.2 | 10 4 1 5 | 880 | 5°C melt | 0.17 | N.G. |

Notes:

a) Cooling done between melts in .020 inch spacer
b) .020 inch spacer
c) Melt wipe
d) Furnace up during shut down
* Electron beam profile

Reproduced from best available copy.

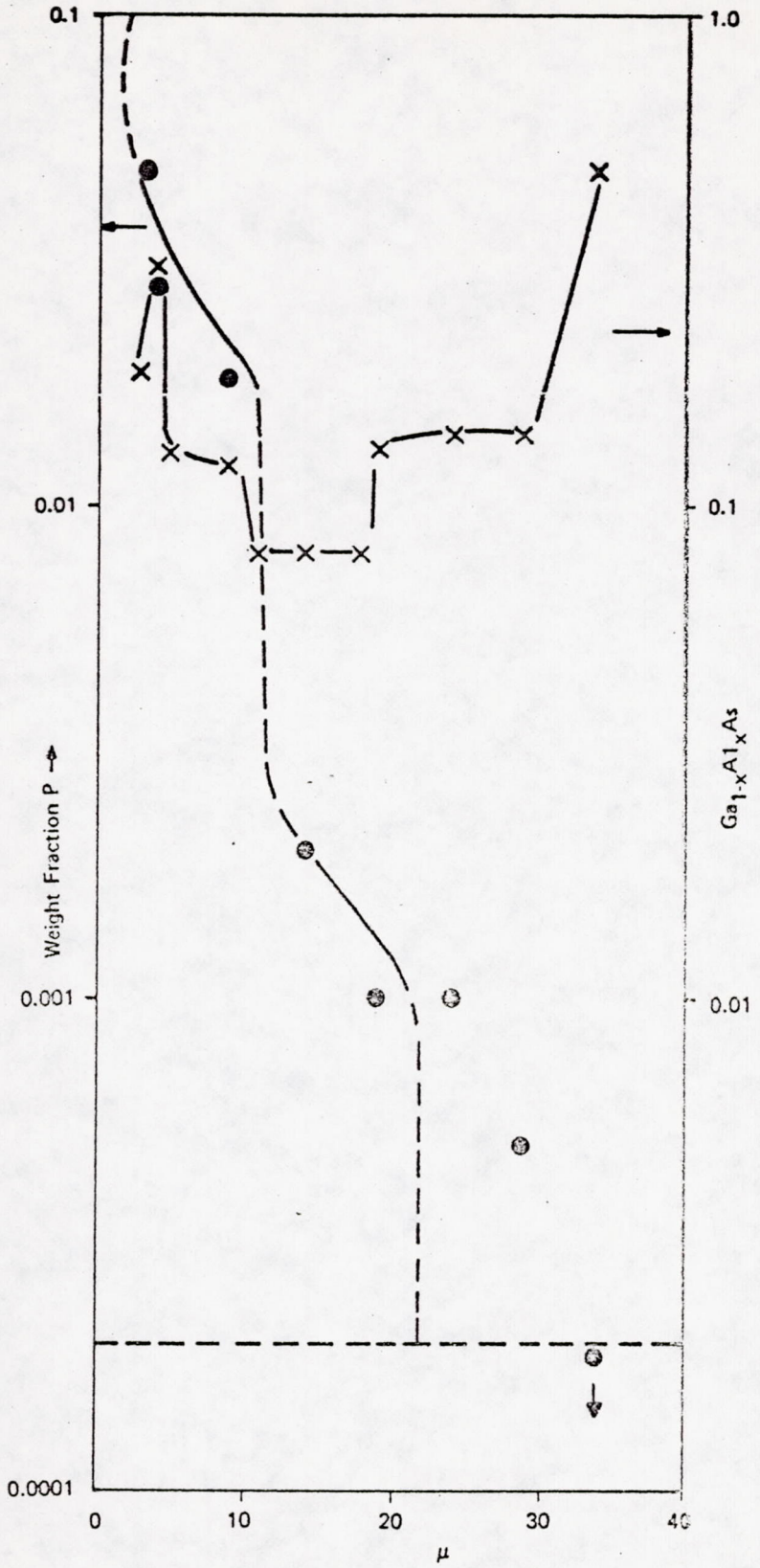


Figure 3-3. Electron Beam Profile of Al and P for P 171

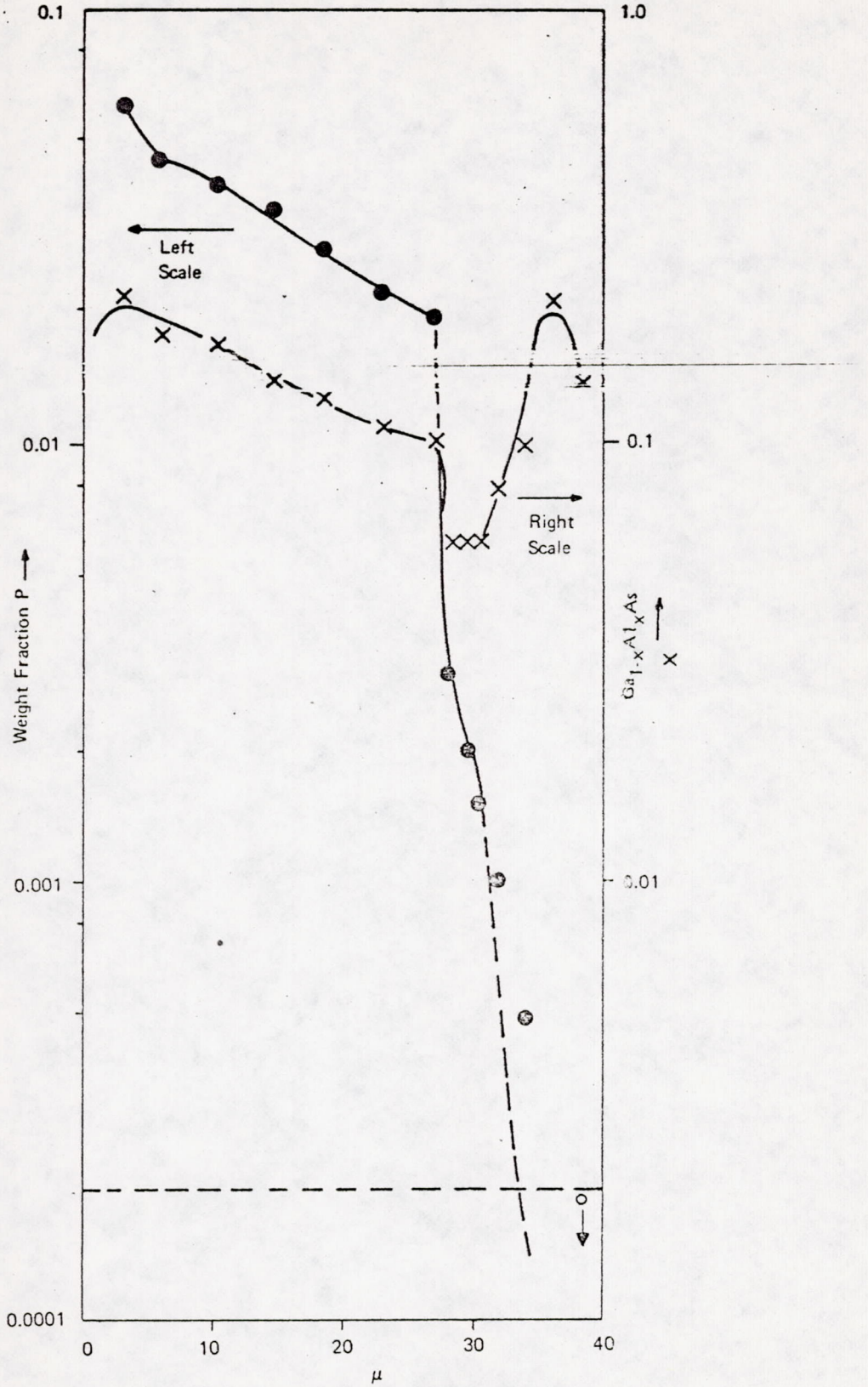


Figure 3-4. Electron Beam Profile of Al and P for P 174

layer. It was concluded that, even though appreciable phosphorous contamination might be necessary to initiate good growth, its presence in the active layer might be detrimental for high quantum efficiencies. This conclusion was further supported by the results of P 176A and P 176B, where growth occurred simultaneously on a GaP and GaAs substrate. For this run, melt 2 duplicated melt 1 in order to "clean up" the phosphorous contamination before growing the active layer from melt 3. This run was the first to show measureable light output of the MBG structure on a GaP substrate. The low quantum efficiencies of the structure were comparable for both substrates. However, the current-voltage characteristics were entirely different. Figure 3-5 shows a typical I-V characteristic for the GaAs substrate, while Figure 3-6 shows these properties for the GaP substrate. It was later shown that for the GaP substrate there is an additional nonlinear resistance in series with the LED due either to poor ohmic contact to the GaP, or to some sort of heterojunction barrier between the GaP and $Ga_{1-x}Al_xAs$.

It was still believed, at the time, that the low efficiencies and peculiar I-V characteristics were related to residual phosphorous contamination, and attempts were made to further reduce the phosphorous. Therefore, for P 179 the 5°C upheat was carried out in the presence of a limited volume of melt 1. This was done by rotating the substrate and a 0.020 inch spacer full of melt 1 to an in-between-melt chamber position prior to the 5°C upheat. The result of this is shown in Figure 3-7. Notice that near the GaP-$Ga_{1-x}Al_xAs$ interface, the phosphorous level is about 0.005, compared with the 0.05 level for an entire melt upheat. In the active region, the phosphorous level dropped to below the detection limit of 0.0003. However, there was no improvement in quantum efficiencies over previous runs with higher phosphorous levels. Indeed, P 182, which was grown at 840°C with even less phosphorous, resulted in even lower quantum efficiencies. The metallurgical features of a typical MBG growth on GaP are shown in Figure 3-8. The surface features can be seen in Figure 9a and the features of the $Ga_{1-x}Al_xAs$ layers are seen in Figure 9b.

Next, several experiments were tried to produce growth surfaces other than the (111). (100) and (031) were tried without success. For both of these surfaces the growths were very nonuniform. An example of the surface for a (100) growth is shown in Figure 3-9. It is not certain what the reasons are for this roughness; however, later experiments, in which the temperature gradient across the solid-liquid interface was increased, improved the smoothness for (100) growths on GaP. This is evidence for a strong dependence of constitutional supercooling effects on growth direction.

Concurrent with the MBG experiments, a program was begun to grow $Ga_{1-x}Al_xAs$ layers with graded compositions on GaP substrates. The layers were grown so that X for $GA_{1-x}Al_xAs$ decreased in a linear fashion from the GaP interface to the surface of the growth. A p-n junction formed parallel to the GaP interface, anywhere along the growth axis, shows that when light emitted at the junction has a direction component towards the GaP substrate it is not strongly absorbed. This structure is a trade off of the external quantum efficiency for ease and relative foolproofness of fabrication. The experiments on this structure are listed chronologically in Table 3-4. The first successful LED structure was P 180. It was fabricated by first growing a graded n-type layer on an n-type GaP substrate, followed by a Zn diffusion to form the p-n junction. Even though the quantum efficiencies were low, the I-V characteristics were much improved over all of the MBG on GaP diodes. This was the first evidence that the I-V properties of the MBG on GaP structures were related to either contact problems or a heterojunction barrier between p-GaP and P-$Ga_{1-x}Al_xAs$, instead of phosphorous contamination.



Reproduced from best available copy.

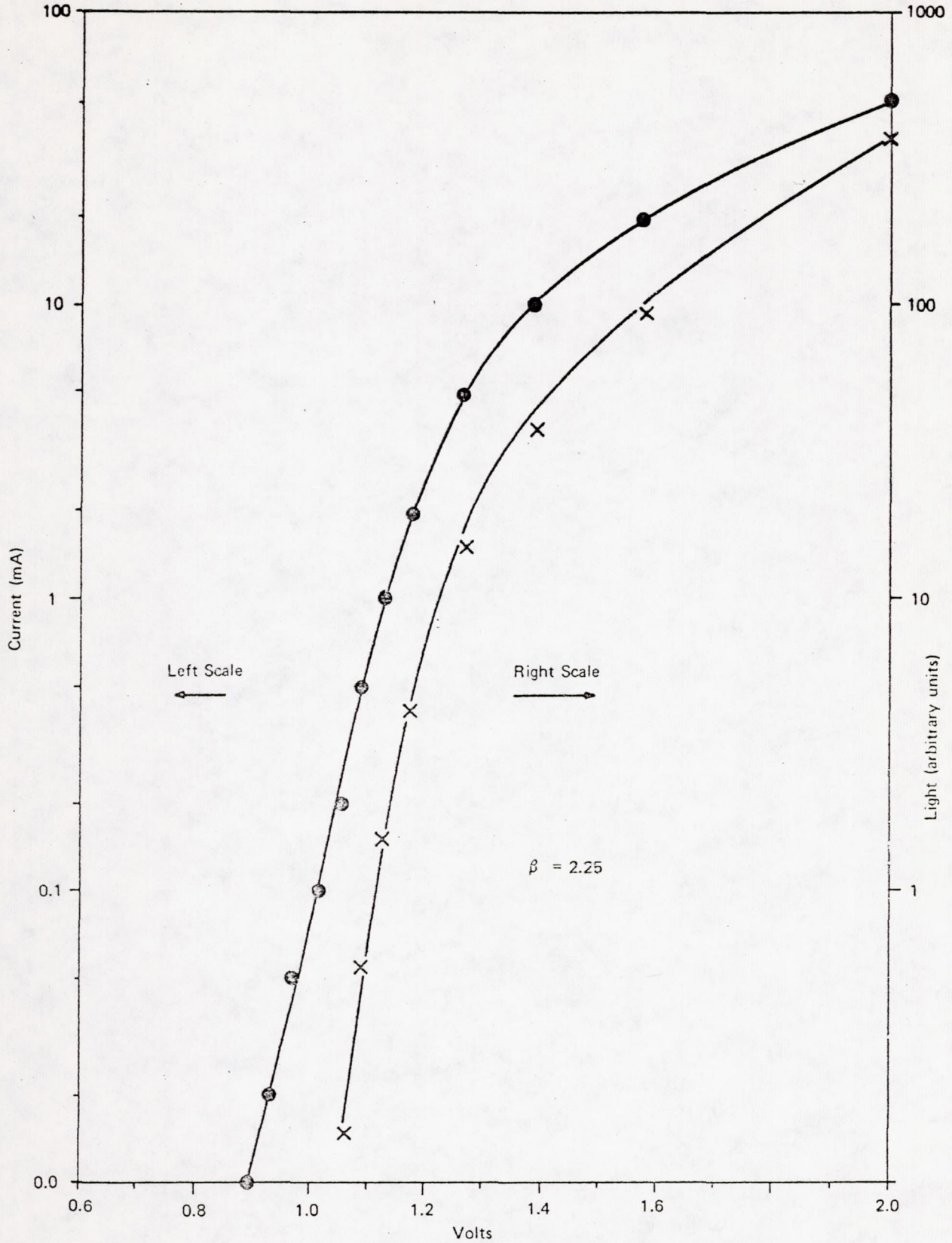


Figure 3-5. Light Output and Forward Current vs Voltage for P 176B

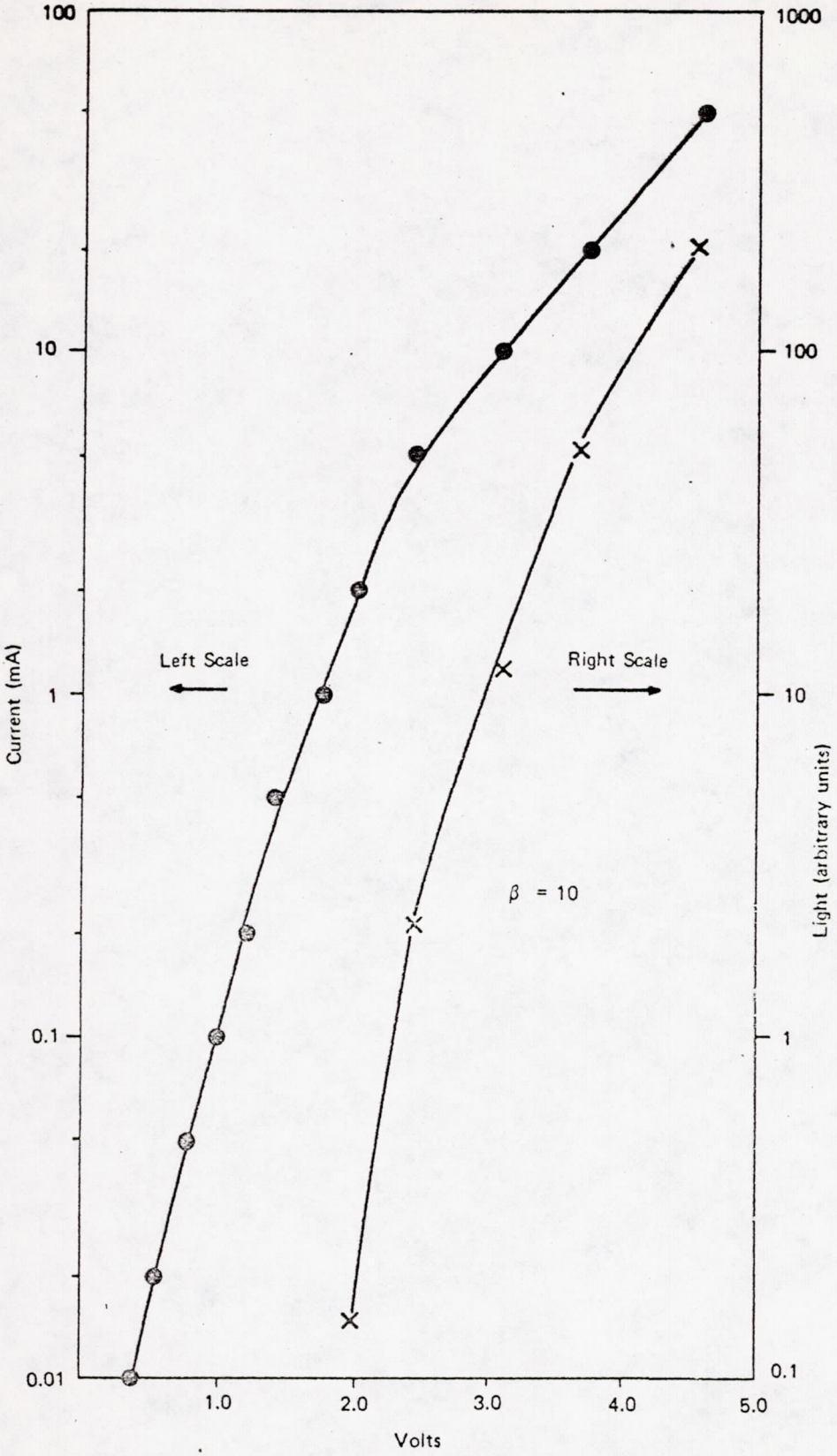


Figure 3-6. Light Output and Forward Current vs Voltage for P 176B

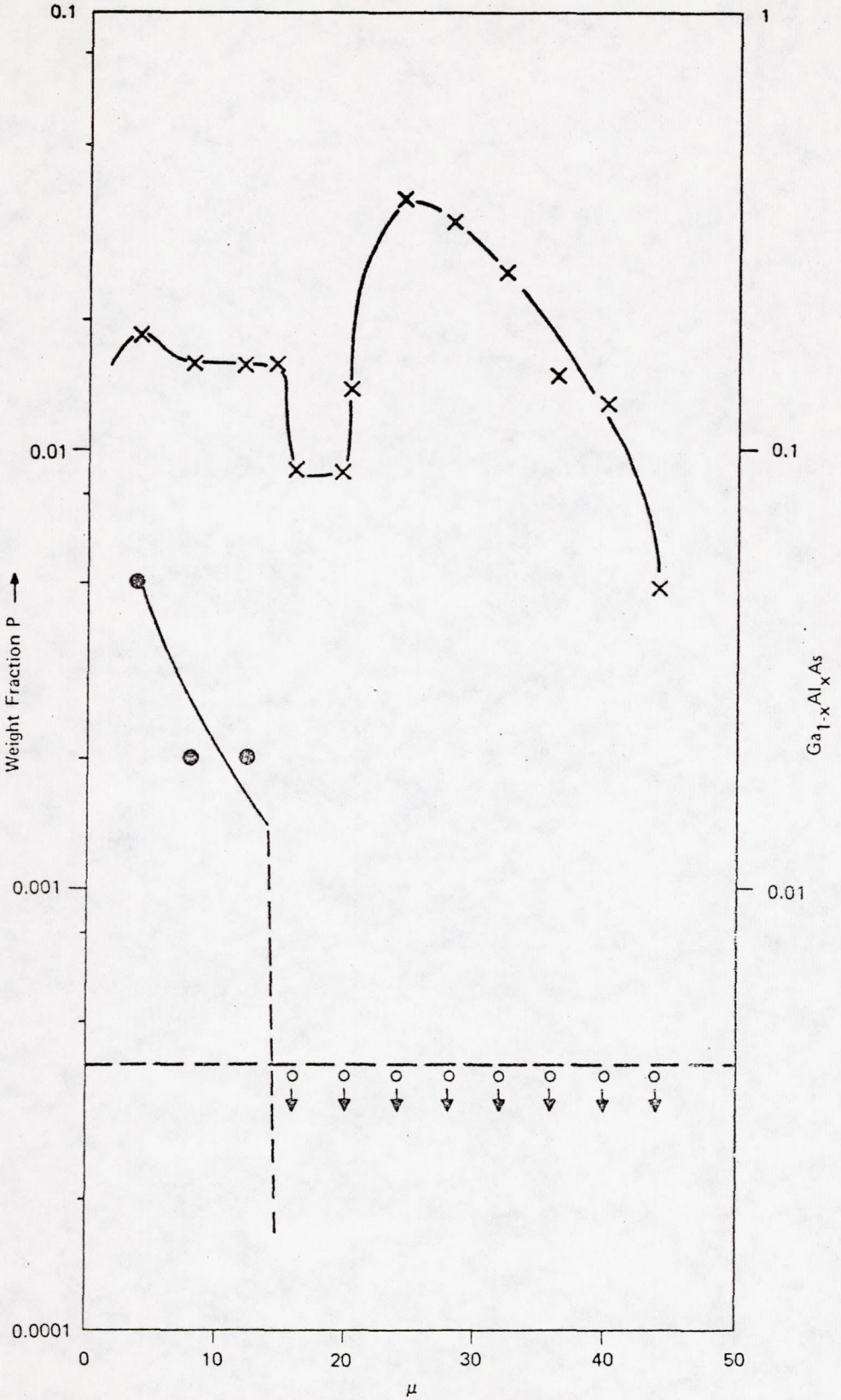


Figure 3-7. Electron Beam Profile of Al and P for P 179

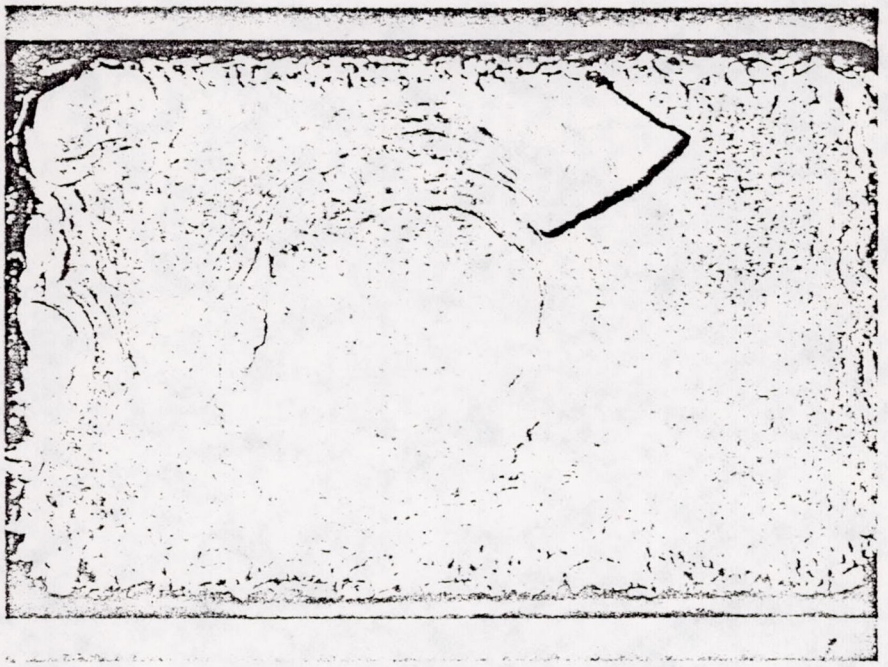

a. Surface

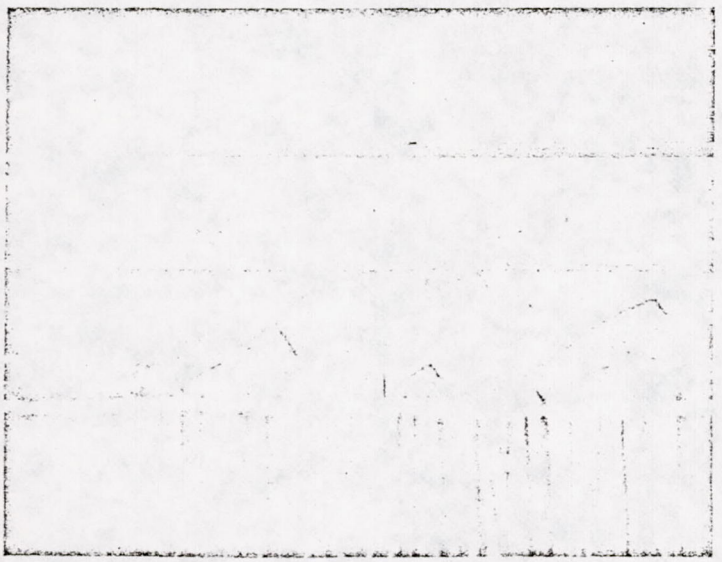

b. (110) Cleavage Face Along Growth Axis

Figure 3-8. Photomicrographs of a Typical MGB Structure on GaP

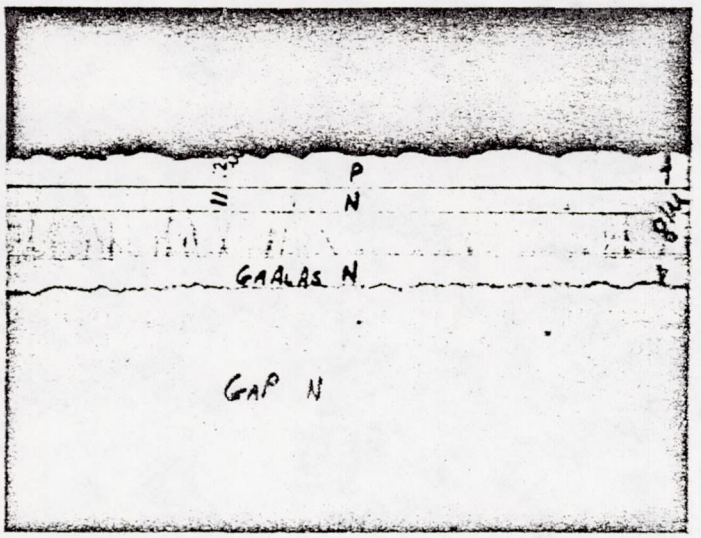


Figure 3-9. Surface of Growth on (100) GaP Surface

The composition and phosphorous contamination profiles of P 180 are shown in Figure 3-10. The p-n junction is located at about the 30$\mu$ position where the phosphorous is below the detection limit.

### 3.1.5. SURFACE MORPHOLOGY AND IMPERFECTION

One of the goals in the growth experiments was to obtain LED structures whose surfaces were suitable for photolithographic processing with photoresists. Most of the surfaces as grown after run P 176 meet this requirements. However, attempts to etch away surface layers, formed during growth termination, resulted in severe roughening. An example of this is shown in Figure 3-11. It is not certain, at present, what causes this roughing, but the best guess is that it is stacking faults or microcracks resulting from the fast cooling rates and strain associated with the termination layers. In some cases microscopie cracks, and even separation of the layer from the substrate, have been observed, i.e., P 196 - see Figure 3-12. These cases are usually associated with conditions that produce the largest strains, i.e., low phosphorous contamination at the interface and large growth rates of the termination layer. The exact conditions leading to these imperfections will be the subject of a future investigation.

Table 3-4

$Ga_{1-x}Al_xAs$ LAYERS WITH GRADED COMPOSITION ON GaP

| Run No. | Orient. | Type | Al Weight per Melt (mg) | | | | Cooling Span per Melt (°C) | | | | Start Temp. | Upheat | Cool Rate (°C/min) | $\eta_{ext}$ |
|---|---|---|---|---|---|---|---|---|---|---|---|---|---|---|
| | | | 1 | 2 | 3 | 4 | 1 | 2 | 3 | 4 | | | | |
| P 177 | 111B | n | n 3.8 | n 1.8 | n 200 | - | 15 | 7 | - | - | 895 | 5°C melt | 0.17 | N.G. |
| P 180[a]* | 111B | n | n 4.2 | n 3.0 | n 1.9 | n 200 | 9 | 9 | 9 | - | 890 | 5°C melt | 0.17 | $1\text{-}3 \times 10^{-4}$ |
| P 191 | 111B | n | n 4.2 | n 3.2 | n 2.0 | n-p 1.5 | 8 | 8 | 8 | 1&2[b] | 895 | 5°C melt | 0.17 | $4.6 \times 10^{-3}$ |
| P 203 | 111B | n | n 4.1 | n 3.1 | n 2.0 | n-p 1.5 | 10 | 9 | 9 | 1&4 | 870 | 5°C melt | 0.17 | $1.1 \times 10^{-2}$ |
| P 207 | 111B | n | n 4.0 | n 3.1 | n 2.1 | n-p 1.6 | 10 | 9 | 9 | 1&8 | 900 | 5°C melt | 0.17 | -- |
| P 208 | 100 | n | n 4.0 | n 3.0 | n 2.1 | n-p 1.5 | 10 | 8 | 8 | 1&8 | 900 | 5°C melt | 0.17 | N.G. |
| P 209 | 100 | n | n 4.0 | n 3.0 | n 2.3 | n-p 1.7 | 7 | 8 | 5 | 1&5 | 900 | 5°C melt | 0.17 | $5.5 \times 10^{-2}$** |
| P 215 | 100 | n | n 4.2 | n 3.2 | n 2.0 | n-p 1.4 | 10 | 8 | 5 | 1&5 | 900 | 5°C melt | 0.17 | N.G. |

Notes:

a) p-n junction formed by Zn diffusion
b) Cooled 1°C with Te doping then 2°C for Zn & Te doping
* Electron Beam Profile
** GaP dome structure

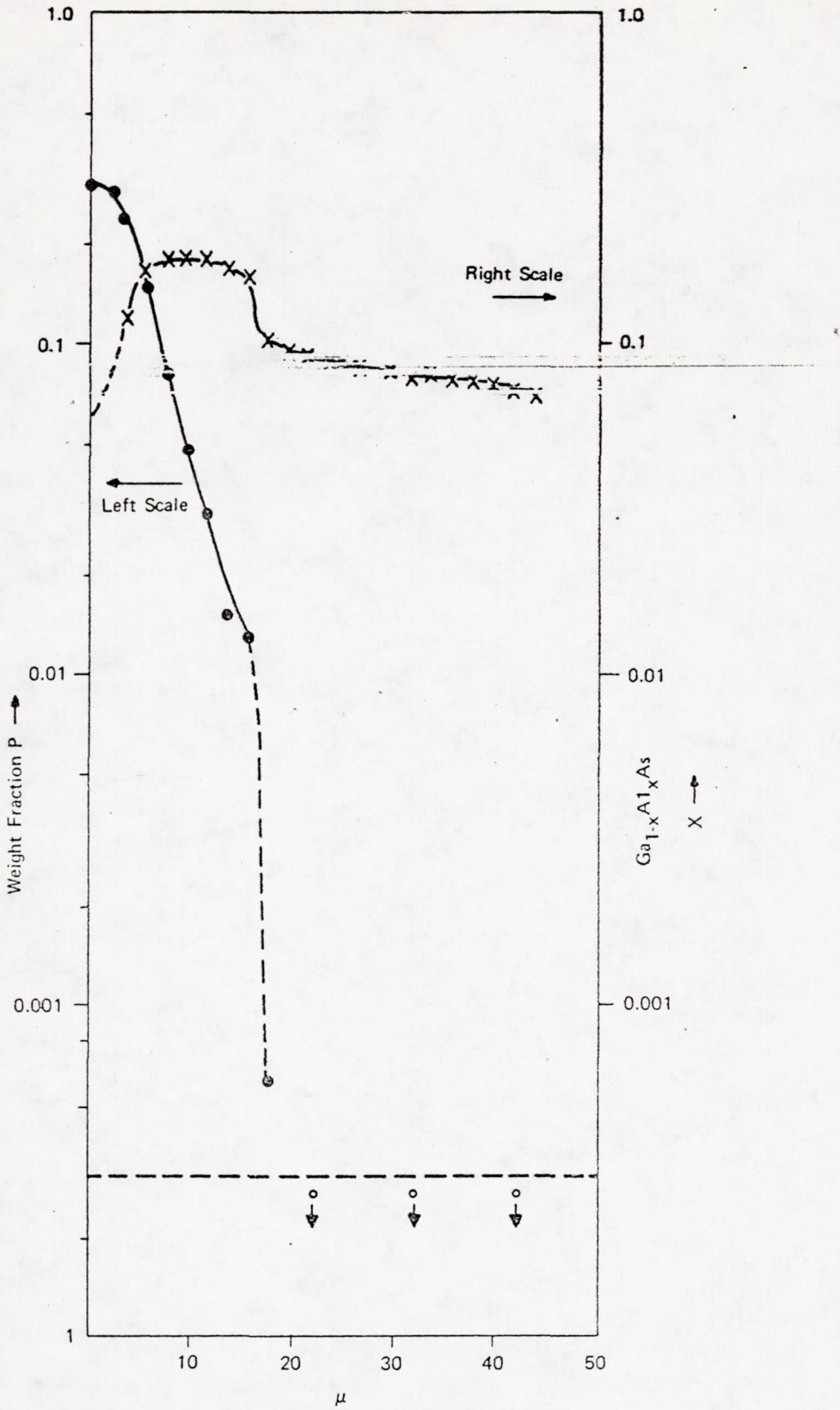


Figure 3-10. Electron Beam Profile of P 180

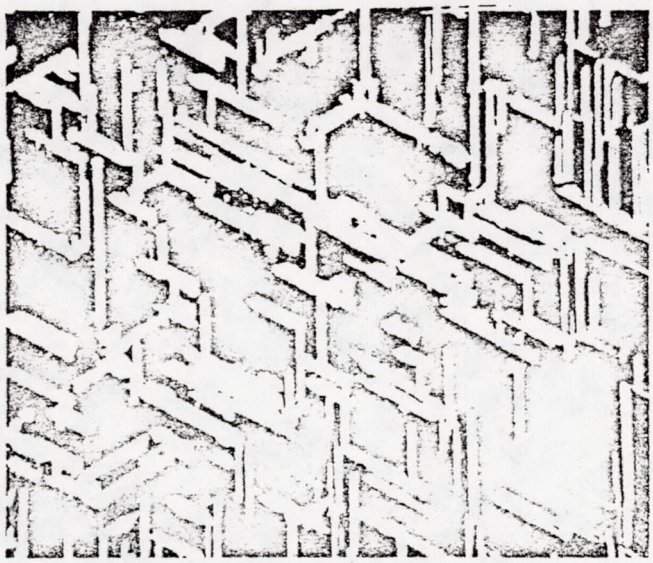

Figure 3-11. Surface of P 180 after HCl Removal of Surface Layer

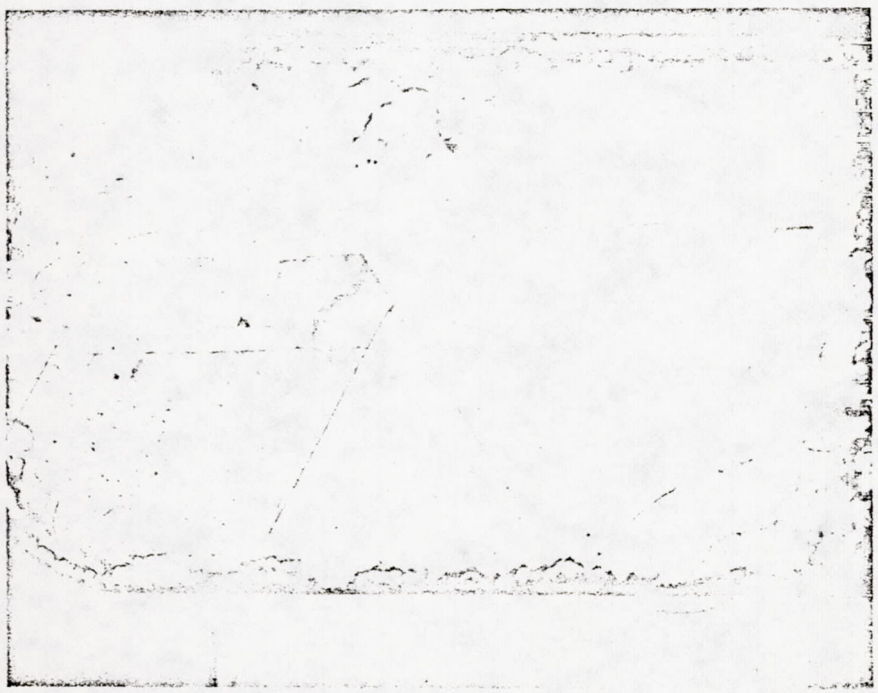

Figure 3-12. Cracked Layer of P 196

### 3.1.6 BACK-CONTACT LED FABRICATION

Another reason for using GaP substrates was to facilitate both n- and p- type electrical contacting on the same face of the diode structure, thus providing a GaP surface free from absorbing contacts. A technology for accomplishing a so-called back contact structure was developed at the IBM facility at Owego, N. Y. under the direction of R. Lynch. This technology was tried on P 203 (see Table 3-4) and produced units with efficiencies just over 1%. An example of such a structure is shown in Figure 3-13. Figure 3-13a shows the GaP face of a diode fabricated from P 203 under incident illumination. Figure 3-14b shows the same diode, viewed through an IR image converter, when forward biased. The light area of the photomicrograph is the area of the active layer which has etched into a mesa-like structure. Another important result of this experiment was the discovery that the I-V characteristics of the back contacted structure are normal, and that, presumably, the MGB structures on GaP would have normal I-V characteristics if contacted in this manner. This possibility will be studied in future investigations.

Back contacted mesa structures were fabricated on a MBG growth on a GaP substrate. This run, P 219, not shown on Table 3-3 is similar to P 198 except for the use of an updoped n-type substrate and no melt wiping. The mesa area and, hence, junction area, was $6.3 \times 10^{-4} cm^2$. As before, the efficiencies were measured, without ohmic contacts, using metal points to make electrical contact. Also, only the light emitted through the GaP surface parallel to the active layer was collected by the Si cell. Efficiencies up to 2.7% into air were measured for currents up to 30 mA. This exceeds that predicted in Subsection 3.1.2, but the approximation used in Subsection 3.1.2 fails because the surface is not much larger than the sum of the area of the side faces. The results here compare favorably with previous authors.[8]

### 3.1.7 SUMMARY

Experiments on growth of MBG structures of $Ga_{1-x}Al_xAs$, on both GaP, and GaP and GaAs, and the growth of a graded layer of $Ga_{1-x}Al_xAs$ on GaP have demonstrated the usefulness of GaP substrates for improving external quantum efficiencies of LEDs. Several undesirable results were obtained during the experiments, notably on occasional layer cracking due to large strains, and a non-linear impedance associated with either electrical contacting of p-type GaP or a barrier between p-type GaP and p-type $Ga_{1-x}Al_xAs$. Thus far, external quantum efficiencies have been obtained on domed shaped devices.

### 3.1.8 FUTURE STUDIES

Since most of the better efficiency results have occurred towards the end of this investigation, it is obvious that many aspects of the MBG growths on GaP will have to be studied before practical devices can be fabricated in a reproducible manner. There are a few studies, however, which deserve high priority considerations:

1) The causes and the elimination of layer cracking and surface roughness
2) Establishing growth condition for (100) surface growth
3) Further optimization of internal quantum efficiencies

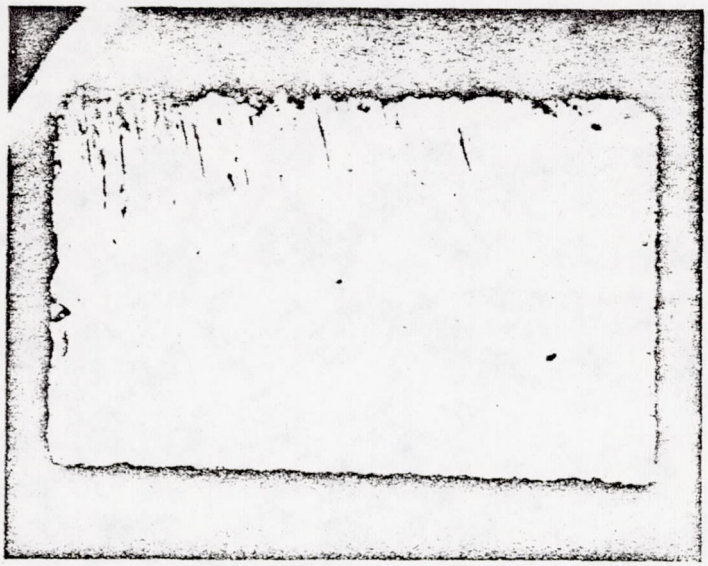

a. Incident Illumination

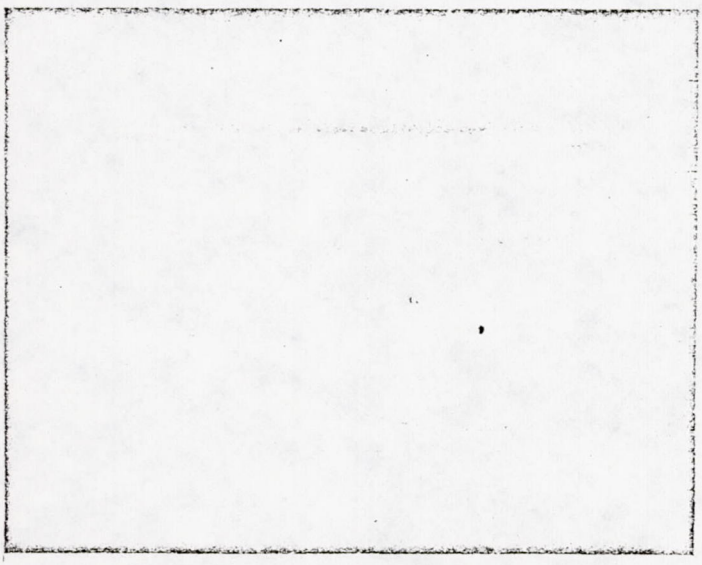

b. Forward Biased

Note: View from GaP face.

Figure 3-13. Photomicrograph of a Back Contacted Graded $Ga_{1-x}Al_xAs$ Layer Grown on GaP - Run P 203

Once these studies have been successfully conducted, it should be possible to move onto the work which will optimize optical coupling, electrical contacting, and life testing.

## 3.2 METAL-GaAlAs CONTACTS AND CONTACT RESISTANCE

### 3.2.1 INTRODUCTION

All the data presented in this section were obtained from $Ga_{1-x}Al_xAs$ films grown by liquid phase epitaxy on single crystal GaAs substrates. N-type $Ga_{1-x}Al_xAs$ was grown on p-type Czochralski grown GaAs substrates obtained from Bell and Howell. The p-type substrate had the following characteristics: carrier concentration, P, = $9.7 \times 10^{18}/cm^3$; mobility, u = 130 $cm^2/Vs$; and resistivity = $7.8 \times 10^{-3}$ ohm cm. P-type $Ga_{1-x}Al_xAs$ was grown on n-type Czochralski grown GaAs, also obtained from Bell and Howell, whose characteristics were typically; $n = 1 \times 10^{18}/cm^3$, u = 2900 $cm^2/Vs$, and = $2.4 \times 10^{-3}$ ohm cm.

For the purpose of studying the several different parameters in the films, a large number of crystals (of varying aluminum concentrations and varying degrees of thickness) were epitaxially grown. The aluminum concentrations in the films were obtained by electron-microprobe techniques. The thickness of the epitaxially grown crystals were obtained by means of microscopy methods. All epitaxial layers of $Ga_{1-x}Al_xAs$ were grown on the (100) set of planes of GaAs.

Over the period during which this work was accomplished, several different metals and alloys were employed as the contacting material. Among these were gold, silver, indium silver, aluminum, gold-zinc, and gold-germanium-nickel. Of these materials, the gold (96%)-zinc (4%) proved to be the best contacting material for the p-type $Ga_{1-x}Al_xAs$ and the Au (83.81%)-Ge (11.43%)-Ni (4.76%) the best for the n-type $Ga_{1-x}Al_xAs$. Consequently, the contact resistance, as a function aluminum content, carrier concentration, and resistivity, will be presented for these latter two alloys.

### 3.2.2 APPLICATION OF METALLURGY

Two methods were employed to place the desired metallurgy on the $Ga_{1-x}Al_xAs$ surface. To accomplish this end, appropriate masks were fabricated to give the desired pattern. For contact resistance measurements, the masks comprised a square array of holes of various diameters (6, 3, 1-1/2, and 3/4 mils). The holes were arranged in columns of equal diameters (four holes per column). The sequence of the four columns of holes was repeated on the mask to give complete coverage over the crystal (eight arrays per mask). Hall masks were also fabricated to give the standard Hall configuration for making dc Hall and resistivity measurements.

The two methods used for applying the metallurgy in these experiments were:

1) Placing the desired mask in contact with the wafer and placing the combination on a holder (capable of being electrically heated), which is then placed in the vacuum system and evacuated to approximately $10^{-5}$ torr. The metallurgy is then evaporated through the desired holes in the pattern.

2) Placing the wafer on the above mentioned holder and placing in the vacuum system. The system again evacuated to approximately $10^{-5}$ torr. In this case, the whole surface is covered with metallurgy. From this step on, photo resist techniques employing masking and subtractive etching are used to produce the desired patterns.

Experimental evidence (regarding contact resistance) has shown that the best results were obtained, for the deposition of AuZn on p-type $Ga_{1-x}Al_xAs$, when the substrate temperature was held at 250°C for the deposition of the metallurgy. In the case of the deposition of AuGeNi on n-type material, the best temperature for the substrate during the evaporation was 185° C.

The thickness of the evaporated AuGeNi layer was measured as 2200 Å; that of the AuZn was 1100 Å.

The sintering operation for both AuZn on p-type material and AuGeNi on n-type material was carried out at approximately 480°C. In a number of experiments, the time of sintering was varied from 5 to 20 minutes, in steps of 5 minutes. There was very little difference in the magnitude of the contact resistance for a sample sintered at 480°C for 10 minutes, and one sintered at the same temperature for 20 minutes.

Sintering was carried out in a forming gas environment.

### 3.2.3 EXPERIMENTAL

Contact resistance measurements were made using two different techniques. The first technique was a modification of a technique developed by Hooper and Sharif[12]. The second technique used is one similar to that reported by L. E. Terry[13]. Both techniques yield values for the specific resistance which were within 2% of each other.

All Hall measurements were made using standard dc techniques. Hall measurements were made on the same material used to make the contact resistance measurements.

### 3.2.4 DISCUSSION

The value of the contact resistance versus carrier concentration for AuGeNi on n-type $Ga_{1-x}Al_xAs$ and for AuZn on p-type $Ga_{1-x}Al_xAs$ is shown in Figures 3-15 and 3-16 respectively. To achieve the values of the specific contact resistance illustrated in these two figures, it was necessary to exercise great care in the preparation of the surfaces and to maintain surfaces that were free of contamination. Also, care was taken that the surfaces not be exposed for any length of time to air, lest oxides be formed. Failure to maintain good surface conditions would result in a larger specific contact resistance than shown in Figures 3-14 and 3-15.

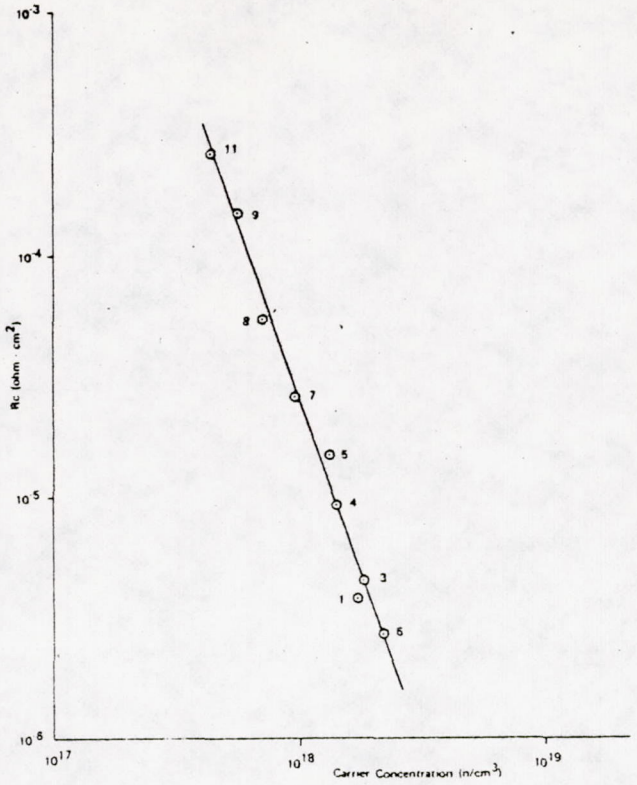


Figure 3-14. Specific Contact Resistance of AuGeNi on N type $Ga_{1-x}Al_xAs$ As a Function of Carrier Concentration

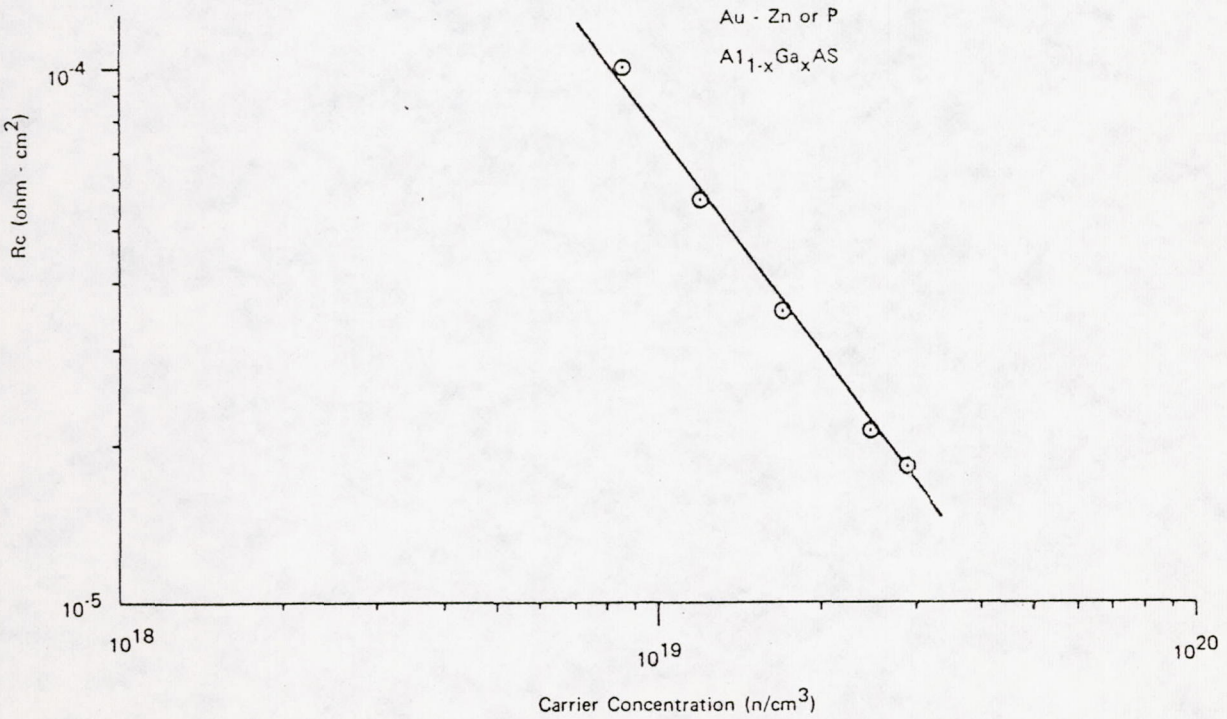


Figure 3-15. Specific Contact Resistance of AuZn on P-type $Ga_{1-x}Al_xAs$ As a Function of Carrier Concentration

The values of the carrier concentration used in these experiments ranged from $4.4 \times 10^{17}$ to $2.4 \times 10^{18}/cm^3$ for the n-type material, $9 \times 10^{18}/cm^3$ for the n-type material, and $9 \times 10^{18}$ to $3 \times 10^{19}/cm^3$ for the p-type material. Both Figures 3-14 and 3-15 show a strong dependence of contact resistance upon the carrier concentration of the material.

Since the band gap in $Ga_{1-x}Al_xAs$ is a direct function of the aluminum content in the epitaxial grown material, the same series of crystals as used in the preceding paragraph, having aluminum content of 25 to 50% for n-type material and 10 to 50% for p-type material, were used for studies for specific contact resistance as a function of aluminum content.

For these samples, the aluminum content was obtained by Electron microprobe methods.

Figures 3-16 and 3-17 show the results of a study of specific contact resistance versus aluminum content for AuGeNi on n-type material and AuZn on p-type material respectively. Both of these figures show essentially the same trend, in that the contact resistance decreases with decreasing aluminum content. However, there is a notable difference: the AuGeNi metallurgy on n-type material gives a specific contact resistance whose value is more than an order of magnitude lower than the AuZn metallurgy or p-type material at the same aluminum content.

Figure 3-18 shows the result of a study of contact resistance as a function of resistivity for n-type $Ga_{1-x}Al_xAs$ using AuGeNi as the contacting alloy. Here again, the lowest contact resistance is obtained from material with a low resistivity value.

### 3.2.5 CONCLUSIONS

The technique of specific contact resistance measurements between $Ga_{1-x}Al_xAs$ and a contacting metal, or alloy, has proven to be an excellent way to evaluate the metallizing processes involved. It also gives a determination of the best suited alloy for a given conductivity type of material.

This work has demonstrated the necessity for clean, oxide-free surfaces prior to the application of metallurgy in order to obtain a low specific contact resistance.

It appears that the resistivity of the $Ga_{1-x}Al_xAs$ epitaxial layer is a major controlling factor in the magnitude of the contact resistance for a given conductivity type of the material.

It has been shown that the contact resistance is a strong function of the carrier concentration, and also that the aluminum content in the grown $Ga_{1-x}Al_xAs$ epitaxial layers. This work indicates that the contact resistance, $R_c$ decreases with increasing carrier concentration for both p and n type material, when contacted with their respective metallurgy.

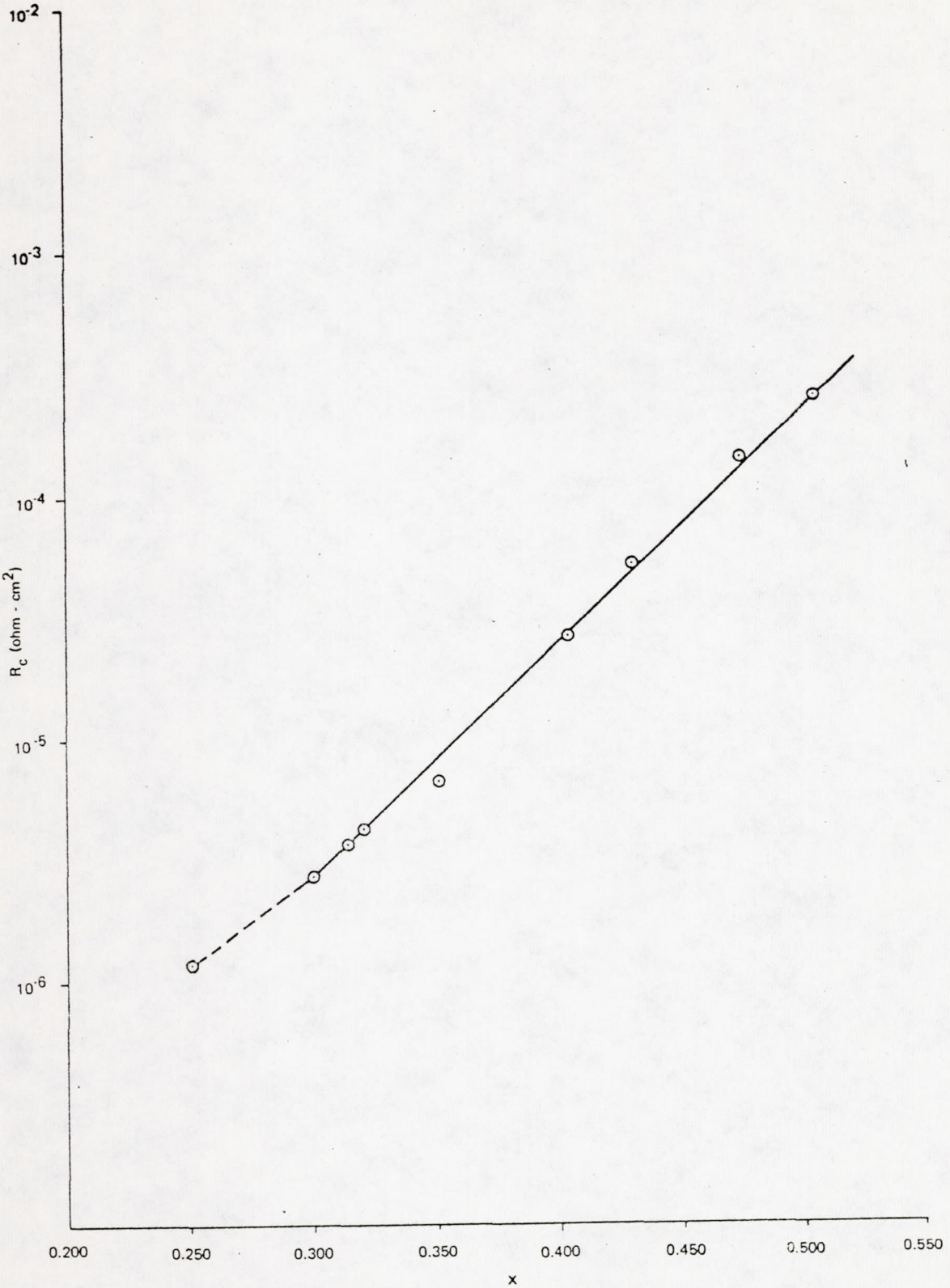


Figure 3-16. Specific Contact Resistance of AuGeNi on N-type $Ga_{1-x}Al_xAs$ as a Function of Percent Aluminum

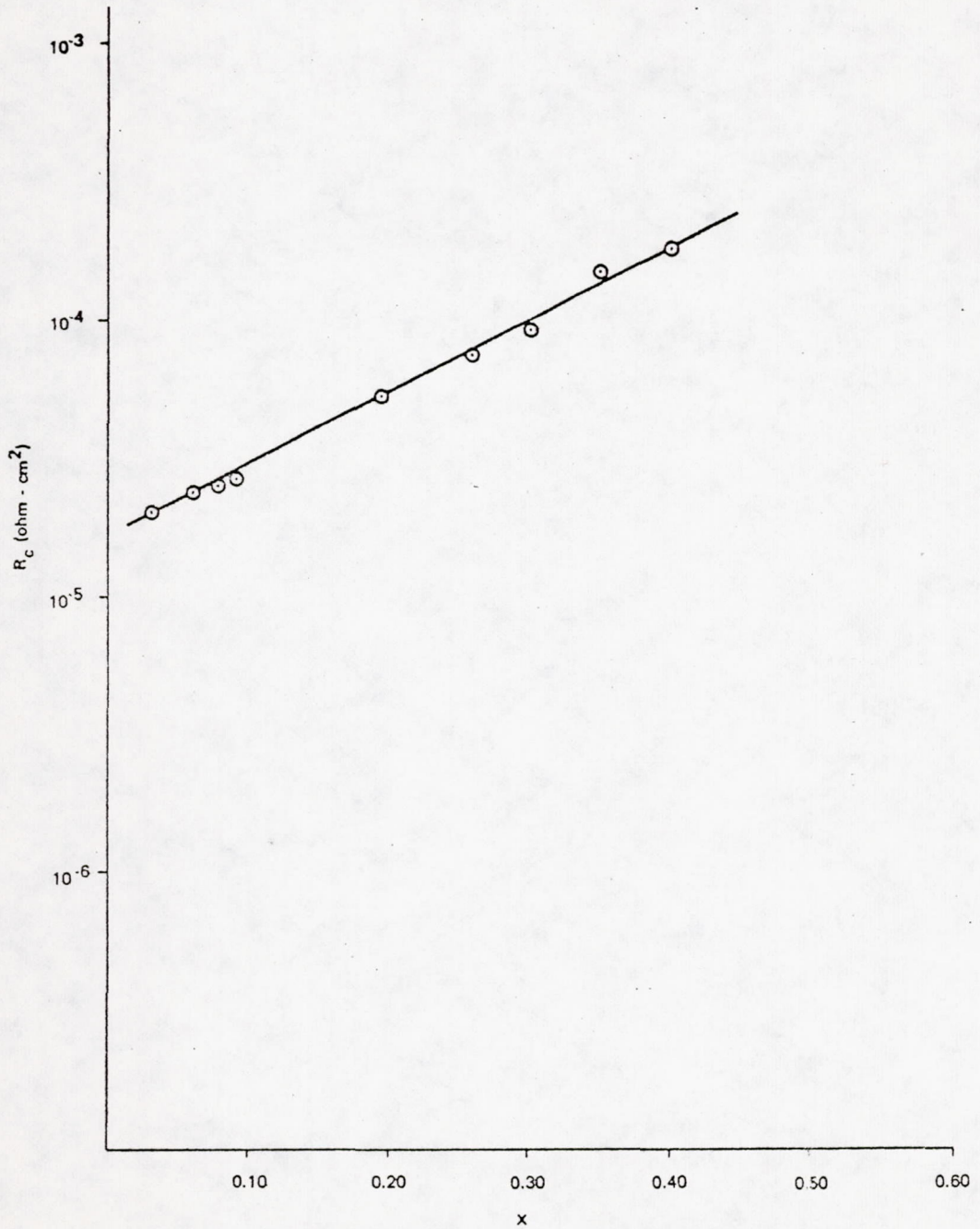


Figure 3-17. Specific Contact Resistance of AuZn on P-type $Ga_{1-x}Al_xAs$ as a Function of Percent Aluminum

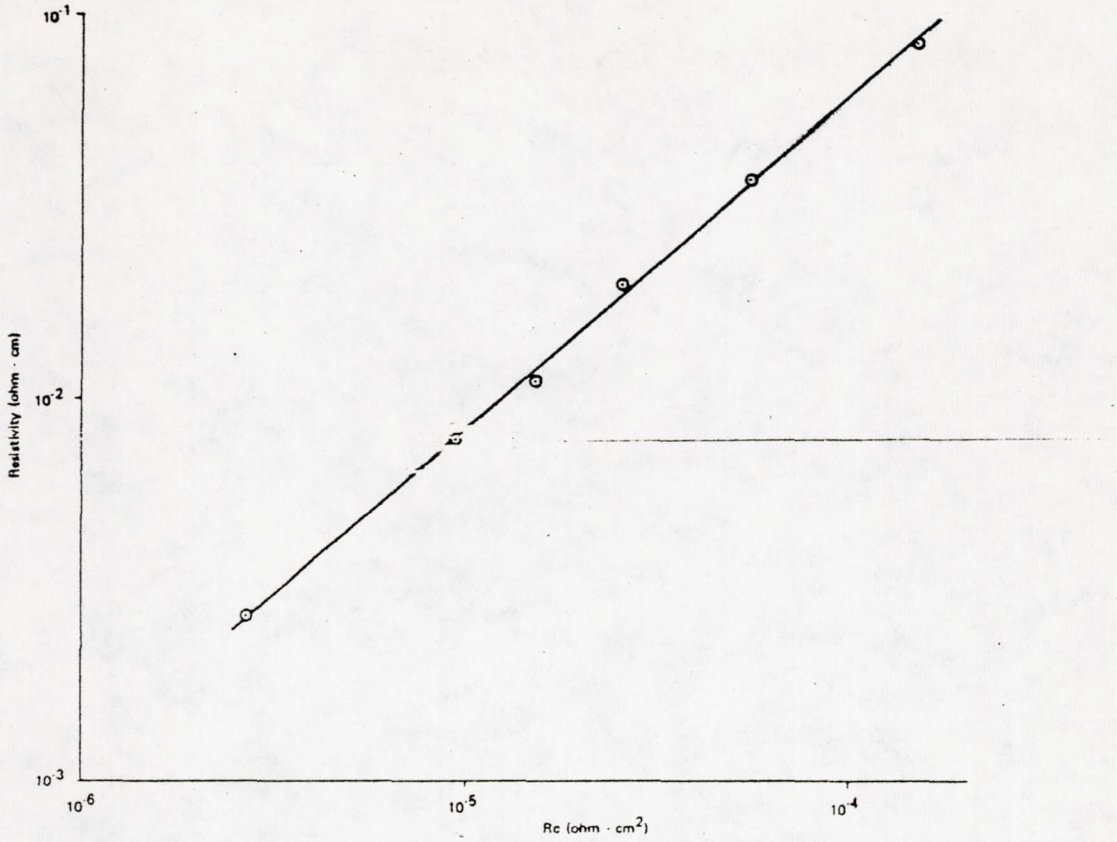


Figure 3-18. Specific Contact Resistance of AuGeNi on N-type $Ga_{1-x}Al_xAs$ as a Function of Resistivity

The objective of the study of specific contact resistance is to find those conditions which produce the lowest total heating in the diode. Four major factors affecting this total heating are:

1) Contact resistance

2) Bulk resistivity

3) Nonradiative transistors

4) Absorption of emitted light.

These factors are not independent but are related in a complicated manner. Measurements reported in this section have shown the relationship between contact resistance, bulk resistivity, and aluminum concentration. However, the relationship between bulk resistivity (carrier concentration) or aluminum fraction and absorption has not been discussed. The absorption coefficient, $\alpha$, increases with increasing carrier concentration due to free carrier absorption. The absorption decreases as the aluminum concentration is increased because of the shift in the absorption edge toward a shorter wavelength. The dependence of the heating on the absorption has the form

$$e^{-\alpha l}$$

where l is an average distance that light travels through the semiconductor. This contribution can be kept low by manipulating either the absorption coefficient or the distance, l.

The bulk resistance, v, of the device is related to the resistivity, $\rho$, by

$$v = \frac{\rho t}{A}$$

where t is the diode thickness and A is its area perpendicular to the current flow. This resistance can be reduced by increasing the carrier concentration (reducing $\rho$); but this contributes to the absorption and makes it more desirable to reduce the diode thickness, t. The thickness, however, cannot be made arbitrarily small because of the requirement of physical strength for diode material at minimum, 125 $\mu$m thick. Likewise, it is not helpful to increase the diode area, A, arbitrarily since the laser threshold is a function of current density rather than current. This means that the total heat deposited will vary linearly with the diode width and thermal density will remain constant.

No useful empirical data are presently available relating the absorption to doping density or aluminum mole fraction because it is very difficult to grow suitable samples. This measurement requires material of 50 $\mu$m to 100 $\mu$m thickness over which there is no substantial variation in carrier concentration on the aluminum profile. Lack of these data prevents a true optimization; but specific observations can be made.

1) Diode thickness should be minimized within the constraint of physical strength required for fabrication.

2) The aluminum concentration in regions outside the junction should be such as to raise the bandgap energy by 0.1 eV to 0.2 eV above the emission energy.

3) The doping density should be as high as possible consistent with high internal quantum efficiency. This value must be determined from the empirical data such as found in Table 3-4.

## 3.3 REFLECTIVE COATINGS

Light is generated in an LED by spontaneous emission due to radiative recombination of hole-electron pairs near the p-n junction. This process produces an isotropic distribution of radiated energy, half of which propagates toward the window material and half away from the window material. The total diode efficiency can be increased if the light traveling away from the exit window can be reflected toward it. The amount of this increase will be dependent upon the reflectivity of the surface and the absorption in the material. To explore this avenue of improvement, the reflectivity of the electrical contacts and reflective coatings on GaAlAs was increased.

Measurements were made on the reflectivity of the electrical contact metallurgy, applied in accordance with the optimum technique for minimizing contact resistance. This was performed by comparing the reflections of a 1.06 $\mu$m Nd:YAG laser beam from GaAlAs material with, and without, the contact coating. The contact metallurgy was the gold-zinc alloy described in Subsection 3.2 of this report. As is described

in Subsection 3.2, the alloy is first applied by evaporative coating and then sintered. During sintering, the alloy diffuses several microns into the semiconductor. The rather low reflectivity of the contact can be rationalized on the basis that this diffusion forms an irregular interface at which the reflection takes place. This irregular interface is analogous, to some extent, with "gold-black"[14], a porous gold coating for which high absorption is observed. Details of the experimental measurements are as follows: a 1 cm square GaAs wafer was first prepared with an appropriate GaAlAs epitaxial layer. Subsequently, half of the epitaxial layer was coated with contact metallurgy and half left uncoated. A Nd:YAG laser beam ( $\lambda = 1.06\ \mu m$) was then directed onto the opposite side of the wafer at an angle of 20° to the surface normal. In this manner the wafer could be positioned so that the beam passing through the wafer is alternately reflected from the coated or uncoated area of the surface. By comparing the ratio of the reflected intensity in these two cases it is possible to reduce some of the uncertainty due to surface and bulk scattering effects. The mathematical expression used for this comparison is derived by summation of successive intensity contributions as the light is reflected back and forth between two nearly parallel surfaces, i.e., no interference condition is assumed and beam walk-off is disregarded. The expression for the reflected intensity $I_R$, is,

$$I_R = I_o \left(R_1 + \frac{R_2(1-R_1)^2}{1-R_1R_2}\right)$$

where $I_o$ is the incident intensity and $R_1$ and $R_2$ are the first and second surface reflectivity respectively. Using the reflective index, n = 3.5, the reflection of the uncoated surface, $R_1$, can be calculated. Substituting this value in the expression, and using the measured ratio of reflected intensity, a value for $R_2$ is determined. Values calculated in this way range from 0.75 to 0.81.

Reflective coatings were applied by sputtering successive layers of SiO and metal. The SiO provides the necessary electrical insulation to prevent short circuiting the p-n junction. A subsequent metal coating gives appropriately high reflectivity. This coating is then protected with an overcoating of SiO. Several metals were tried as reflective layers, specifically gold, silver, copper, and aluminum. Of these, good adhesion was achieved only with aluminum. Since it is anticipated that these coatings will be applied to LED surfaces on which the dimensional tolerances are close, it is important to know the precision with which the area coated can be controlled. The thickness of the LEDs is about 100 $\mu$m. Figure 3-19 shows the edge of a 100 $\mu$m thick test sample which has been coated over 40 $\mu$m of its thickness. The coating width was controlled by vignetting the diode surface from the evaporation source with the holder. It has been found that this technique works well when it is desired that the coating not extend near one edge, for instance when danger of shorting exists.

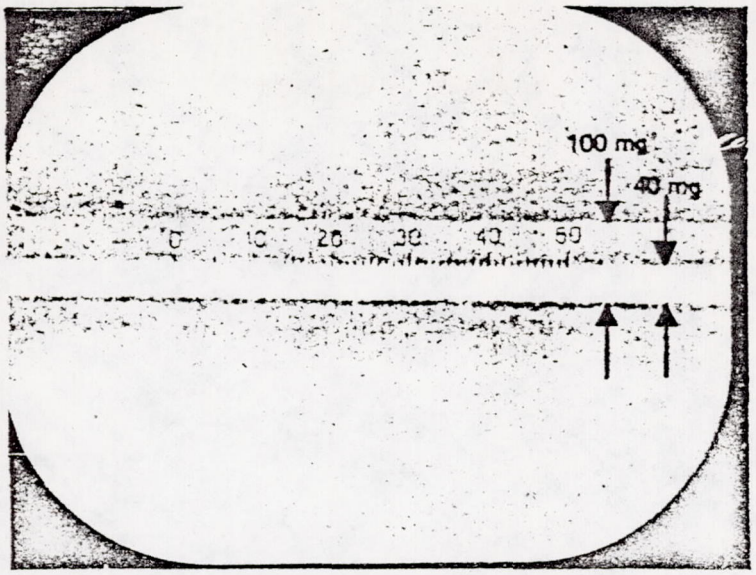


Figure 3-19. Reflectively Coated GaAs Chip

For testing, a 600 Å layer of SiO was applied, followed by approximately 1500 Å of Al and 1000 Å overcoating of SiO. The reflectivity of this coating was gretaer than 80%. Considerable uncertainty exists in the exact reflectivity due to uncertainty of bulk scattering loss in the material. These measurements show that effective reflective coatings can be applied to the diodes. It is, therefore, of interest to estimate the improvement in diode performance that can be gained with these measured reflectivities. As a model for this estimate, assume that the diode is composed of parallel strata of material from which light is specularly reflected, and that some fraction, A, is emitted into an approximately 30° cone which is transmitted from the window. Due to the isotropy of emission, a like fraction propagates into the p-type region, where it is partially absorbed, and partially reflected, at the boundary. The total light emitted from the upper surface is the sum of that propagating toward the window and the additional fraction after reflection and absorption incurred in two transits through the p-type material. In general, this can be represented by:

$$A + RAe^{-2\alpha t}$$

where A is the fraction of light emitted into the emission cone from an infinitesimal region of the p-n junction, da; R, the reflectivity at the boundary; $\alpha$, the absorption coefficient in the p-region; and t is the thickness of the p-type material through which the light passes twice. Without a reflective coating on the diode surface, about 30% will be reflected because of the refractive index mismatch. Since this amount of light reflection is less than half the reflection from the contact metallurgy, we must differentiate between those cases. The enhancement observed will be the ratio of the above expression evaluated for the reflective coatings, and its comparable evaluation without the coatings. For typical material the absorption coefficient, $\alpha$, will have a value between 10 and $10^2$ $cm^{-1}$. Substition into the previous expression leads to an estimated enhancement of 14% (when the p-region thickness is 15 $\mu$m) for all areas backed with perfect reflective coatings rather than electrical contacts. The enhancement of the reflective coatings over encoated areas is 30 to 36%. This enhancement is sufficient to consider reflective coating some portion of the diodes surface; however, since the electrical contact area also serves as the thermal contact for the diode, it should be made as large as practical.

## 3.4 LOW MELTING POINT GLASS ADHESIVE

The high index of refraction characteristic of GaAlAs semiconductor material results in a small critical angle for total internal reflection which, as has been mentioned in previous sections, limits the external quantum efficiency of the LEDs. In the use of LEDs for laser pumping, it is possible to avoid semiconductor air interfaces if one fills the space between the laser rod and the diode with a material of the same refractive index, or higher, as the laser rod.

Figure 3-20 schematically indicates the situation when light passes through three successive media with parallel surfaces and refractive indices $n_0$, $n_1$, $n_2$.

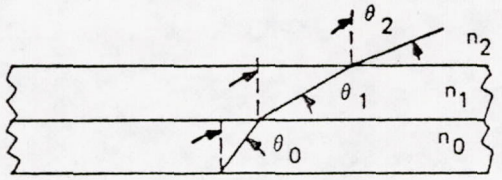


Figure 3-20. Refraction in Multilayered Medium

The angles of refraction of a ray traversing these media, $\theta_0$, $\theta_1$, and $\theta_2$, are related through Snell's Law.

$$n_0 \sin\theta_0 = n_1 \sin\theta_1 = n_2 \sin\theta_2 \qquad 3.4\text{-}1$$

The critical angle for total internal reflection occurs when a ray passes from a region of higher index to lower, and the refracted angle in the second medium becomes $\pi/2$. Then,

$$\theta^c = \sin^{-1}\left(\frac{n_l}{n_h}\right) \qquad 3.4\text{-}2$$

where $n_l$ and $n_h$ represent the lower and higher index respectively and $\theta^c$ is the critical angle.

It can be seen from the relationship in the case of three successive media that if,

$$n_0 > n_1 \geq n_2$$

then the critical angle is,

$$\theta_0^c = \sin^{-1}\left(\frac{n_2}{n_0}\right) \qquad 3.4\text{-}3$$

This situation is the optimum, since light must enter the final medium of index $n_2$, then the critical angle should be no smaller than that produced by the final medium. The customary situation is when,

$$n_0 > n_1 < n_2$$

For this case

$$\theta_0^c = \sin^{-1}\left(\frac{n_1}{n_0}\right) < \sin^{-1}\left(\frac{n_2}{n_0}\right)$$

This situation is avoided if the diodes are attached to the laser material by an adhesive which has an equal or higher index.

Two other sources of loss must also be considered to complete the treatment. They are Fresnel reflection and absorption loss. Fresnel reflection occurs at any discontinuity in the refractive index and is described by

$$R_\sigma = \frac{\sin^2 (i-r)}{\sin^2 (i+r)} \qquad R_\pi = \frac{\tan^2 (i-r)}{\tan^2 (i+r)}$$

where $R_\sigma$ and $R_\pi$ are the intensity reflection coefficients for light polarizations perpendicular to and parallel to the plane of incidence respectively. i and r represent the incidence and refracted angles at the interface. An average value of the intensity reflection coefficient is

$$\bar{R} = \frac{1}{2} \frac{\sin^2 (i-r)}{\sin^2 (i+r)} \left\{ 1 + \frac{1-\sin^2 (i+r)}{1-\sin^2 (i-r)} \right\}$$

The absorption loss, $L_j$, will be represented by the expression

$$L_j = \exp (-\alpha_j l_j / \cos \theta_j)$$

where $\alpha_j$ is the material absorption characteristic; $l_j$ is the thickness of the $j^{th}$ layer and $\theta_j$ is the angle of propagation in the medium. In the GaAlAs region surrounding the junction, the absorption $\alpha_0$ will be approximately 10 $cm^{-1}$. The absorption of the low melting point glass was found to be less than 3 $cm^{-1}$. Measurement of undoped YAG shows in the neodymium pump band at 8070Å.

To determine the transmission for the case illustrated in Figure 3-21 we must take the product of the individual reflection and absorption terms. Reflection

$$T_1 = \left\{1 - \frac{1}{2}\frac{\sin^2(\theta_0 - \theta_1)}{\sin^2(\theta_0 + \theta_1)}\left[1 + \frac{1-\sin^2(\theta_0+\theta_1)}{1-\sin^2(\theta_0-\theta_1)}\right]\right\}$$

$$T_2 = \left\{1 - \frac{1}{2}\frac{\sin^2(\theta_1 - \theta_2)}{\sin^2(\theta_1 + \theta_2)}\left[1 + \frac{1-\sin^2(\theta_1+\theta_2)}{1-\sin^2(\theta_1-\theta_2)}\right]\right\}$$

The total transmission, T, is then,

$$T = L_0 T_1 L_1 T_2$$

Using the mentioned values of absorption coefficients, $l_0 = l_1 = 25 \times 10^{-4}$ cm, and indices of refraction of 3.5, 2.5 and 1.82 for the GsAlAs, the LMP glass, and YAG respectively, one finds that the maximum transmission factor, i.e., normal incidence ($\theta_0 = 0$), is 92%. This reduces to zero when total internal reflection is reached which for $n_0 = 3.5$, $n_1 = 2.5$, $n_2 = 1.82$, then $\theta_0 = 31.4°$. The dependence of the transmission, $T_1$, as a function of the incidence angle, $\theta_1$, is shown in Figure 3-21.

The purpose of these experiments was to develop the preparation technique and material to use as an adhesive in bonding semiconductor diodes to yttrium aluminum garnet (YAG). The material used for this purpose should bond well to the semiconductor and YAG surfaces, have a refraction index higher than YAG ($n = 1.82$) have a lower melting point than the diode solder, be transparent at the diode emission wavelength, and form bonds which will endure cycling over a large number of operations without fatigue.

Glassy materials having many of these properties can be formed by mixtures of arsenic, selenium, sulphur and bromine.

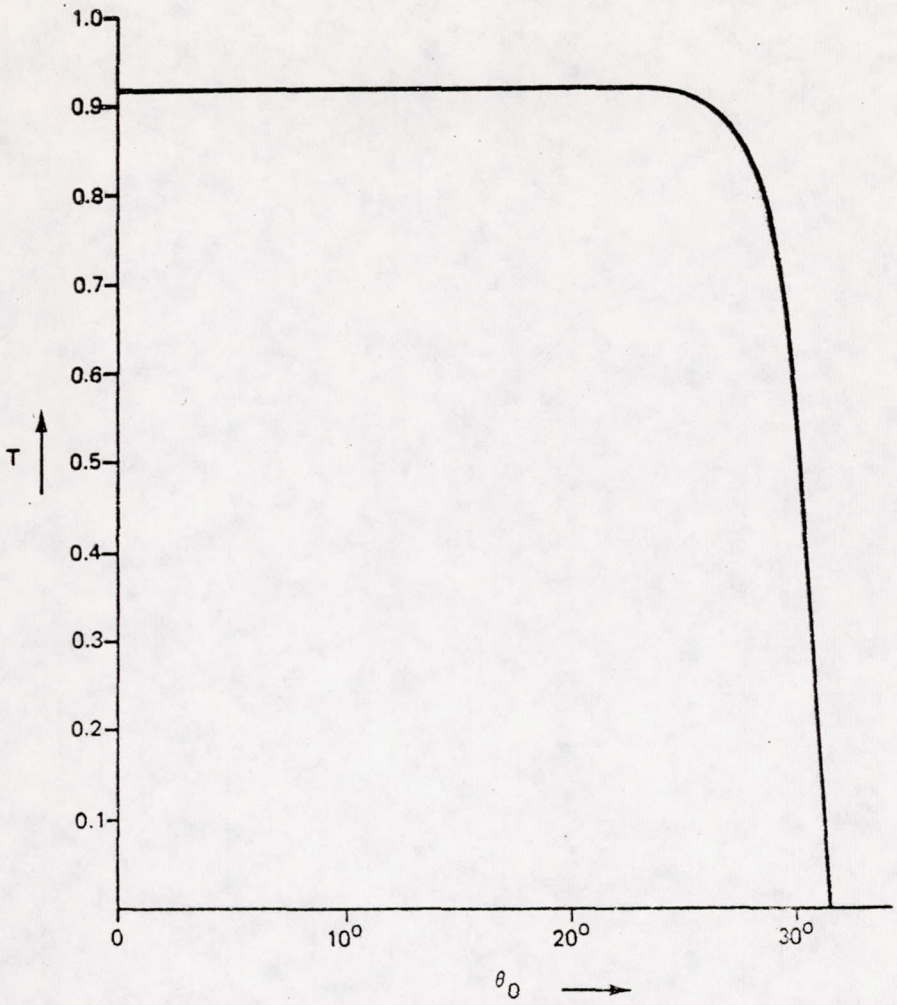


Figure 3-21. Transmission of Pump Radiation vs Interface Incidence Angle

During this program, eight batches of glass were prepared by the technique described by Fisher [15] and Neuse. The mixture of constituents chosen for these batches was:

| | |
|---|---|
| Arsenic | 5 g |
| Sulphur | 10 g |
| Bromine | 1 cc |

Several advantages cited by Fisher and Neuse for this mixture provide the basis for its selection. The refractive index, n, is approximately 2.5 which satisfies the requirement,

$$1.82 \leq n \leq 3.5.$$

The material transmits the 8000 Å to 8100 Å pump radiation without absorption. The melting range of the material fits well with the solder hierarchy selected for use, i.e., its melting range is lower than that of the lowest melting solder. The material softens at 68° C and is completely fluid at 174° C. This mixture also has a wide thermoplastic temperature range of about 100° C which is located within the anticipated operating temperature (~45° C) for the diode devices. Within that range the glass will yield to expansion and contraction of the adjacent material.

Experimental measurements of the glass absorption spectrum was made by bonding a 1 mm thick sample to a glass microscope slide. This piece was mounted in the sample holder of a Cary 14 spectrometer and an uncoated microscope slide was placed in the reference beam. The measured spectrum is featureless from 7900 Å to 9000 Å with an apparent transmission of 82%. If it is assumed that this difference in transmission is due to Fresnel reflection the refractive index can be deduced from these data. The transmission through the three surfaces of the test sample can be expressed as

$$T_{glass} = \left[1 - \left(\frac{n-1}{n+1}\right)^2\right]\left[1 - \left(\frac{n-1.5}{n+1.5}\right)^2\right]\left[1 - \left(\frac{1.5-1}{1.5+1}\right)^2\right]$$

where n is the refractive index of the LMP glass; 1.5 is the refractive index of the microscope slide, and each of the square bracketed terms represents the transmission through a single surface. The transmission through the slide in the reference beam is represented by

$$T_{ref} = \left[1 - \left(\frac{1.5-1}{1.5+1}\right)^2\right]^2$$

since there are only two surfaces to consider. The ratio of these two can be used to find n.

$$\frac{T_{glass}}{T_{ref}} = \frac{\left[1 - \left(\frac{n-1}{n+1}\right)^2\right]\left[1 - \left(\frac{n-1.5}{n+1.5}\right)^2\right]}{\left[1 - \left(\frac{1.5-1}{1.5+1}\right)^2\right]^2} = 0.82$$

This expression is satisfied by n = 2.4 which is near the expected value of the refractive index for this mixture. The agreement indicates that the absorption or bulk scattering loss in the material is no greater than about 10%/cm.

To determine the usefulness of the glass as an adhesive in space applications, several tests were performed. First, it was determined that the glass would wet the semiconductor and YAG material. This was done by applying the glass to GaAs wafers and to YAG material. After wetting tests were successful, the materials were bonded together with the glass adhesive.

Current-voltage (I-V) curves of diodes to which the glass adhesive was applied were unchanged by the application. Cycling tests conducted over a 2 week period showed no change in diode output over a 20 hour operating time. During this cycling test the diodes were driven at 300 mA current (40 A/cm$^2$). The power applied to the diode was 0.45 W. This power is about 1/2 of that anticipated under laser operation. Since these diodes were mounted on commercial headers, which do not have thermal conductivity equal to that anticipated by mounting them on berylium oxide, the disparity between the operating temperatures is small. Figure 3-22 shows the relative output of

a diode as a function of drive current for three different conditions. First, the diode was operated without coating. Next, a thin layer of glass was applied to the surface and the power was measured. Finally, a cylindrical dome of a diameter approximately twice the diode width was applied to the diode. The higher power observed for this dome is the result of decreased total internal reflection.

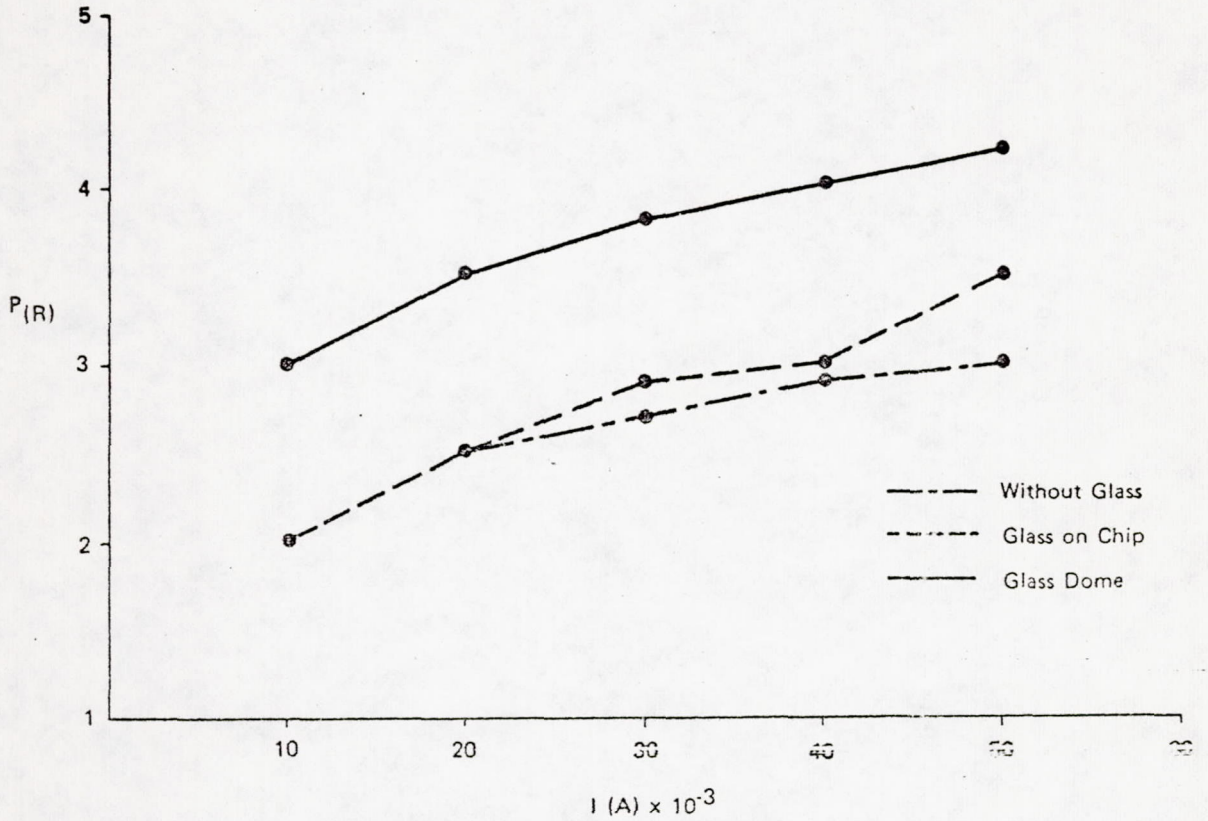


Figure 3-22. Diode Output (Relative) vs Drive Current

No cracking or crazing was observed on the diodes operated in the cycling tests. Some cracking did appear on diodes which were covered with thick glass layers which extended over the header. No observation of long term stability of this material has been made.

An application technique was investigated in which a thin film ($\approx 125\,\mu$ m) of the glass was applied to a microscope slide. The slide was subsequently cut with a string saw to simulate diode fabrication condition. Microscopic examination of the piece showed chipping along the edges but generally good adhesion to the remainder of the surface. It appears that the wafer surface can be coated with LMP glass before the diodes are cut and sufficient material will remain to form the desired bond with undoped YAG.

Figure 3-23 shows the results of thermal-vacuum testing of the LMP glass. Several small (0.1 g) samples having irregular shapes were placed in the vacuum bell and the vapor pressure monitored as the pressure was increased. The initial pressure measured ($3 \times 15^5$ Torr) was the same as that measured in the system before the addition of the samples. As the temperature was increased the vapor pressure rose as shown in Figure 3-23. Time was allowed at each temperature for the system to stabilize. Above the temperature at which the glass became completely liquid a sharp drop in pressure was observed. This indicates the complete distillation of the most volatile component of the mixture.

## 3.5 LED CONSTRUCTION AND EVALUATION

### 3.5.1 DEVICE DESCRIPTION

The final phase of this program was to construct several light emitting diodes that could be placed in direct contact with an optical configuration used for pumping a Nd:-YAG laser (see Figure 2-4). The device would have its top surface clear of all contact metallurgy and wire bonds which might normally obstruct the emitted radiation. The optical system in this case is envisioned as a garnet elliptical cylinder focusing on a laser rod. The structure by necessity requires that both n and p ohmic contacts be placed on the bottom surface.

Figures 3-24 and 3-25 show the GaAlAs light-emitting diode configuration which was grown on GaP substrate material. The rectangular chips were constructed having a 0.07 cm width, 0.125 cm length, and 125 cm thickness. This so called "flip chip" device provides a clear optical window transparent to the emitted radiation, and closely matches the index of refraction of the optical system. Connections to the bottom of the chip are made by flowing electroplated solder between the device metallurgy and a hybrid circuit board metallurgy. The hybrid circuit board is composed of high thermal conductivity beryllium oxide which has been metalized with chrome, nickel, and gold by sputtering and electroplating.

Photolithographic techniques are then used to develop the interconnection metallurgy pattern which ultimately is used to connect the chips in series (Figure 3-26). The feasibility devices are mounted on single section pieces from the array board shown in Figure 3-27. A summary of device characteristics is shown in Table 3-5, and the spectral emission characteristic is presented in Figure 3-28.

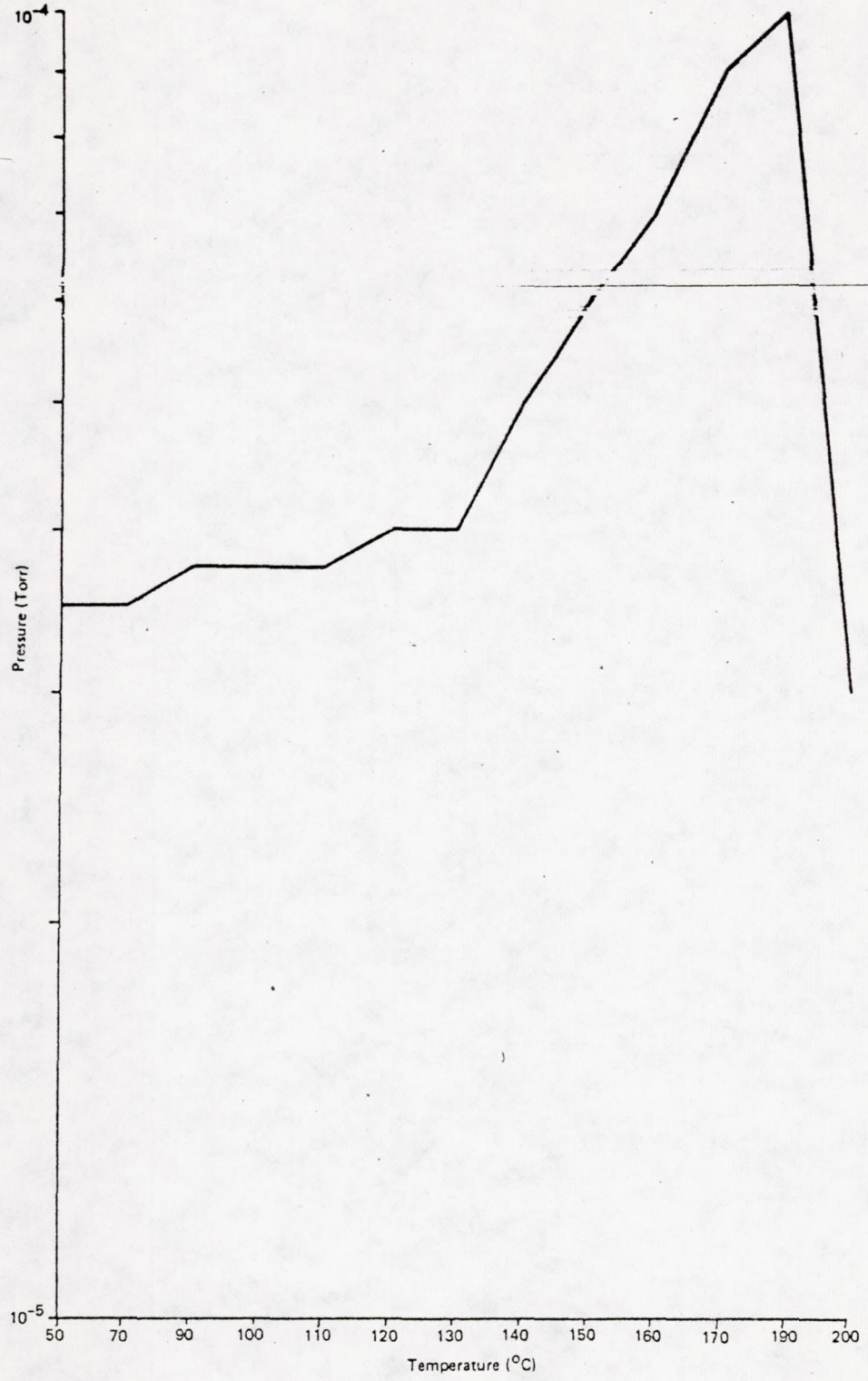


Figure 3-23. Glass Vapor Pressure vs Temperature

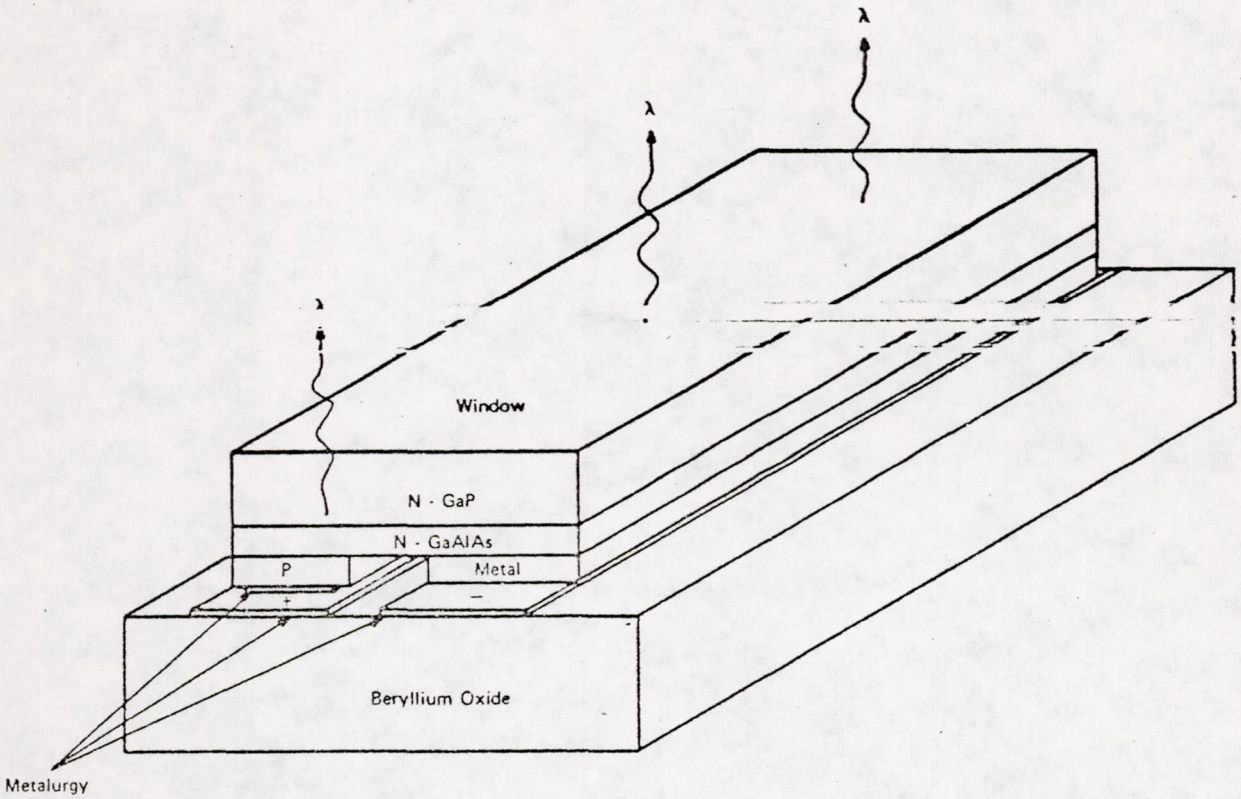


Figure 3-24. LED Structure

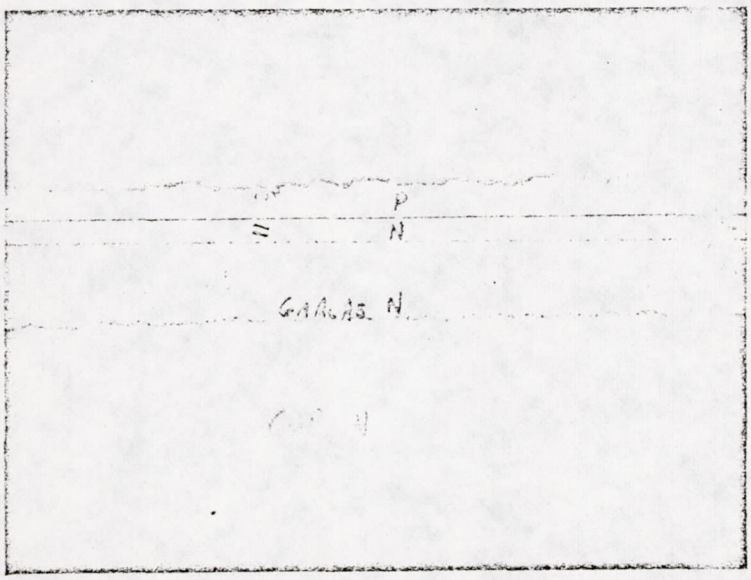


Figure 3-25. Cross Section of Solution Grown Wafer Before Processing

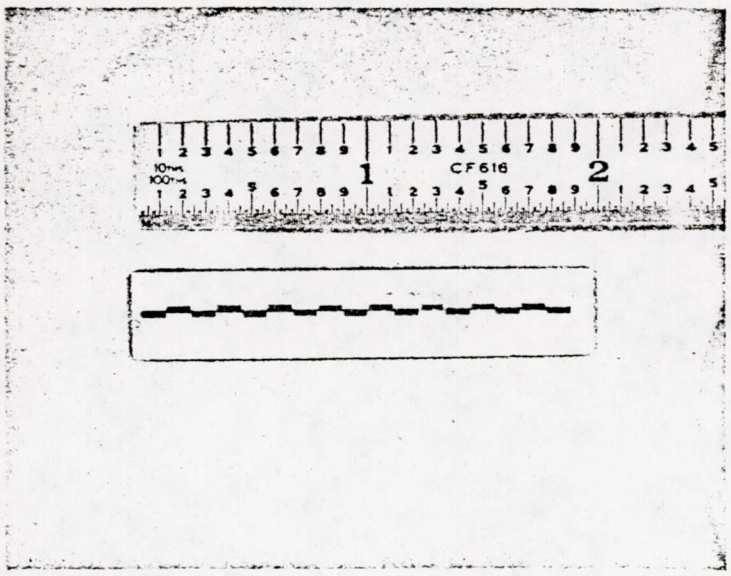


Figure 3-26. Series Embodiment for a LED Pumping Array

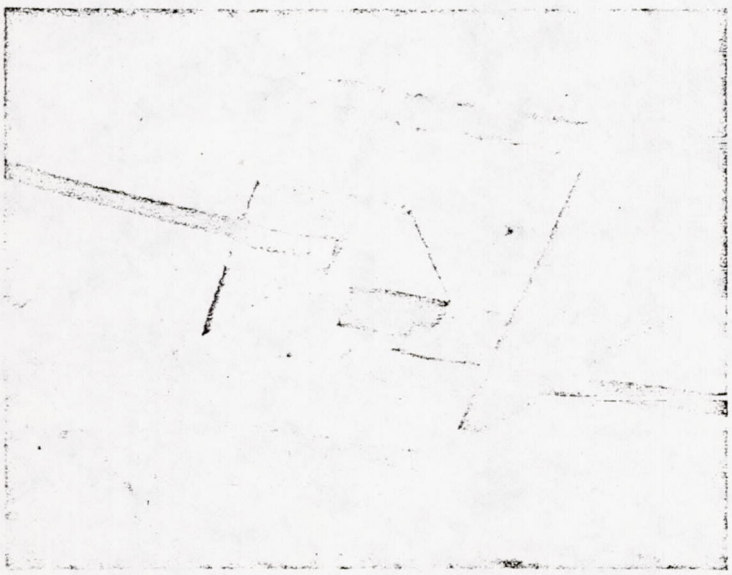

Figure 3-27. Assembled Device for Evaluation

Table 3-5

DEVICE CHARACTERISTICS SUMMARY

| Parameter | Typical Value | Units |
|---|---|---|
| Peak Emission | 8580 | Angstrom |
| Emission Width 50% Points | 410 | Angstrom |
| Forward Voltage Drop @50 mA | ≈1.25 | Volts |
| External Quantum Eff. into Air | 1.0 | Percent |
| Dynamic Resistance | < 2 | Ohms |
| Chip Size: 0.125 cm × 0.07 cm GaAlAs grown on GaP | | |

The DC current-voltage curves for three "flip chip" diodes have been determined at 300°K. No particular effort for device heat sinking was made during these measurements. For diodes DI, DII, and DIII, results of these measurements are shown in Figures 3-29, 3-30, and 3-31. From the forward slopes of the current-voltage curves, DC-series resistance, $R_S$, values between 1.15 Ω and < 1.66 Ω have been obtained. All devices investigated started to emit incoherent infrared radiation at about a 1.1 V forward bias, as observed with an infrared image converter.

For devices DII and DIII, the DC current-voltage curves are plotted on a semilog scale, as shown in Figures 3-32 and 3-33. The results for these presentations have already been corrected for the DC voltage drop caused by the diode series resistance.

The current-voltage curves of forward biased light emitting diodes can be described by the equation:

$$I = I_0 \exp\left(\frac{qV}{nkT}\right)$$

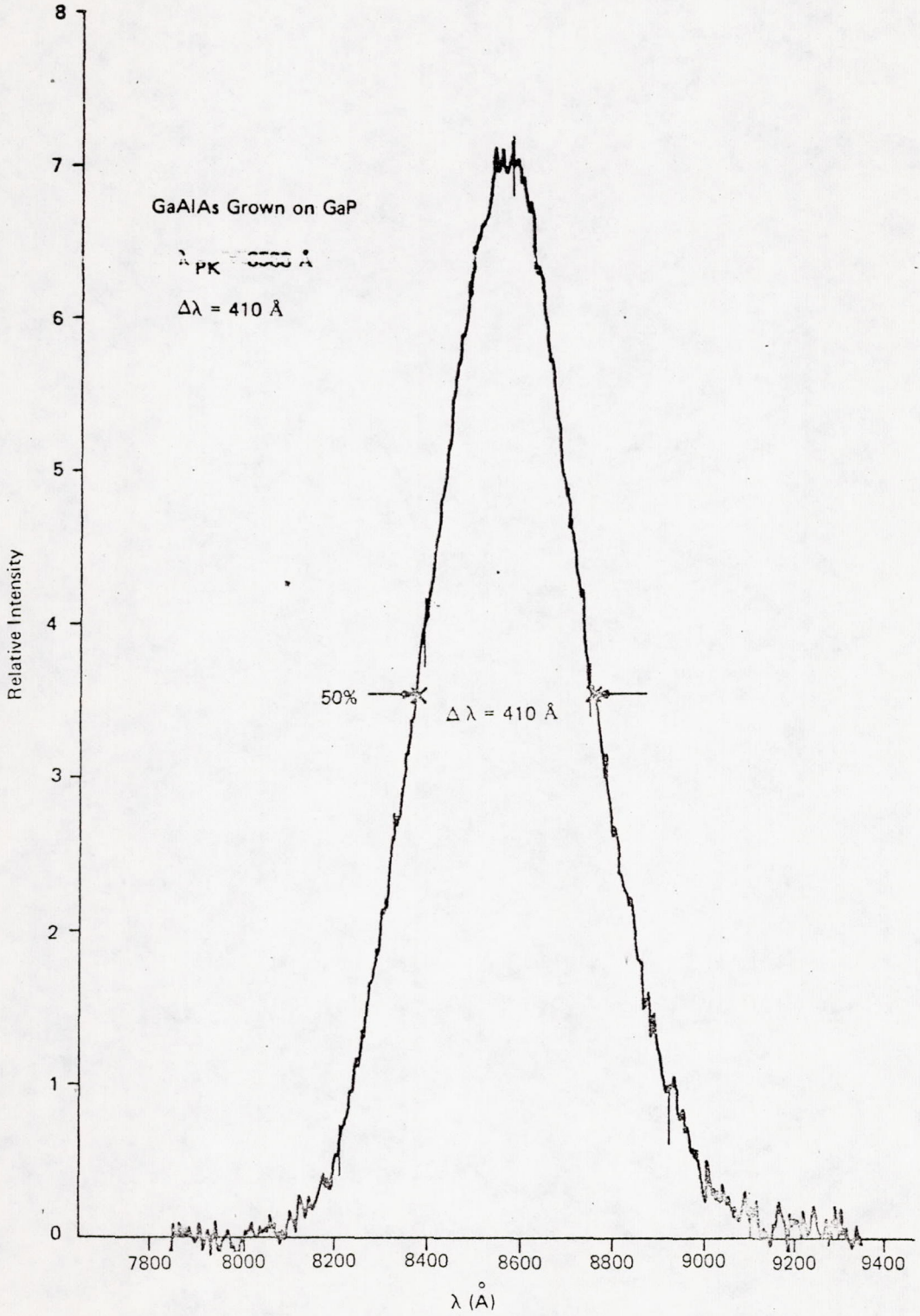


Figure 3-28. Emission Spectrum from Flip Chip Device

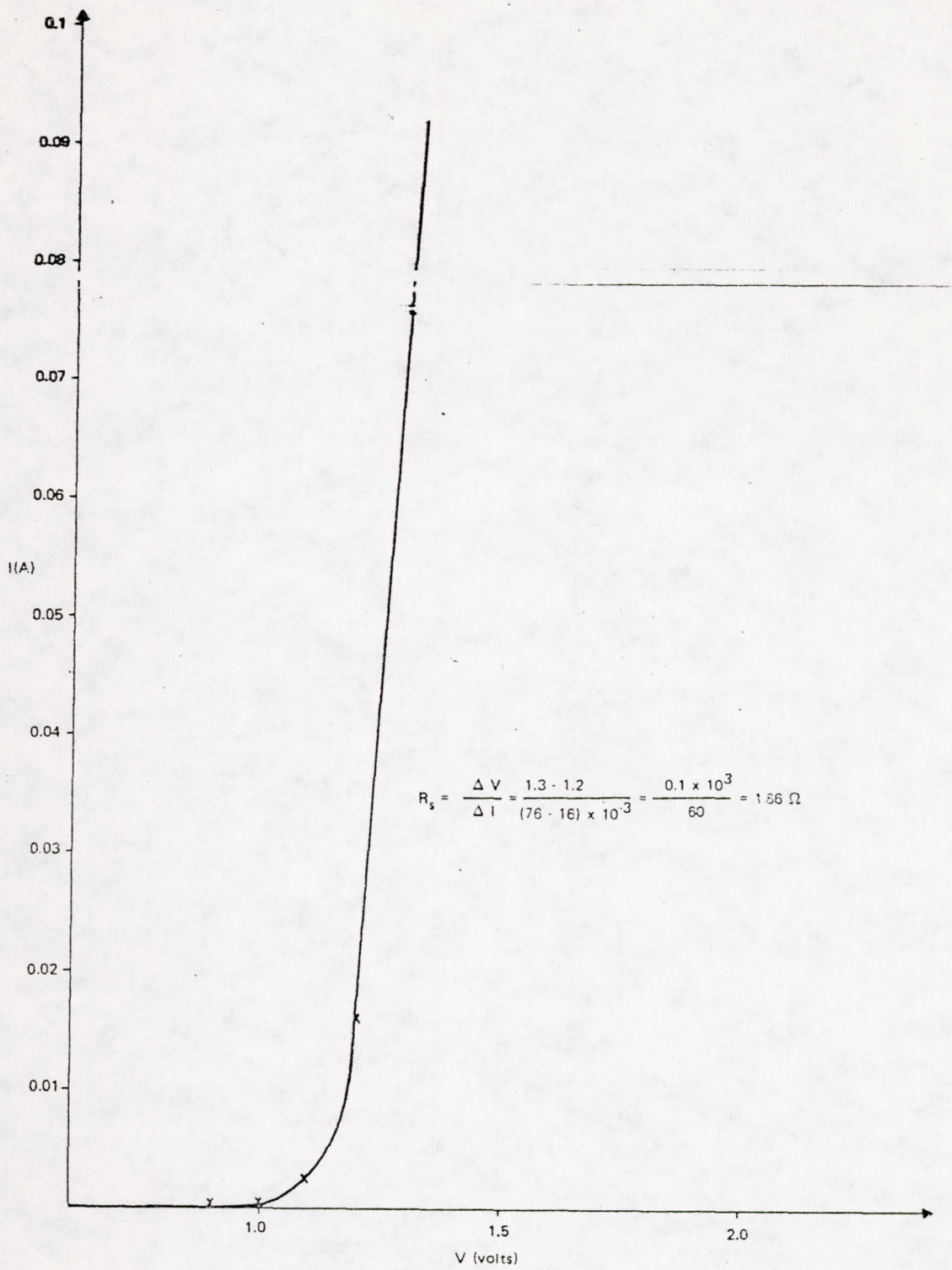


Figure 3-29. DC Current-Voltage Characteristic,
GaAlAs LED with GaP Window,
Diode Area: 10 mil by 100 mil, Diode DI

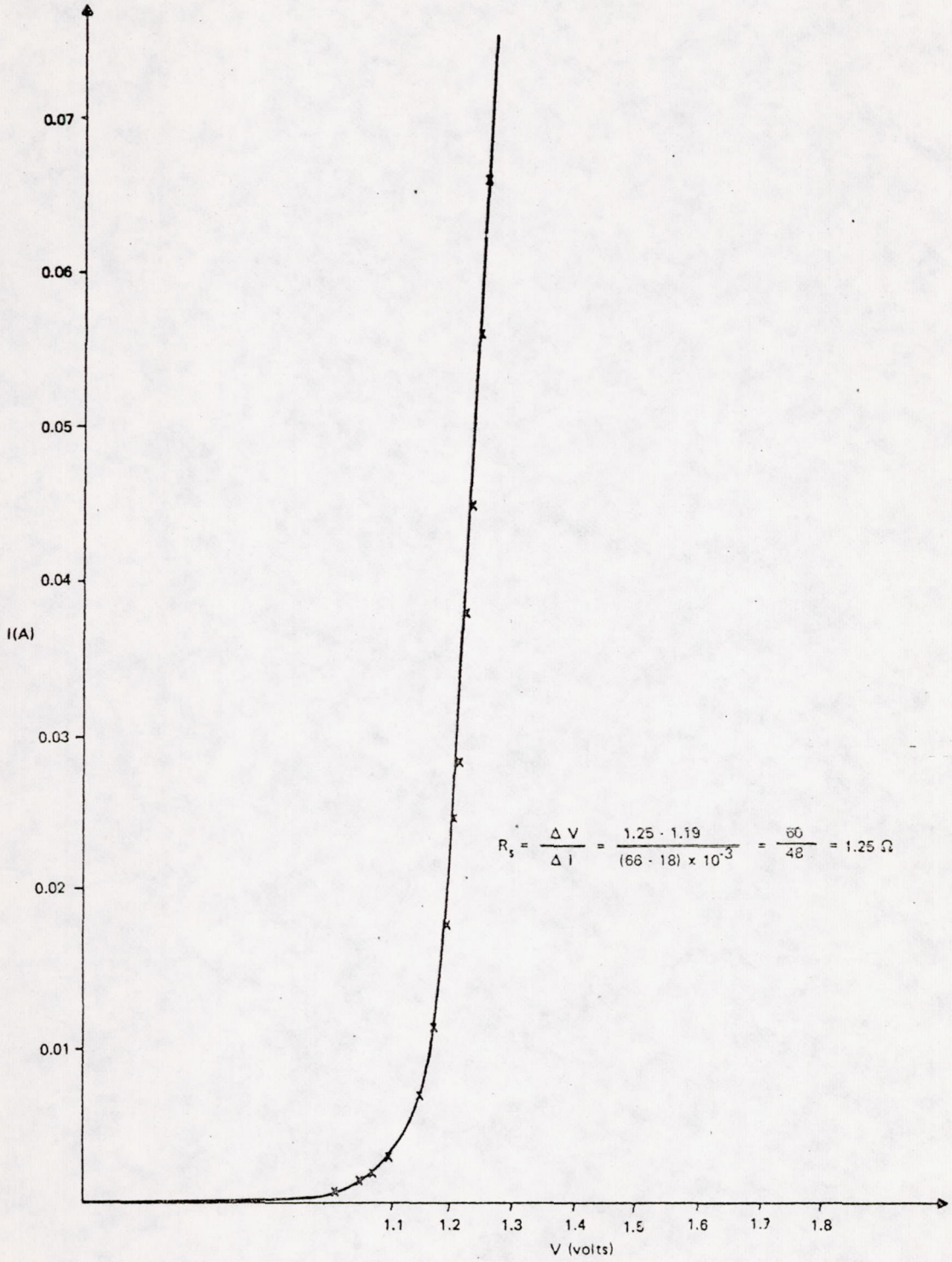


Figure 3-30. DC Current-Voltage Characteristic,
GaAlAs LED with GaP Window,
Diode Area: 10 mil by 100 mil, Diode DII

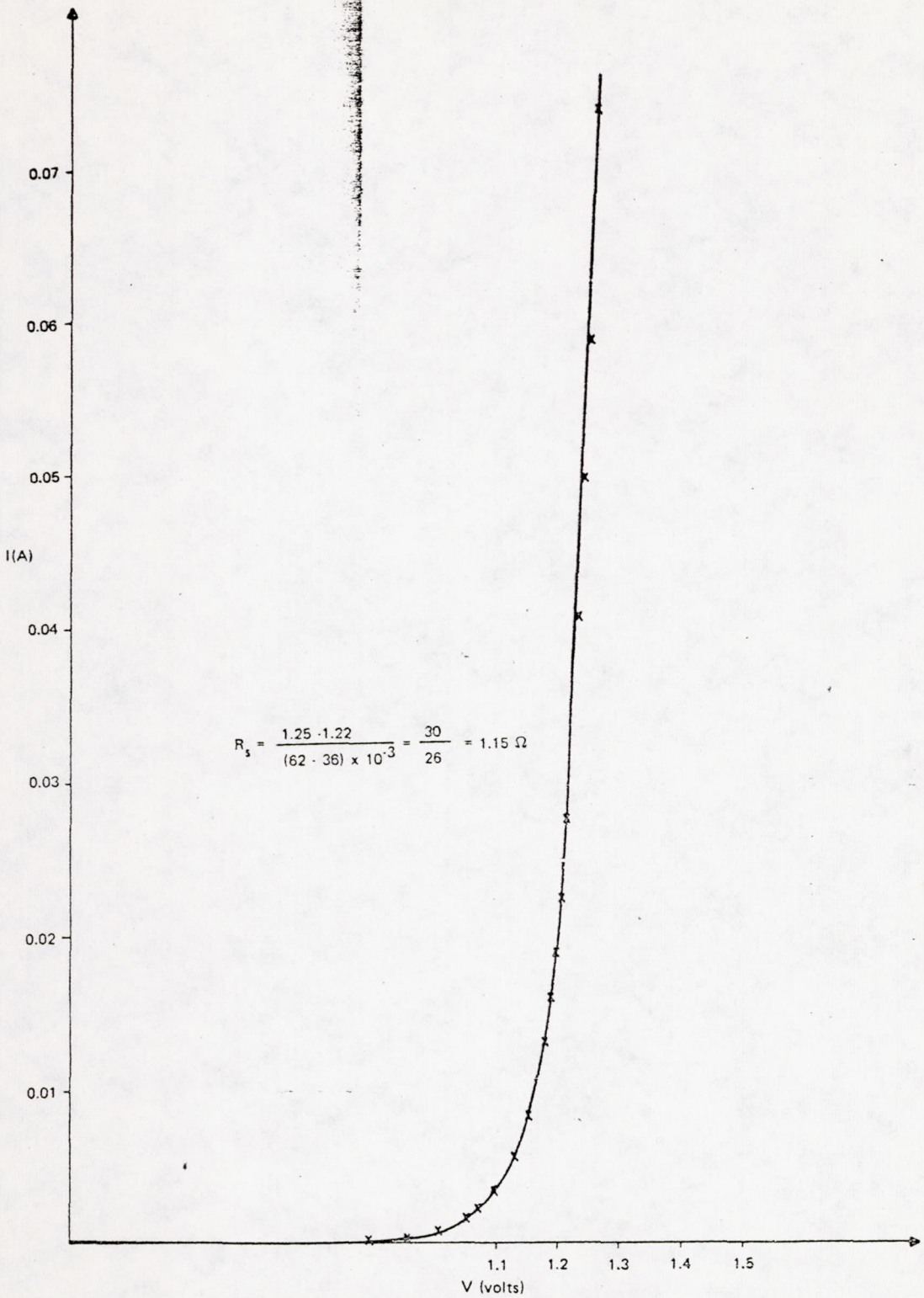


Figure 3-31. DC Current-Voltage Characteristic, GaAlAs LED with GaP Window, Diode Area: 10 mil by 100 mil, Diode DIII

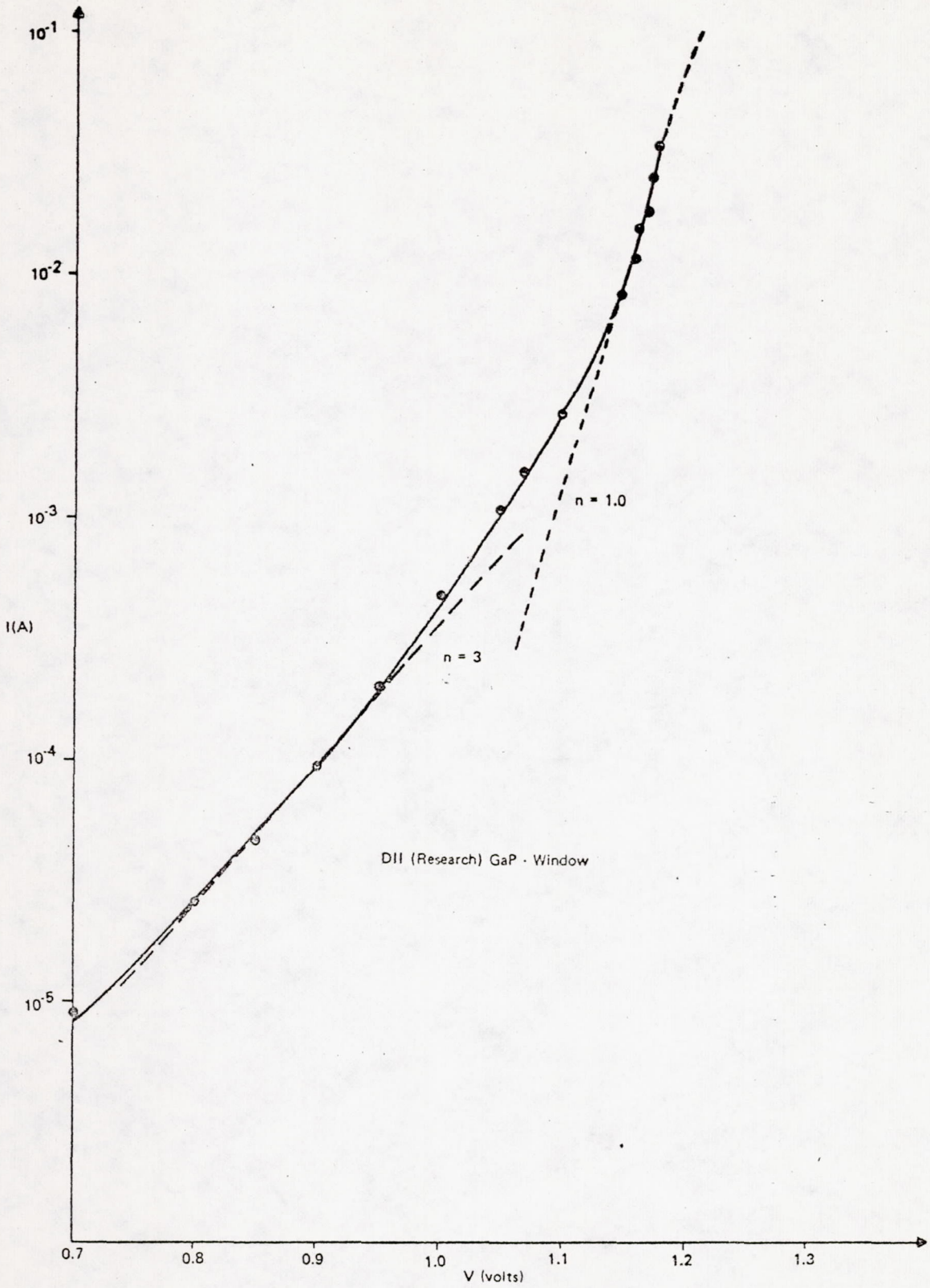


Figure 3-32. Voltage Dependence of Diode Current

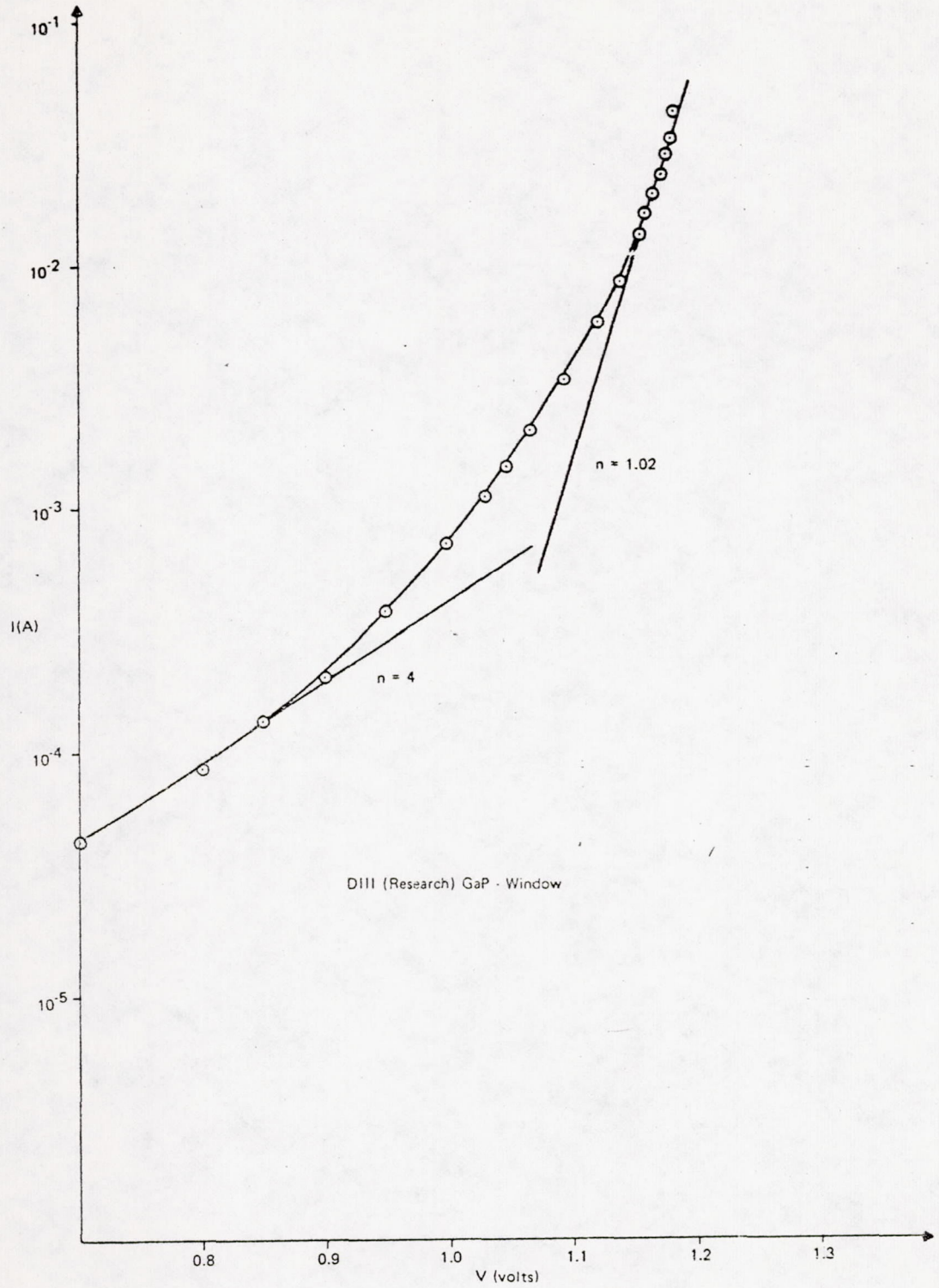


Figure 33. Voltage Dependence of Diode Current

where

V = applied bias voltage

q = $1.6 \times 10^{-19}$ Coulomb-electronic charge

k = $1.38 \times 10^{-23}$ Joules/° K — Boltzman constant

$I_0$ = Diode saturation current

T = 300° K and n is a constant.

The constant n can be determined from the slopes of the current-voltage curves in Figures 3-32 and 3-33. It indicates whether the dominant currents are diffusion currents caused by recombination of injected charge carriers in the device p- or n-region in case of n = 1, or whether the dominant current flow is caused by recombination of injected carriers in the space charge region via traps for values of n = 2. At current values greater than 7 $\mu$ A, the dominant current flow for all devices investigated is caused by recombination of carriers injected into the p- or n-region, as indicated by n-values of n ≈ 1. At voltages between 1.05 V to 1.15 V, the dominant current is caused, in part, by recombination of charge carriers in the space charge region shown by n-values of 2. Whether currents possibly due to tunneling for n-values of $3 \leq n \leq 4$ have to be considered for bias voltages below 1.05 V has not been established.

The current-voltage characteristics for diodes DII and DIII were also measured repeatedly under pulsed conditions at 300° K. For these measurements, a Rutherford Pulse Generator Model B7B, and a Tektronix Model 547 scope, with Dual Trace Plug-in Type 1A1 were used. The AC current was determined from the voltage drop across a 49 Ω resistor in series with the device, as shown in Figure 3-34.

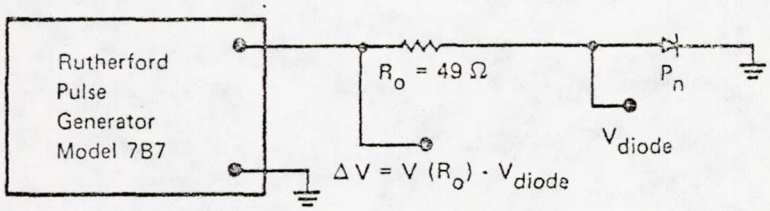


Figure 3-34. AC Measurement Circuit for Device Evaluation

For all AC measurements, the pulse repetition frequency (PRF) was 20 Hz and the pulse width 500 $\mu$s. No significant change in current-voltage characteristics due to degradation has been observed on these devices during repeated measurements. The AC current-voltage curves for these diodes are shown in Figures 3-35 and 3-36. Current values in excess of 300 $\mu$A, at 1% duty factor, could be achieved without noticeable diode heating effects, even though no special effort was made for special heat sinking. Again, emission of incoherent infrared radiation was observed at 1.1 V forward bias with an infrared image converter.

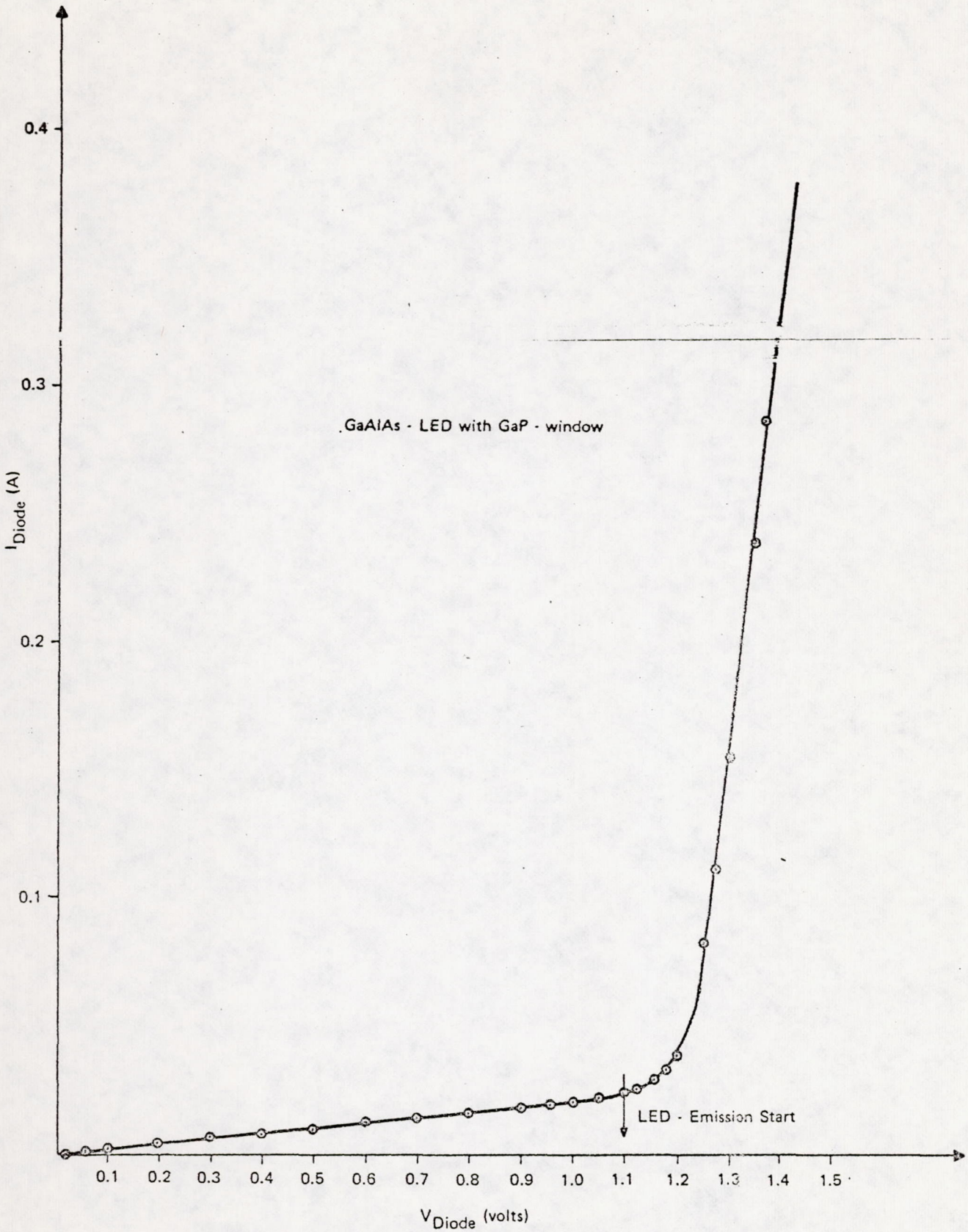


Figure 3-35. AC Current-Voltage Characteristic,
Pulse Width: 500 $\mu$s, PRF: 20 Hz,
Diode Area: 10 mil × 100 mil, Diode DII

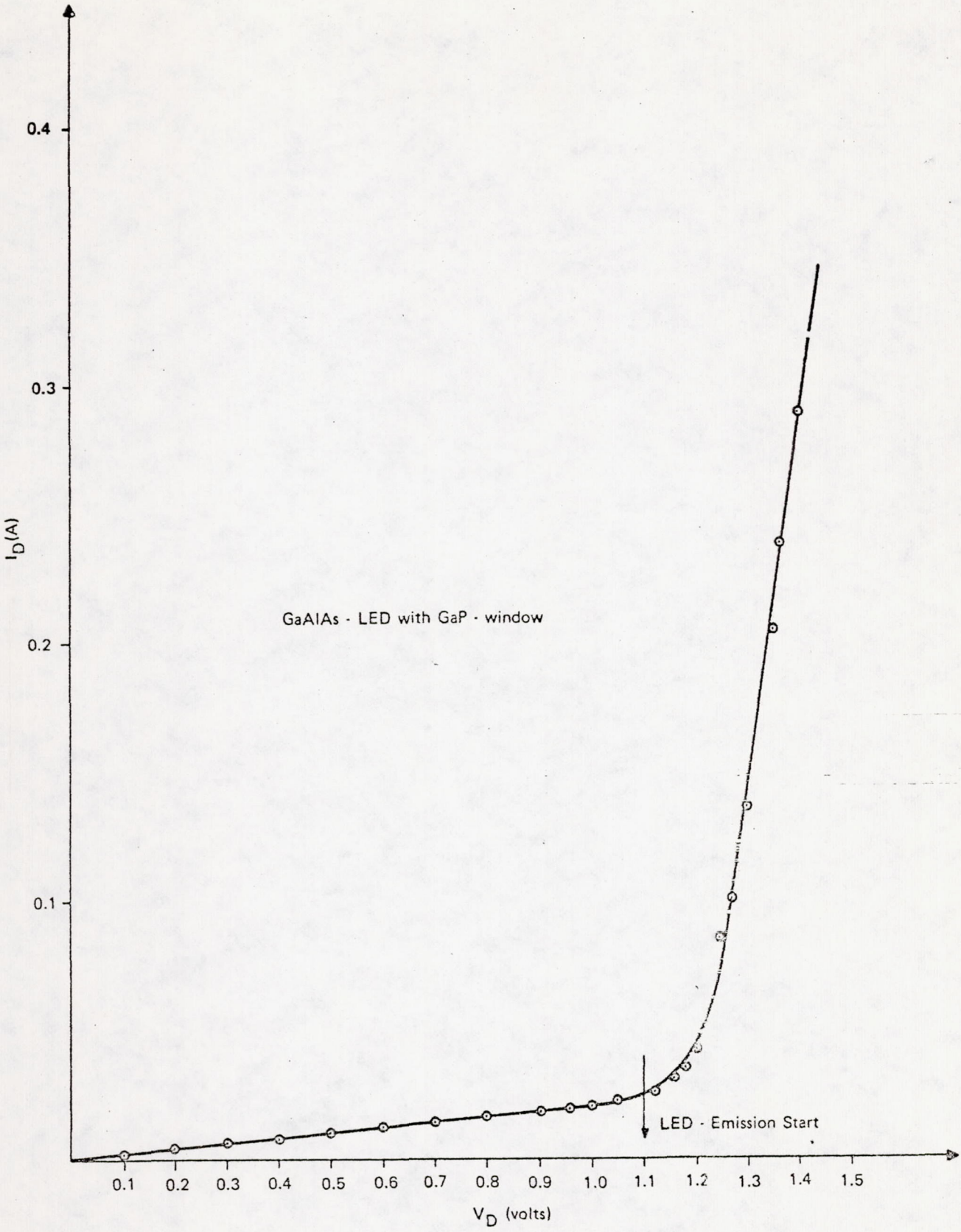


Figure 3-36. AC Current-Voltage Characteristic,
Pulse Width: 500 $\mu$s, PRF: 20 Hz,
Diode Area: 10 mil × 100 mil, Diode DIII

## 3.6 PROJECTED LIFE TESTING

Realistic testing under simulated operating conditions is indispensible for measuring diode operating life. Reliability estimates can be made only after credible data are available as a basis. To begin this data collection, diodes produced under this contract are divided into two groups of ten each for testing at different current densities. One group will be tested at 100Å/cm$^2$ and the other at 200Å/cm$^2$. The diodes are individually soldered to beryllium oxide substrates, which are, in turn, soldered to copper heat sinks. This simulates array mounting satisfactorily. By measuring the diode emission spectrum, the junction operating temperature can be derived and used as a test of this assumption.

Testing will consist of frequent measurement of diode output power during continuous operation, and occasional measurement of the diode emission spectrum. Such measurements will adequately record the diode performance changes in a way which can be related to useful operating conditions. Results of this test will be repeated by letter when complete.

## Section 4

## RECAPITULATION AND DISCUSSION OF PROGRAM RESULTS

Several problems with diodes, currently used for Nd:YAG laser pumping, prompted the pursuit of this research program. Specifically, mechanical interference and vulnerability of electrical contacts on the upper diode surface, absorption of light in relatively thick epitaxial overgrowth, and thermal problems due to thick epitaxial growth between p-n junction and heat sink were some of the problems faced. The contact problem suggested that the position of the contacts be arranged on the same face of the diode opposite the diode emission. The absorption and thermal problems indicated that the epitaxy should be thin and that, if support was provided by thick material above the p-n junction, it should be transparent to the emitted radiation.

Two candidate materials seemed worthy of consideration as the transparent window on which active layers could be grown: GaP and high band-gap GaAlAs. The single crystal GaP, which has recently become available, is transparent to the 8000Å pump radiation. However, there exists a slight lattice mismatch between that crystal and GaAlAs. No such mismatch would exist if a thick layer of aluminum GaAlAs were grown, but this alternative was judged less promising because of the difficulty in maintaining uniform high aluminum concentration during a several hour growth and preserving adequate doping in a subsequently grown active region. Properly prepared GaP wafers served as substrates for epitaxial growth of thin active layers of GaAlAs.

Initial growths, made by techniques minimizing phosphorous contamination of the melt, resulted in irregular interfaces between substrate and overgrowth. This problem was eliminated by a slight up-heat and etch phase, upon introduction of the wafer to the melt. It was then necessary to grade out the phosphorous dissolved from the wafer, before growing the active layers, or suffer a very low quantum efficiency. When this last condition was met, diode material with high internal quantum efficiency (>50%) resulted.

Upon growth of efficient material, the task of suitable device fabrication remained. The previous considerations required that the contacts be placed on the back surface of the diode. Further consideration of maximum packing density in a linear diode array with series electrical connections, dictated an arrangement of parallel stripe contacts on adjacent p and n semiconductor regions. The choice of method for creating these parallel regions was not easily made. Mesa etching and isolation diffusion each offered a feasible technique for producing such diodes, and the choice of the former was rather arbitrary. This technique proved satisfactory and, after application of photolithography and etching, contacts were applied.

Reproduced from best available copy.

Bonding of the diode chips to the thermally conducting substrate was a development task successfully performed under this contract. Because of the high power density operation anticipated, it was important that the diodes be soldered in place, thereby minimizing the thermal resistance rather than bonding with silver-loaded epoxy, which was the prevailing fabrication technology. Electroplating solder and thermal compression bonding proved a satisfactory combination. However, careful control of solder thickness is needed to avoid short circuits. This is easily done through plating time and current control.

Work was also done on two related topics: (1) low melting point glass adhesives, and (2) reflective coatings of diode surfaces. The low melting point glass has a desirable high index of refraction, but several of its other properties were unknown. As part of this program, several batches of glass were prepared and tested for adhesion properties and behavior under thermal-vacuum conditions. Reflective coatings were applied and the reflectivity of electrical contacts was measured.

Considerable effort was expended in optimizing the electrical contact metallurgy for minimum resistance. This is particularly important for pumping arrays, since operating currents are very high. The reflectivity of an optimally applied ohmic contact was measured in this program and found to be relatively low. Therefore, reflective coatings, applied over regions of the diode not contacted, enhanced the light output more than reflection from the contacts. This problem is complicated by the problem of heat conduction from the diodes which occurs via the electrical contact surfaces. Reductions in the width of electrical contacts, to allow reflective coatings, will increase operating temperature of the diode and, thereby, reduce the diode efficiency at a rate of approximately 2.7% per degree centigrade. Careful design optimization is necessary.

The devices produced under this program have most of the desired characteristics sought. They are correct in form, having contacts on the side opposite the light emission. They have demonstrated efficient light emission (1% to 2.7%) from thin epitaxial layers grown on a substrate of diverse material. This gives the thermal characteristics and low absorption desired. The emission wavelength and bandwidth of the diodes fabricated was not that desired for Nd:YAG pumping. The emission wavelength is readily achievable through control of the active layer aluminum content. However, the emission bandwidth is not so tractable and will require further experimentation. The emission bandwidth of the devices produced are tolerable, but an improvement in the pumping efficiency would be achieved by a reduction in bandwidth.

## Section 5

## NEW TECHNOLOGY

### 5.1 EPITAXIAL GROWTH OF GaAlAs on GaP

Liquid phase epitaxial growth of GaAlAs on single crystal GaP has been successfully performed. Additionally, active p-type and n-type GaAlAs layers have been grown in light emitting diode structures, which have performed with a maximum of 2.7% efficiency from a planar diode into an air interface. This efficiency exceeds the average efficiency achieved with presently used technology by a factor of 2.5.

This technological advance is significant because it reduces diode processing cost while improving performance. The cost saving stems from the elimination of the tedious and precise lapping operation presently used and required to remove light absorbing semiconductor substrates. Since GaP is transparent to the emitted radiation, it can be left on the diode.

### 5.2 MINIMUM BANDGAP LED STRUCTURE

A new type of structure called a minimum bandgap (MBG) structure has been successfully grown on GaP (111) substrates. This structure should provide greatly improved external quantum efficiencies using appropriate device geometries. The name of this new structure (MGB) derives from the characteristic that all of the GaAlAs outside the region where radiative recombination occurs has an energy bandgap larger than that of the active region. Because of this, the peak energy of the light emitted in the active region is less than the absorption edge of the material outside the active layer; hence, light produced in the active region will not be strongly absorbed outside the active layer. The MBG structure is shown schematically in Figure 2-3.

### 5.3 TECHNIQUES FOR FABRICATION OF DOMED LEDs

A new technique for forming hemispherical device structures was developed for the GaP-GaAlAs devices. Efficiencies of 5.5% were observed on the dome shaped devices. This technique which is suitable for volume production is described in detail in Appendix A.

### 5.4 LED PUMP ARRAY DESIGN AND ASSEMBLY

The design and execution of the LED pump arrays described in this report are new. The use of plated series circuitry on berylium oxide boards, conforming in length and width to the laser mode volume, represents a technological advance. This is also true for the technique of simultaneous reflow of preplated solder connections on the entire array. These concepts and processes are completely described in Appendix B.

## Section 6

## CONCLUSIONS

It is concluded from this program that efficient GaAlAs diodes, grown by liquid epitaxy on GaP single crystal substrates, are feasible.

These experiments have shown the MBG diode structure can yield increased efficiency over the conventional diode structure. The most efficient diodes produced on this program have reached 80% of the ideal performance as described in Subsection 3.1.2. The efficiency achieved on some material, during the very limited number of growth runs throughout this program, was better than that of the presently used GaAlAs diodes. Therefore, efforts to grow these diodes in production quantities are desirable. However it must also be concluded that problems of layer cracking due to strain are not completely solved. (reference Section 3.1)

Secondly, it may be concluded that fabrication of the "back-contact" diode structure is feasible, and that no insurmountable problems exist in placing these diodes in closely packed, carefully aligned arrays. Additionally, no factors exist which would cause this fabrication cost or array assembly cost to be disproportionately higher than that of the presently used diodes. (reference Appendix B)

The relationship between aluminum concentration, doping density, and contact resistance is now known to a sufficient extent that contact resistance can be minimized. The necessity for clean, oxide-free surfaces prior to metallurgy application has been demonstrated (reference Subsection 3.2)

To date, no conclusion can be drawn about the use of low melting point glass in laser device construction, since the information gained in this program is not exhaustive. No characteristics of the glass preclude its use, but insufficient data exists concerning its life properties to draw conclusions at present. (reference Section 3.4)

Optimized device structures may include reflective coatings on side surfaces. The faces on which the electrical contacts are placed will not have reflective coatings since the difference in reflectivity is less than 25% and it is important to have broad contact surfaces for thermal conduction.

## Section 7

## RECOMMENDATIONS FOR FURTHER ACTIVITY

Diode yield rates during this research phase have been low. Although it is not an unexpected situation to begin with a low yield, one improvement, which would increase yield and should be sought, is the avoidance of layer cracking of the epitaxial layers, which spoiled otherwise useful wafers. This effect can probably be associated with the total thickness of the epitaxy in such a way that, by limiting thickness, it can be avoided. This possibility should be pursued further.

The most important subjects for further investigation are:

1) Improvement in epitaxial surface quality. Present surfaces are frequently too rough for the application of photoresists. This has made diode processing difficult.

2) Causes and elimination of layer cracking

3) Establishing conditions for (100) surface growth. It is believed, on the basis of experience with GaAs, that (100) growth would reduce etch problems.

4) Further optimization of internal quantum efficiency. Growths to date have not established a recognizable relationship between efficiency and aluminum concentration, cooling rate, or growth temperature. (reference Subsection 3.1)

As previously indicated, isolation diffusion is a technique of diode fabrication which could also have been tried, rather than mesa etching. This alternate course should be pursued because this technique may enable the processing of wafers which have a slightly rougher surface than required for etch techniques, and because etch depth control requirements on very thin epitaxy are stringent. No untried technology is required for this procedure — only the application of previously proven techniques to the new material.

Most importantly, work should now be pursued to utilize the advances made in this research to produce larger quantities of the diodes. Enough of these diodes should be produced to build several arrays for test in laser devices, and to establish extensive lifetime and performance data.

## Appendix A

## GaP DOMED DIODE PREPARATION

Concurrent with the course of this investigation a method was developed to produce hemispherical domes of GaP. The usefulness of hemispherical domes for LED structures has been previously shown[8]. The GaP domes for this program were formed in the following manner:

1) Bond two GaP wafers, of thickness t, together with glycol pthalate
2) Dice the wafer produced in 1) into cubes with sides of 2 t
3) Ball mill cubes into spheres
4) Polish spheres with a chemical etch, i.e., 1:1 HCl: $H_2$ $O_2$
5) Separate spheres into hemispheres by heating or dissolving away the glycol pthalate.

An example of such a hemisphere is shown in Figure A-1. This structure was used with LED layers with graded compositions.

On run P 209, a graded layer, diodes were formed into a hemispherical dome configuration. The $Ga_{1-x}Al_xAs$ layers were etched to form an x-y linear array of $150\mu m \times 200\mu m$ mesas on $250\mu m$ centers. The wafers were then cut into two small pieces and cemented together, such that the $Ga_{1-x}Al_xAs$ mesas of each piece were touching. Since the total growth, plus GaP substrates, was about $625\mu m$, the cubes were cut 0.125 cm on a side. Quantum efficiency was measured, using a calibrated Si cell, and an electrical contact to the diode was made via pointed metal probes using a micromanipulator. This method resulted in both a large and nonlinear contact resistance, which limits the current to about 10-20 mA through the diode. Even under the low current density condition, one diode yields a quantum efficiency of about 5.5%, which compares favorably with previously published values[8]. This result clearly demonstrates the use of GaP substrates lead to much improved LED devices.

Figure A-1. GaP Hemispheres

## Appendix B

## PROCEDURE FOR DEVICE FABRICATION

When the LED-structure has been proven, the following procedure, for making ohmic contacts on the crystal wafer and for packaging, was applied.

### B-1. APPLICATION OF "P"-TYPE METALLURGY

For applying a p-type ohmic contact on gallium aluminum arsenide, the wafer is placed on a hot stage inside a vacuum evaporator. The temperature of the hot stage is controlled by a thermocouple inserted into the wafer holder. Prior to evaporation of a gold-zinc alloy film of a 1000A onto the wafer surface, the wafer holder, hot stage, and the wafer are masked appropriately with an aluminum mask. The gold-zinc alloy is usually evaporated, with the wafer at a temperature between 200° C and 300° C. After evaporation of the alloy, the wafer is cooled in a nitrogen atmosphere.

### B-2. PHOTOPROCESSING AND ETCHING OF "P"-TYPE METALLURGY PATTERN

After the p-type metallurgy has been applied on the wafer, KTFR-photoresist is used for establishing a 150 $\mu$m wide stripe pattern by using photolithography. Prior to photoresist exposure, the KTFR is prebaked, at about 100° C. After developing and inspection of the KTFR-pattern it is postbaked at about 125° C.

Etching of the gold-zinc alloy film, for establishing the p-contact pattern, involves a metal etchant comprised of potassium iodide, water, iodine, and methanol. The unwanted alloy film is removed completely by a controlled etching, and the process is monitored and observed under the microscope. After inspection of the metallurgical etch pattern on the wafer, the KTFR is removed by means of a suitable photoresist stripper. The unfinished wafer is then inspected to guarantee quantitative removal of the KTFR.

### B-3. PHOTOPROCESSING AND ETCHING OF 250 $\mu$m WIDE MESA DIODES ON THE WAFER

The wafer is processed, as outlined in Section II, except on a mask yielding 250 $\mu$m wide mesa diodes is used for KTFR-exposure. The mesa mask has to be aligned in such a way that the 150 $\mu$m wide p-metallurgy stripe is just within the 250 $\mu$m opening-that is offset to one side.

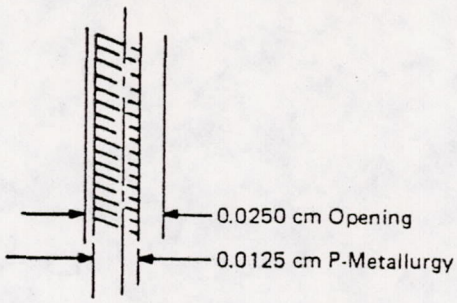


After exposure, developing, and post baking of the resist the wafer is mounted with black wax on a glass substrate so that the periphery of the wafer is also protected from the etchant with wax. The mesa diodes are then etched with a bromine-methanol solution under suitable illumination. The unmasked p-region of gallium aluminum arsenide (approximately 10 microns thick) is then removed by the etchant. After removal of the wafer from the glass substrate and dissolving the black wax completely in trichlorethylene, the KTFR is stripped with 100 photoresist stripper. Wafer inspection follows and the wafer is passed on for application of the n-type metallurgy.

## B-4. APPLICATION OF "N"-TYPE METALLURGY

Prior to evaporation of gold germanium nickel alloy, a metal mask is aligned which properly defines the metallization pattern for the n-contacts. The previously applied p-type metallurgy and the mesa diodes are covered, and the opening of the metal mask is centered over "+" signs etched into the wafer during the process step outlined in Step B.4.3 above. The "+" signs serve as alignment aid.

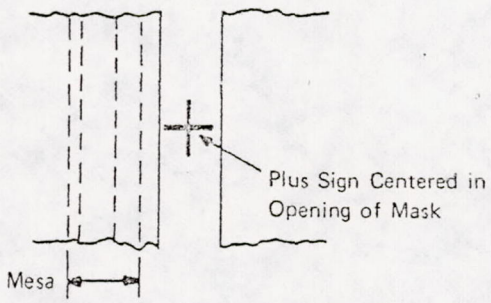


After proper alignment of the mask, wafer final inspection of the complete mask-wafer holder assembly takes place. The assembly is then placed on the hot stage, inside the vacuum chamber. The chamber is evacuated and evaporation of the gold germanium nickel alloy is accomplished, with the wafer at a temperature of about 160° C. After evaporation of the alloy, the wafer is cooled down in a nitrogen atmosphere and removed from the mask and wafer holder.

## B-5. CONTACT ALLOYING

Contact alloying is carried out, under forming gas, in a tube furnace having a temperature in the range between 400° C to 500° C. After contact alloying, the wafer is inspected and stored for further processing.

## B-6. REMOVAL OF PART OF THE GaP-SUBSTRATE FROM PROCESSED WAFER

The wafer is mounted on an adjustable polishing fixture, with the processed surface down on the lapping block. The GaP substrate is then lapped, successively, with 3 micron and 0.3 micron oxide slurry to achieve a 4 to 5 mil thick n-layer of gallium phosphide. The final finish is a mechanically polished n-layer of gallium phosphide, forming the LED-window.

## B-7. WAFER CUTTING INTO DIODE BAR AND DEVICE SEPARATION

The individual diodes, with dimensions 250 $\mu$m by 0.25 cm, are cut with a string saw, by mounting the wafer with the isolated p- and n-regions upside down. The sawed edges of the individual diodes are then etched briefly with a bromine methanol solution to remove mechanical damage caused by cutting. Afterwards, devices are rinsed in methanol and subsequently in acetone.

## B-8. PLATING OF BERYLLIUM OXIDE CARRIER BOARDS

The beryllium oxide carrier boards, used for diode mounting, are coated by sputtering successively thin layers of chromium, nickel, and gold. On top of the sputtered gold layer, a 1.5 to 4 micron thick gold layer is deposited electrolytically. Then the metallization pattern is etched out, utilizing photolithographic techniques. Finally, a lead-tin alloy film is deposited on the gold pads.

## B-9. REFLOW SOLDERING OF DIODE CHIPS TO CARRIER BOARD

Prior to device mounting with a Kulicke and Soffa wedge bonder, the heating column of the bonder is set to 200° C, and the wedge temperature at about 300° C. The weight for wedge compression bonding is also properly adjusted. The diodes can then be mounted on the board after a line is scribed 150 $\mu$m from the edge of the anode side of the board connection pattern. A light coating of Indalloy flux is applied on the metal pads of the board, prior to chip positioning. This flux will hold the chips temporarily in position after chip positioning parallel to the scribed line along the anode side of the device. The wedge bonding tip is then placed in the center of the chip and held until a slight reflow around the edges of the chip is observed. After withdrawal of the wedge tip and removal of the board from the bonder, the diodes are cleaned with trichlorethylene to remove the solderflux. The devices are then ready for testing.

Additional external leads of nickel, for anode and cathode connections, can be a added, by first tinning the leads with 60/40-solder, and by soldering these leads to the pads of the hybrid board, with the same procedure used for chip mounting.

Figure B-1 shows the vacuum evaporator. Figure B-2 shows the hot stage and evaporation filament inside the vacuum chamber. Figure B-3 shows the furnace set up for contact alloying. Figure B-4 shows the adjustable lapping and polishing fixture and the fixture for wafer and mask holding during evaporation.

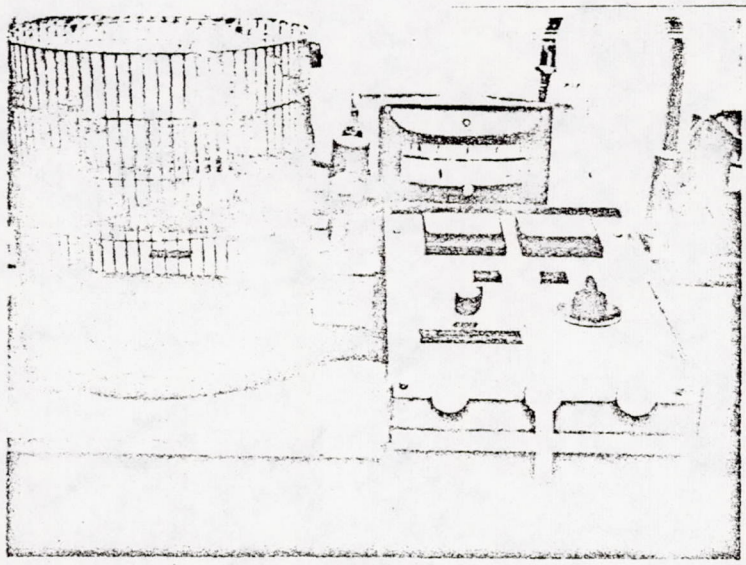

Figure B-1. Vacuum Evaporator

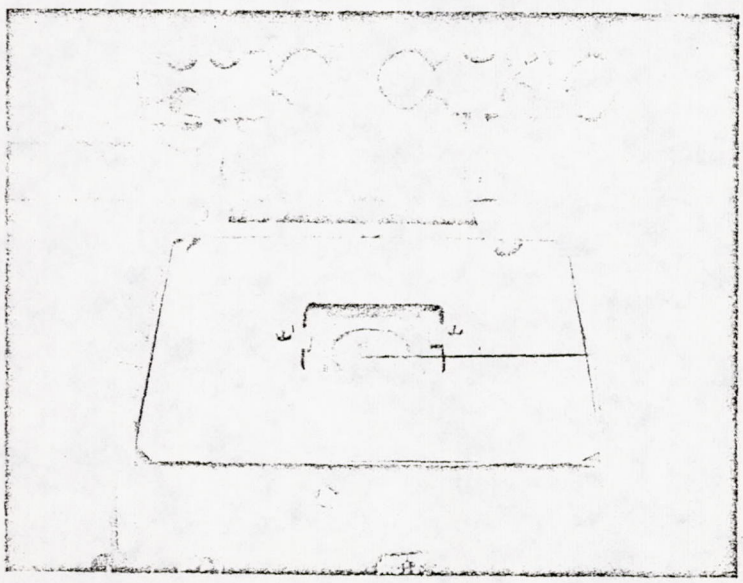

Figure B-2. Hot Stage and Filament

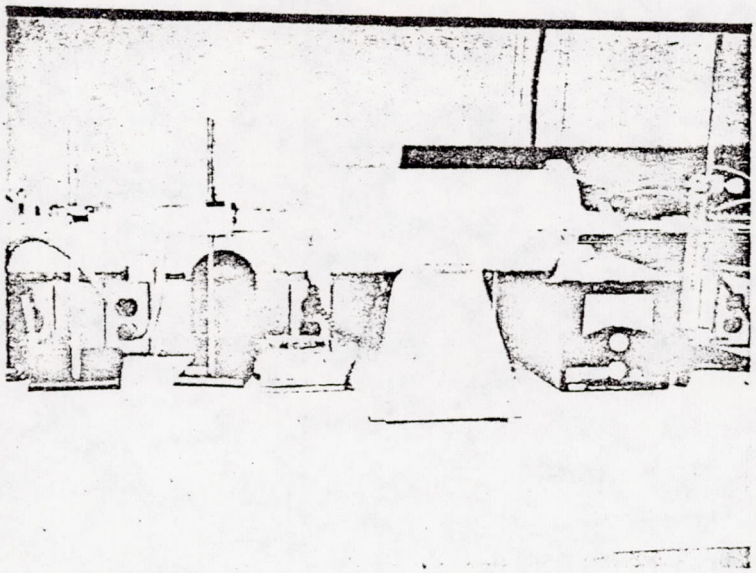

Figure B-3. Alloying - Sintering Furnace

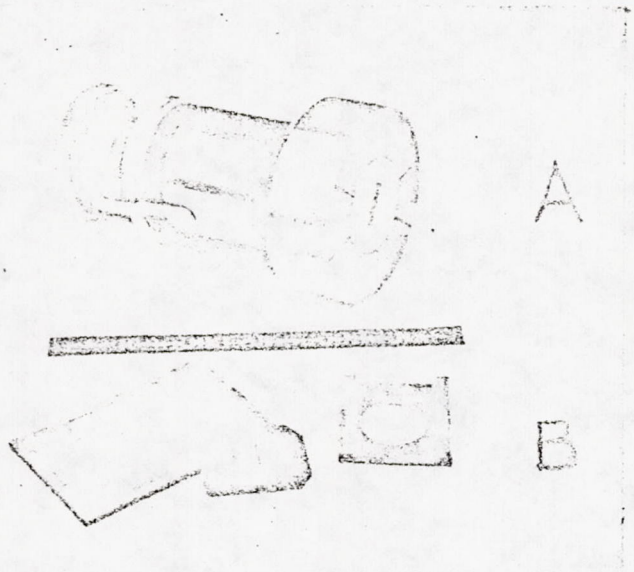


Figure B-4. Adjustable Lapping & Polishing Fixture, and Fixture for Holding Wafer and Mask During Evaporation

## REFERENCES


1. H. Rupprecht, J. M. Woodall and G. D. Pettit, Appl. Phys. Letters 11, 81 (1967).

2. I. Hayashi and M. B. Panish, J. Appl. Phys. 41, 150 (1970).

3. H. Kressel and H. Nelson, RCA Rev. 30, 106 (1969).

4. Zh. I. Alkrov, et al, Soviet Physics Semiconductors 4, 1573 (1971).

5. I. Hayashi, M. B. Panish and F. K. Reinhart, J. Appl. Phys. 42, 1929 (1971).

6. H. Nelson, RCA Rev. 24, 603 (1963).

7. J. M. Woodall, H. Rupprecht and W. Reuter, J. Electrochem. Soc. 116, 899 (1969).

8. E. G. Dierschke, L. E. Stone and R. Haisty, Appl. Phys. Letters 19, 98 (1971).

9. J. M. Woodall, J. Electrochem. Soc. 118, 150 (1971).

10. J. M. Woodall, J. Crystal Growth (in press).

11. R. M. Potemski and J. M. Woodall, J. Electrochem. Soc. (in press).

12. R. Hooper and L. Sharif, "Metal-Semiconductor Contact Resistance" Semiconductor Research and Development Laboratory, Texas Instruments, Inc., Dallas, Texas.

13. L. E. Terry, "Metal-Semiconductor Contacts and Contact Resistance", Electrochemical Society Fall Meeting - Montreal, Canada, Oct. 6-11, p. 466, 1968.

14. L. Harris, J. of Opt. Soc. Am. 51, 80 (1961)

15. A. G. Fisher and C. J. Neuse, J. Electrochem. Soc., 116, 1718 (1969)

16. F. Stern, Applied Optics, Vol 3, p. 111, Jan. 1964.



Reproduced from best available copy.